Visualisation of Articular Motion in Orthopaedics

Visualisation of Articular Motion in Orthopaedics

Proefschrift

ter verkrijging van de graad Doctor aan de Universiteit Leiden,
op gezag van de Rector Magnificus prof. mr. P.F. van der Heijden,
volgens besluit van het College voor Promoties
te verdedigen op donderdag 10 februari 2011
klokke 15:00 uur

door

Peter Roelof Krekel

geboren te Den Haag
in 1982

Samenstelling promotiecommissie:

Voor mijn opa.

vi

Contents

1

Introduction

1.1 Motivation

Medical visualisation is the research field that deals with the graphical representation of medical data. Its main goal is the extraction of insight from that data by leveraging the human visual system. Examples can be found in many clinical procedures, for example in liver surgery, where medical visualisation is used to predict the vascularity of a liver after a resection (Lang et al., 2005), neurosurgery, where it assists in finding neuronal connections between regions in image data of the brain (Blaas et al., 2005) and virtual colonoscopy, where it improves the semi-automatic detection of polyps (Zhao et al., 2006).

The improved availability and quality of scanning equipment such as computed tomography (CT) and magnetic resonance imaging (MRI) have both enabled and necessitated the more wide-spread adoption of medical visualisation applications. The excellent resolution and contrast of image data generate new possibilities for the extraction of clinically relevant information. In orthopaedics, these developments are generally aimed towards improving the supportive role of image data in clinical decision-making. This applies to several aspects of patient treatment, as is illustrated by Figure 1.1. A good example is the visualisation of the fixation strength of a prosthesis, which can be determined by means of finite element modelling (Huiskes and Chao, 1986, Dick et al., 2008).

In parallel with improvements to scanning equipment, the quality of orthopaedic care has improved. For example, total knee prostheses inserted between 1998 and 2007 have half the risk of requiring revision when compared to prostheses inserted

Medical Visualisation in Orthopaedics
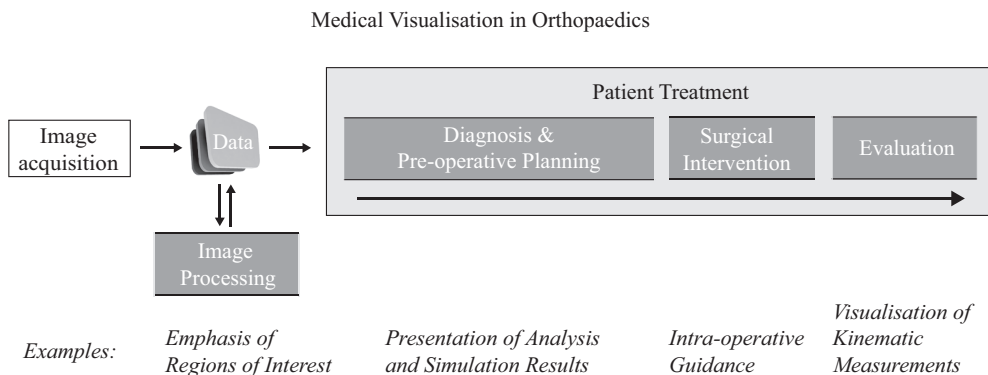
Figure 1.1: The application areas of medical visualisation in orthopaedics. In image processing, medical visualisation improves the usability of acquired image data by emphasising regions of interest. In diagnosis and pre-operative planning, medical visualisation can be used to intuitively present numerical data and assist the decision-making. Intra-operative visualisation methods such as computer navigation support surgical interventions, although this subject is not covered in this thesis. Finally, medical visualisation is used in the evaluation process, for example to provide insight in kinematic data.

between 1988 and 1997 [1]. Similarly, the revision rate of total hip prostheses inserted in 1979 was 15% after ten years, whereas this rate decreased to 6% for prostheses inserted in 1995 [2]. However, there are surgical procedures where the outcome is less satisfactory.

For example, the success rate for shoulder replacements is substantially lower than for knee and hip replacements (Wirth and Rockwood, 1994). This can be attributed to the overall complexity of the shoulder joint and the relatively small incision (see Figure 1.2). Additionally, the lack of experience of many surgeons contributes to reduced success rates (Lo et al., 2003, Hagen et al., 2010). Hasan et al. report that 44% of shoulder replacements are performed by low-volume surgeons (i.e. surgeons performing one or two operations per year), compared to 3% for hip replacements and 2% for knee replacements (Hasan et al., 2003).

Other examples include shoulder fractures, where approximately 73% of patients that receive a shoulder prosthesis do not regain satisfactory function (Goldman et al., 1995) and hip impingement, where between 20% and 32% of the patients are not satisfied after open surgical treatment (Beck et al., 2004, Krueger et al., 2007).

The above examples indicate that there are still challenges ahead in orthopaedics.

---

[1] data obtained from Swedish Knee Arthroplasty Register 2009
[2] data obtained from Swedish Hip Arthroplasty Register 2007

Figure 1.2: Shoulder replacement surgery. The incision is relatively small and the density of muscles, ligaments and bones complicate accurate alignment of prosthesis components.

In this thesis we investigate how medical visualisation may contribute towards addressing these challenges. Specifically, we study how medical visualisation provides insight into the articulation and range of motion (ROM) of joints, with the purpose of supporting surgical decision-making that addresses pathology at the articulating joint.

1.2 Medical quick guide

In this section, the joint diseases and traumatic injuries discussed in this thesis are shortly described. The first two, osteoarthritis and rheumatoid arthritis, are relevant for Chapter 2, 3 and 4. Proximal humerus fractures and femoroacetabular impingement are discussed in Chapter 7.

1.2.1 Osteoarthritis and rheumatoid arthritis

Osteoarthritis and rheumatoid arthritis are diseases that affect the bone and cartilage. In general, people suffering from either of the conditions are severely limited in their activities of daily living. Patients often refrain from using the joints, as motion is usually accompanied by pain (synovitis). In addition, motion limitations are caused as a direct result of the degenerated state of the joints.

Osteoarthritis is a (non-)inflammatory disease that deteriorates the cartilage between the articulating bones, leading to limited mobility and pain. It is more prevalent in midlife and beyond. Above the age of 65, 90% of the population suffers from osteoarthritis to some extent. For the shoulder this percentage is roughly 10% in both men and women (De Filippis et al., 2004, Saase et al., 1989).

Rheumatoid arthritis is an autoimmune disease that causes chronic inflammations to the joints and surrounding tissues. It is characterised by painful and stiff joints and when left untreated it leads to irreversible joint damage. Rheumatoid arthritis is diagnosed more often in women than in men. A prevalence study performed in the United Kingdom reports a prevalence of 1.16% in women and 0.44% in men (Symmons et al., 1994). In the Netherlands the prevalence is 1.10% in women and 0.71% in men (Hoeymans et al., 2010).

Initial treatment is conservative and consists of physical therapy and the administration of medication. However, when osteoarthritis and rheumatoid arthritis progress a surgical procedure may be required to reduce the pain and restore mobility of the patient. This can be achieved by replacing the joint with a prosthesis, a procedure known as joint replacement or arthroplasty. Nowadays arthroplasty is a common treatment for arthritic joints, most often applied to knees and hips and less commonly to the shoulder[3].

1.2.2 Proximal Humerus Fractures

The shoulder is comprised of three bones that move with respect to the thorax: the shoulder blade (scapula), the clavicle (clavicula), and the upper arm bone (humerus). When the head of the upper arm bone breaks this is known as a proximal humerus fracture (PHF) (see Figure 1.3). In general, these fractures are caused by high impact of the humeral head on the shoulder blade, e.g. as the result of a falling accident. The incidence increases with age and is higher in women. The reported incidence varies between 1/952 and 1/1.370 (Palvanen et al., 2006, Hagino et al., 1999, Lind et al., 1989).

---

[3]data obtained from American Academy of Orthopaedic Surgeons (AAOS)
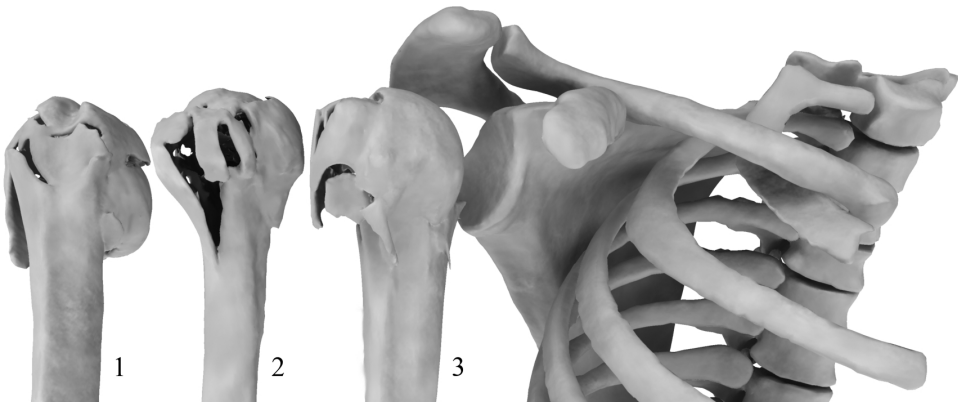
Figure 1.3: Three examples of proximal humerus fractures. As can be seen there is considerable variability in the shape of these fractures.

There are several treatment options for these types of fractures, consisting of conservative treatment or surgical intervention, depending on the type of fracture, but also on personal preference of a surgeon. The surgical options range from simple refixation surgery to shoulder replacement surgery. The treatment decision is typically based on assessment of static image modalities such as radiographs and CT, the age and personal situation of the patient and fracture classification systems found in the literature.

Classification systems attempt to relate the appearance of the fracture to clinical outcome with the goal of integrating this knowledge in treatment decision-making. Many studies on these classification systems exist, all leading to the conclusion that the systems have a large inter-observer variability (Bernstein et al., 1996, Kristiansen et al., 1988, Sidor et al., 1993, Siebenrock and Gerber, 1993). A second problem is that these classifications only assess a static image, while the multidirectional movable shoulder joint would need a dynamic evaluation tool in decision analysis on the optimal treatment.

Shoulder fractures are a typical example of injury where the decision-making process is primarily governed by surgical experience. The outcome of a treatment decision depends on many aspects that are not easily assessed using visual inspection of the available image modalities. Regardless of this fact, these classification systems are commonly used in treating these types of fractures. The relationship between shape and outcome depends on underlying principles such as vascularity, muscle attachment sites, joint articulation and potential impingement when the shoulder is moved in different directions. Although many attempts have been undertaken, it is

extremely difficult to capture this variability in a classification system.

In this thesis the simulation of one such principle is described. In Chapter 5 and 7 the dynamically simulated joint articulation and collision aspects are used as guidelines for the assessment of shoulder fractures. We restrict our research to these parameters because the image modality that was available for this study (CT) does not provide the information needed to assess aspects such as vascularity and muscle attachment sites.

1.2.3   Femoroacetabular Impingement

In femoroacetabular impingement (FAI), morphological changes to the bone of the hip joint lead to bony impingement. This results in limited hip motion, pain and progressive damage to the cartilage. Recent work suggests that FAI may lead to osteoarthritis (Ganz et al., 2003). Although the etiology of FAI is still unclear, a variety of causes are described, such as excessive sporting activities and post-traumatic deformities (Leunig et al., 2005). The prevalence of FAI is approximately 10% to 15%, although it is seldomly symptomatic (Leunig et al., 2005, Gosvig et al., 2008). Patients are often between 20 and 40 years old (Tannast et al., 2007b).

Two types of FAI are recognised; the cam type and the pincer type. The former refers to a deformation of the femoral head, typically on the anterior side. The latter refers to deformations of the acetabular rim. Cam and pincer deformities individually reduce the space available for movement and lead to FAI symptoms. The two types are reported to occur simultaneously in 86% of patients (Beck et al., 2005). Treatment options vary and include resection of the colliding bones at the hip by a surgical dislocation or arthroscopic surgery. Satisfactory outcome varies and is reported to range from 68% to 100%, arthroscopic management having slightly better results than open surgery (Larson and Giveans, 2008, Beck et al., 2004, Krueger et al., 2007).

The dynamic spatial relation between the femoral head and the acetabular rim is difficult to assess using traditional static image modalities. In Chapter 7 a case study is presented in which we use dynamic ROM simulations to support the treatment decision regarding a patient with FAI.

1.3   Goal

The goal of this thesis is to study medical visualisation and its supportive role in the orthopaedic treatment decision-making process that affects the articulation of spheroid joints and their ROM. We specifically focus on the ROM of the shoulder joint and, to a lesser extent, the hip joint.

1.4 Contributions

The contributions of this work include the following:

- We present a new segmentation technique specifically designed for rheumatoid glenohumeral joints. Segmentation of CT scans of heavily affected joints is a challenging problem. To facilitate pre-operative planning solutions a fast and accurate method is required. The solution presented in this thesis is able to segment the CT scans in under two minutes.

- We present a system that interactively simulates and visualises patient-specific bone-determined ROM of spheroid joints. The system can be used to plan shoulder replacement surgery and to dynamically assess the ROM of prostheses, PHFs and hip joints with FAI. To technically validate the system we have performed a cadaveric evaluation study. With regards to PHFs, we draw several conclusions on the consequences of fracture morphology on bone-determined ROM. Three case studies are presented that describe the application of the ROM simulator to a PHF case, a case of prosthetic dislocation after primary hip arthroplasty and a case of femoroacetabular impingement.

- We present a technique for the comprehensive visualisation of multi-joint kinematic data used in orthopaedics and rehabilitation medicine. The technique is integrated in the data acquisition process and allows researchers to explore the data rather than to validate a pre-determined hypotheses.

1.5 Structure of this thesis

In this thesis we discuss image processing, diagnostics, pre-operative planning and the evaluation of kinematics. The structure of this thesis is defined by the order in which these concepts are encountered in the treatment of patients, followed by a description of possible clinical applications. For an overview of the structure, see Figure 1.4.

In Chapter 2 we present an application of medical visualisation in image processing. A novel segmentation method that combines surface and volume processing techniques is described, forming a fast and effective approach that segments the humerus and scapula from CT scans of arthritic shoulder joints. The severely pathological state of the joint is associated with irregularities of the bone surface and large variations in bone density, thereby complicating segmentation and posing a challenging problem.

In Chapter 3 a technique is presented for the simulation and visualisation of patient-specific bone-determined ROM for shoulder arthroplasty. The techniques are

Structure of this Thesis

Pathology	Image Processing	Diagnosis & Pre-operative Planning	Surgical Intervention	Evaluation
RA/OA	Chapter 2	Chapter 3, 4		
PHF		Chapter 5, 7		Chapter 6
FAI		Chapter 8		
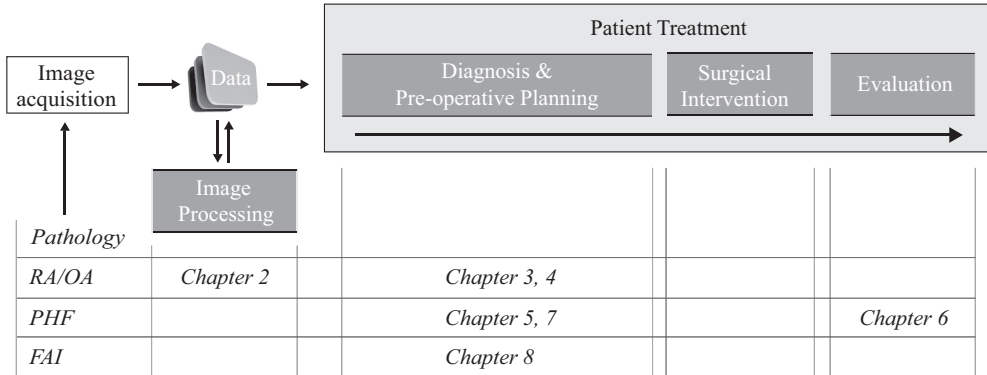
Figure 1.4: The structure of this thesis. RA/OA = Rheumatoid arthritis/osteoarthritis, PHF = Proximal humerus fracture and FAI = Femoroacetabular impingement.

integrated in a pre-operative planning solution, allowing the surgeon to make adjustments to the prosthesis position and alignment. Adjustments to the pre-operative plan affect the ROM, which is subsequently recalculated and depicted using a comparative visualisation technique. Optimisations have been implemented to enable interactive utilisation of the system.

In Chapter 4 we describe a validation study on the prediction of impingement using the ROM simulator. Two cadaveric shoulders were replaced with a modular shoulder prosthesis. A computer navigation system was used to register the occurrence of impingement and these registrations were compared to the predictions by the ROM simulator.

In Chapter 5 we study the implications of shoulder fracture morphology on the bone-determined ROM of the glenohumeral joint. We demonstrate that specific fracture patterns lead to reduced bone-determined ROM and that there is a relation between morphological properties of the humeral head and the available range of bone-determined ROM.

Following the work on ROM simulation, Chapter 6 discusses a novel visualisation technique for the analysis of multi-joint kinematic data. Through a combination of a forward and inverse visual query system, large collections of multijoint kinematic data can be compared and relations between kinematic parameters can be found without a pre-determined hypothesis.

Chapter 7 describe clinical applications of the ROM simulation system. We present

three case studies in which the system supported treatment decisions.

Finally, in Chapter 8 we discuss important conclusions that follow from this thesis and we present a brief outlook on the future of medical visualisation.

2

Combined surface and volume processing for fused joint segmentation

Peter R. Krekel[1,2], Edward R. Valstar[1,3], Frits H. Post[2],
Piet M. Rozing[1], Charl P. Botha[2]

[1]*Department of Orthopaedics, Leiden University Medical Centre*
[2]*Visualisation Group, Delft University of Technology*
[3]*Biomechanical Engineering, Delft University of Technology*

Abstract

Segmentation of rheumatoid joints from CT images is a complicated task. The pathological state of the joint results in a non-uniform density of the bone tissue, with holes and irregularities complicating the segmentation process. For the specific case of the shoulder joint, existing segmentation techniques often fail and lead to poor results. This chapter describes a novel method for the segmentation of these joints.

Given a rough surface model of the shoulder, a loop that encircles the joint is extracted by calculating the minimum curvature of the surface model. The intersection points of this loop with the separate CT-slices are connected by means of a path search algorithm. Inaccurate sections are corrected by iteratively applying a Hough transform to the segmentation result.

As a qualitative measure we calculated the Dice coefficient and Hausdorff distances of the automatic segmentations and expert manual segmentations of CT-scans of ten severely deteriorated shoulder joints. For the humerus and scapula the median Dice coefficient was 98.9% with an interquartile range (IQR) of 95.8% - 99.4% and 98.5% (IQR 98.3% - 99.2%) respectively. The median Hausdorff distances were 3.06 mm (IQR 2.30 mm - 4.14 mm) and 3.92 mm (IQR 1.96 mm - 5.92 mm) respectively.

The routine satisfies the criterion of our particular application to accurately segment the shoulder joint in under two minutes. We conclude that combining surface curvature, limited user interaction and iterative refinement via a Hough transform forms a satisfactory approach for the segmentation of severely damaged arthritic shoulder joints.

2.1 Introduction

In orthopaedic surgery, CT-scans are routinely used to diagnose and plan joint replacement surgery for severe cases of osteoarthritis and rheumatoid arthritis. These diseases are the two most common forms of arthritis and are characterised by heavy deterioration of the cartilage and bone surface of joints. The CT-scans yield anatomical information that is hard to obtain through other means. A wide variety of orthopaedic applications require CT-scans to provide pre- and intra-operative assistance to the surgeon (Krekel et al., 2006, Di Gioia III et al., 2007, Sato et al., 2000).

Segmentation of the data enables the surgeon to distinguish the geometry of the different bones of the joint. This allows for fast assessment of the state of the pathological joint and provides means to set up a pre-operative plan for surgery. One of the target applications for our segmentation routine utilises the bone geometry for biomechanical modelling of the shoulder. The challenging aspect of this segmentation problem is that bone tissues need to be separated, rather than just classified.

For arthritic joints the segmentation process is typically complicated by large variations in bone density and irregularities of the bone surface (see Figure 2.1 for an example slice of such a dataset). The varying bone density complicates interpretation of the data. In addition, the joint often appears to be fused in the CT data due to the significantly decreased joint space. As the cartilage of pathological joints wears off, the joint space can become virtually untraceable. This is further complicated by the limited resolution of the CT scanning equipment. Manual slice-by-slice segmentation is labour intensive and may take up to two hours per dataset.

Existing segmentation techniques, including a high-level integration of level-sets and watershed segmentation, have limited success with this specific segmentation task, as discussed by Botha (Botha, 2005). Although these techniques lead to accurate segmentation results, they require adaptation of numerous parameters. This is a time-consuming process and therefore these techniques are not suitable for clinical protocols.

One of the promising techniques for separating skeletal structures is presented by Kang et al. (Kang et al., 2003). The technique consists of 3D region growing with locally adaptive thresholds, followed by a mixture of 3D and 2D morphological operations to close holes in the segmentation. The resulting segmentation is then smoothed by adjusting its containing iso-surface. The technique is applied to the hip, the knee and the skull. The authors state that a site-specific approach is required for separating different bony structures at joints *before* their techniques can be applied and that this separation is site specific. In our opinion, the determination of this site-specific separation method is one of the most challenging tasks in the case of the shoulder due to its deformed shape.
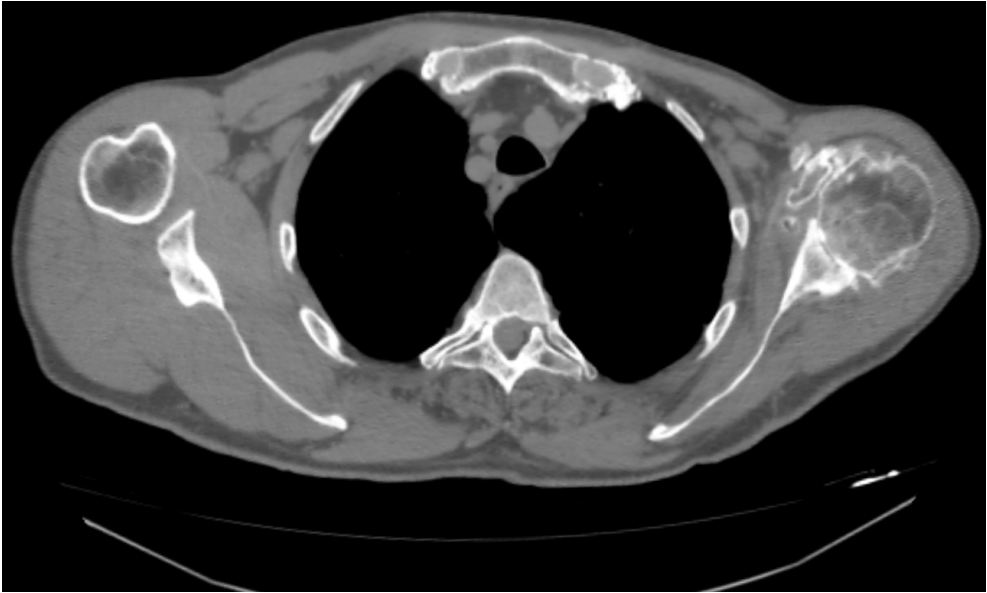
Figure 2.1: A single slice of a CT-dataset used in this study. The image shows the right and left shoulder in the transverse plane (i.e. view from feet to head). As can be seen, the left shoulder joint (on the right side of the image) is heavily deteriorated due to rheumatoid arthritis, complicating segmentation of this shoulder.

In the work of Zoroofi et al. rheumatoid hip joints are segmented by making use of histogram-based thresholding (Zoroofi et al., 2003). A number of landmarks are chosen relative to the convex hull. These points are used to construct an initial ellipsoid around the femoral head. This ellipsoid is used to derive an initial estimate of the joint space, which is subsequently refined on a Hessian-filtered version of the data. Although their method yields accurate segmentation results for less arthritic joints, the joint spaces of severely arthritic and extremely arthritic hips were only correctly segmented 30% and 12% respectively.

Branzan-Albu et al. and Tremblay et al. describe a technique for segmenting shoulders from T1-weighted MRI images of healthy shoulders (Branzan-Albu et al., 2004, Tremblay et al., 2004). Although this work is based on MRI data rather than CT data, it is relevant because it specifically targets the shoulder. A separate 2D segmentation is performed on each 2D slice. This segmentation is based on Wiener filtering, Sobel edge detection and region growing. Morphological techniques are used to successfully reconstruct a smooth 3D segmentation from the 2D segmentations. However, this work focuses on healthy subjects with large acromiohumeral and

glenohumeral distances. Their technique does not address the problems of decreased joint space and bone decalcification. It does however indicate the promise of MRI-based techniques for the segmentation of the shoulder skeleton.

Model-based segmentation techniques can also lead to a successful solution for the segmentation of anatomical shapes (Tao et al., 2002, Pitiot et al., 2004, Wu and Sun, 2006). In orthopaedics, statistical shape models for hips and knees have been investigated (Rajamani et al., 2007, Fleute and Lavallee, 1998). However, the great variability in healthy shoulder bone anatomy, together with the numerous small and unpredictable variations due to the rheumatoid state of the shoulders that we wish to segment, greatly complicate the successful application of shape models (Prescher, 2000, Von Schroeder et al., 2001).

We were inspired by curvature-based segmentation techniques that operate directly on 3-D surface meshes. For example, by adapting the morphological watershed to segment regions of similar surface curvature on 3-D meshes, object surfaces can be decomposed into meaningful regions (Mangan and Whitaker, 1999, Page et al., 2003). This generally works well for the segmentation of solid objects that give a sharp contour in the image data. However, for organic structures watershed techniques lead to less satisfactory results.

To the best of our knowledge no algorithm exists that can be used for the segmentation of severely deteriorated shoulder joints from CT data. The discussed techniques require extensive adaptation to be applicable to this difficult segmentation problem. Usage of these adapted techniques would require image processing expertise and therefore they cannot be included in day-to-day clinical workflow.

In this chapter we describe a new technique that exploits the spherical shape of the humeral head to automatically segment the rheumatoid joints. The centre of rotation of the glenohumeral joint can be determined by applying a Hough transform directly on the CT data, as described in (Van der Glas et al., 2002). In the pathological case, this spherical shape may have partially disappeared and often appears to be fused with the shoulder blade. However, the remaining curved shapes give an indication of where the joint gap is located. Our technique utilises this knowledge and, with a minimum of user interaction, segments highly pathological glenohumeral joints in less than two minutes.

The major contribution of our work is that we combine curvature information of surface data with path searching techniques on volumetric data. By combining these techniques, we retain fine details of the volumetric data, enabling this fast routine to result in accurate bone models. Concepts traditionally from visualisation are combined with concepts traditionally from image processing in order to solve a challenging segmentation problem. Expert orthopaedic surgeons stated that the segmentation process is sufficiently accurate and fast to be included in a clinical protocol, enabling
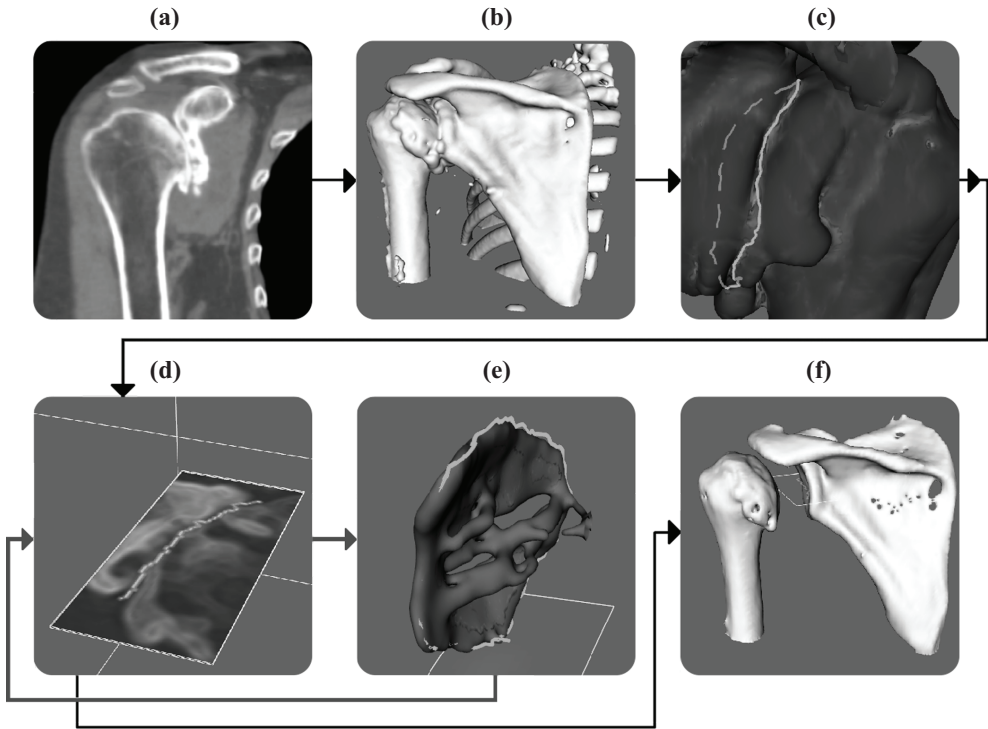
Figure 2.2: Overview of the stages of our segmentation method. (a) The input data. (b) The data after pre-processing, described in Section 2.2.1. (c) The joint separation loop, described in Section 2.2.2. (d) Slice-by-slice separation contours (Section 2.2.3). (e) The Hough feature volume (Section 2.2.4). (f) The final segmentation result, obtained after iteratively applying the slice-by-slice separation contours and the Hough feature volume (Section 2.2.5).

a wide variety of diagnosis and surgical planning purposes.

The remainder of this chapter is structured as follows: Section 2.2 presents the details of our new segmentation technique and section 2.3 documents the results of an evaluation we performed on ten pathological shoulder CT datasets. In Section 2.4 we present our conclusions and plans for future work.

2.2 Method description

The severity of rheumatoid arthritis can be represented by the widely accepted Larsen-score (Larsen, 1995). It is determined using radiographs and indicates how much bone damage has been done by the disease. A high Larsen score generally means that a corresponding CT-scan will be difficult to segment. We have developed our techniques for segmentation of the highest severity level (level 5) of this score. This level of the Larsen-score implies that the joint has deformed from its normal anatomical shape and the density of the bones is not uniformly distributed. In addition, holes are scattered over the articular surface of the bone. For many of the slices the joint space is not visible. These factors lead to a challenging segmentation problem.

Our segmentation technique consists of four stages (see Figure 2.2) of which the first stage is a preprocessing stage to counteract variability in the scan parameters and to alleviate noise. During the second stage a contour is determined that encircles the glenohumeral joint. The third stage connects the pairwise intersection points of this loop and the individual CT-slices. This temporary segmentation is refined during the fourth stage by creating a surface model of the connecting lines and applying a Hough transform to this model to determine how plausible the different parts of the segmentation are. The Hough transform allows us to improve the segmentation results at noisy parts of the CT-data, difficult to interpret due to the rheumatoid state of the joints.

2.2.1 Preprocessing

Clinical CT data is most often anisotropically sampled with the slice thickness being greater than the pixel size. To facilitate later processing steps, the data is isotropically resampled with trilinear interpolation, after which it is smoothed with a Gaussian filter with a standard deviation of 1.5 and radius of 2 voxels to counter noise. The window size is chosen so that the joint space is preserved after smoothing. The smoothed volume is used for the second stage of our approach that requires a volume with larger scale features. The unsmoothed isotropic volume that is used for the actual slice-by-slice segmentation should contain all details of the original volume. To enhance the edges of the volume, it is sharpened with the following voxel-wise operations: 1) The volume and its gradient magnitude are summed; 2) The gradient magnitude of this sum is subtracted from the volume.

The Hounsfield Scale is defined such that distilled water results in a Hounsfield Unit (HU) of 0, whereas air at Standard Temperature and Pressure results in a HU of -1000. With these standards cortical bone has a HU of 400 and rheumatoid bone has a HU of 200. Surrounding muscle tissues have a HU of 50. As a result of this, the
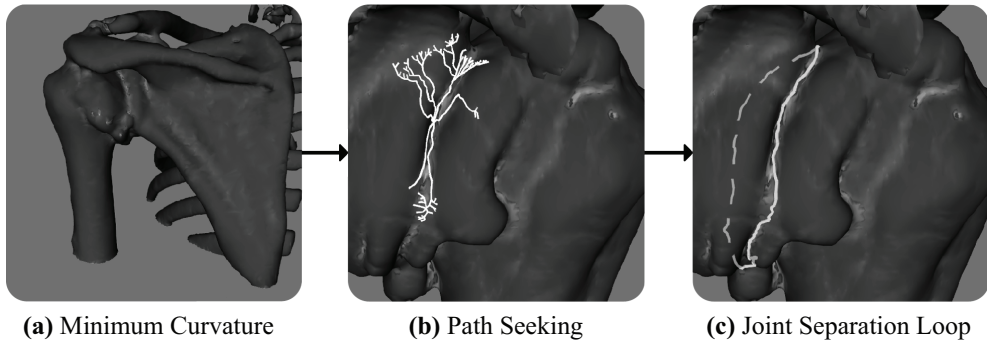
(a) Minimum Curvature   **(b)** Path Seeking   **(c)** Joint Separation Loop

Figure 2.3: Extraction of the joint separation loop. (a) First, the minimum curvature of the rough surface model is calculated. Areas with negative minimum curvature are highlighted. (b) The user selects a highlighted part of the surface model where the glenohumeral joint is located and this initiates a path searching algorithm. (c) The path seeking algorithm uses a cost function to encircle the glenohumeral joint and return this edge loop as output.

gradient magnitude of the pathological articular surface varies between 0 and 160.

2.2.2   Joint separation loop

We define the joint separation loop as the contour that encircles the fused humerus and scapula, running along the valley, an elongated surface depression, where the bones meet. The joint separation loop will be used in later stages to derive a surface that separates the humerus and scapula. In this section we document the determination of the joint separation loop. Figure 2.3 gives an overview of this stage.

To initiate this stage, the smoothed volume is converted to a coarse surface model of the bones using the Marching Cubes algorithm (Lorensen and Cline, 1987). Although healthy bone has a HU of approximately 400, experiments showed that a threshold value of 100 captures most of the bone geometry when it is in a pathological state.

Due to joint space narrowing the result is a single surface model that represents a fused scapula (i.e. shoulder blade) and humerus (i.e. upper arm). The different shapes of these bones result in a clearly visible valley between the scapula and the humerus that can be extracted by finding an edge loop that runs along vertices where the minimum curvature has a great magnitude.

In order to determine the required surface curvature, based on our triangular mesh, we have used the technique described by Page et al. (Page et al., 2002). Their

method determines the surface curvature at each vertex of a mesh as follows: First all triangles in a neighbourhood of configurable size around the vertex are extracted. Then the normals of these triangles are combined with an inverse distance weighted averaging to determine the normal at the vertex. Finally this central normal and the positions of the vertices of the surrounding triangles are used to derive a curvature tensor, of which the Eigen-analysis yields the principal curvatures at the central vertex.

To extract the joint separation loop, the user selects any part of the glenohumeral joint. The vertex closest to the point selected by the user acts as the seed for a surface constrained region growing method. The seed is the initial region. Neighbouring vertices, i.e. nodes, are iteratively added to the region until the joint is completely encircled.

At each iteration, a cost function is evaluated for every node neighbouring the current region:

$$C^L = \sum_{k=1}^{N} ||x_k - x_{k-1}|| \times (1 + ||\alpha||) \qquad (2.1)$$

The cost function is a modification of Dijkstra's shortest path algorithm which minimises the length of a path between two nodes (Dijkstra, 1959). Parameter x refers to the position of a node. Parameter α prevents sharp inflections in the different branches and is described below.

Because the glenohumeral joint is a ball and socket joint, we can safely state that the joint separation loop will be located roughly in a single plane. To determine whether the direction of a growing tip of the path deviates from the direction of its predecessors, we evaluate the angle between the vector perpendicular to the front half of its preceding segments and the vector perpendicular to all of its preceding segments. Figure 2.4 illustrates how this angle α is determined.

Because we are interested in the joint separation loop, the paths should specifically connect nodes that have a negative minimum curvature. Therefore, when the minimum curvature of a particular path is positive for three consecutive steps, it is assumed the path has left the joint gap. The path is then discontinued. The number of three was chosen so that occasional bumps in the surface do not restrain the algorithm from finding a solution, while paths do not continue to expand outside of the joint gap.

The expectation is that a path evolves in two directions from a starting point and will eventually encircle the joint. In other words, the two tips of the path should meet each other. At each iteration, we check whether a newly added node neighbours any
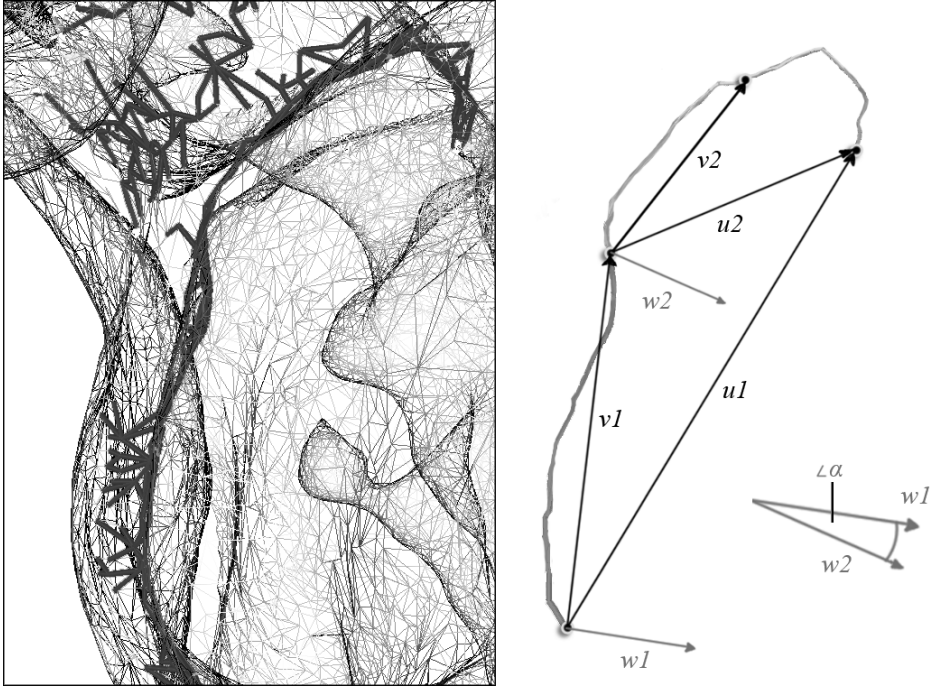
Figure 2.4: Parameter α of equation 2.1. The angle in radians is calculated between the vector perpendicular to the front half of the preceding segments and the vector perpendicular to all of the preceding segments. The vectors $\vec{w}1$ and $\vec{w}2$ are directed perpendicular to $\vec{v}1$, $\vec{u}1$ and $\vec{v}2$, $\vec{u}2$ respectively. If the path takes sharp turns, the value of α will increase, thus increasing the total cost of the path. This prevents sharp inflections.

other part of the path. If so, this could indicate a successful encirclement. Two further conditions have to be satisfied:

1. The two tips have to run in opposite directions when they meet. This is the case if the dot product of their respective directions is negative.

2. The total path has to form a closed loop. This is the case if the accumulated path normal is close to 0. The accumulated path normal is defined as the sum of all surface normals crossed by the path, each scaled by the inverse of the sum of the edges before and after the vertex that it is defined on.

When the algorithm terminates, the result is a closed loop that encircles the gleno-humeral joint. We refer to this loop as the joint separation loop.

2.2.3 Slice-by-slice separation contour

In this stage the joint separation loop is used to derive, for each slice of the unsmoothed isotropic volume (see Section 2.2.1 Preprocessing), a 2-D contour separating humerus and scapula. Together, these contours will form a surface that separates the humerus and scapula in 3-D. On each slice, the two intersection points of the joint separation loop with that slice serve as the end-points of the 2-D separation contour.

In the case of a healthy joint, the humerus and scapula would be separated by a region of low intensity voxels. In our case, the more dense outer layers of the humerus and scapula are pressed together, resulting in a transition region of more or less consistent, but not necessarily low, density. The 2-D separation contour attempts to connect its endpoints whilst remaining within this transition region and crossing pixels of similar values to the values of the endpoints.

To connect a pair of endpoints a path seeking algorithm is used. The cost function attempts to minimise the variation between consecutive pixels in the path. In our data, bone has a HU of at least 100, while soft tissue surrounding the bone has a range somewhere around 0 HU. To capture this variation, we determine the absolute difference between the HU of a pixel and the HU of its predecessing pixel, divided by 100 and clipped to [0.0, 1.0]. These last two steps are required to control the influence of the variation within the cost function, relative to the additional parameter that is introduced in Section 2.2.5.

The cost function is defined as:

$$C^H = \sum_{k=1}^{N} \min(1, \frac{||H_k - H_{k-1}||}{100})$$

(2.2)

where H is the HU of a pixel. From both points a path evolves that minimises the cost function. When the two paths find each other, the path seeking algorithm terminates and re-initialises for the point pair of the next slice.

It is highly unlikely that the segmentation is correct after the initial pass, because the pathological state of the shoulder allows the paths to run through cortical bone, the thin outer layer of bone that normally has a high density and strength. However, even an erroneous segmentation provides a useful basis for the subsequent refinement stage.

2.2.4 Hough feature volume

In this stage the 2-D separation contours are used to derive a feature volume, based on the Hough-transform, that will be used in the subsequent stage to extract a surface
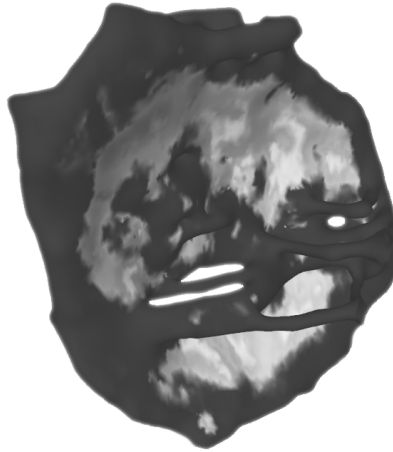
Figure 2.5: Surface model of the stacked 2-D separation contours. Highlighted areas indicate a high confidence value γ, further explained in Section 2.2.4.

that accurately separates the humerus and the scapula.

An encapsulating surface is constructed of the rasterised separation contours (see Figure 2.5). The surface is Laplacian smoothed with 20 iterations. This method yields suitable surface normals for further analysis. In spite of this, it would be interesting to investigate alternative volume-preserving smoothing methods in the future, such as those proposed by Taubin and Vollmer et al. (Taubin, 1995, Vollmer et al., 1999).

We apply a Hough transform to the smoothed surface (Duda and Hart, 1972). For each point on the smoothed surface we follow its extended normal through an empty volume, rasterising it using Bresenham's algorithm (Bresenham, 1965). The result is a volume where each voxel contains a scalar equal to the number of times that an extended surface normal of the smoothed surface has intersected that particular voxel. Due to the sphericity of the humeral head and hence the smoothed surface, the area under the centre of the head contains consistently higher values.

Again, for each point on the smoothed surface we follow its extended normal through the Hough volume and determine the position of the voxel that contains the highest number of intersections. This position is referred to as the point origin of the surface point that it corresponds with. The confidence value γ of a surface point is defined as the ratio between the Hough value at its point origin and the maximal value of the Hough volume. In other words, if a point origin is located at a globally high Hough value, it is likely that the surface point is located within the joint space

(a) Hough Volume   *(b) CT slice*   *(c) Confidence γ*   *(d) Agreement λ*
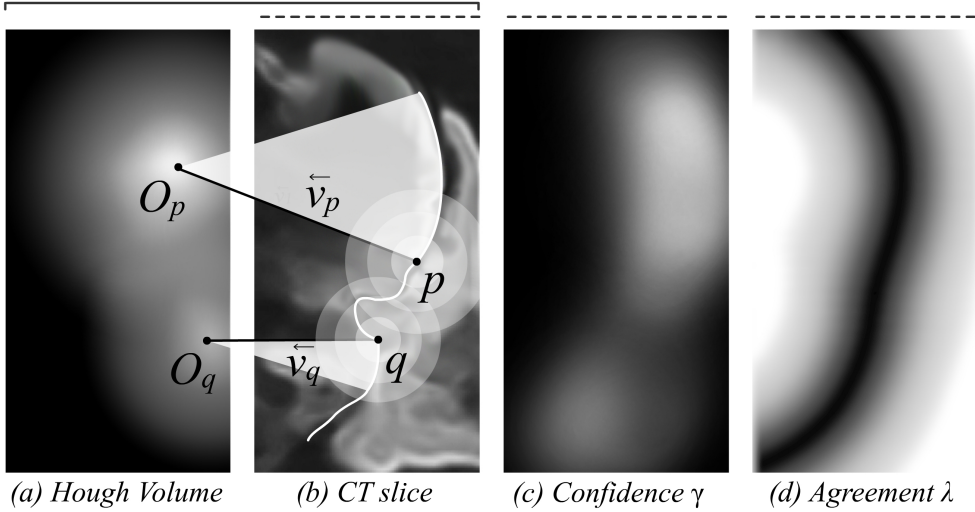
Figure 2.6: (a) The Hough volume is determined by applying a Hough transform to the surface formed by the slice-by-slice separation contours. (b) For each point on this surface a point origin O is determined, together with a vector $\vec{v}$ pointing to this point. (c) Confidence γ is a fraction of the Hough value of the surface point's point origin, relative to the maximum value in the Hough volume. The values of O, $\vec{v}$ and γ are 3D-splatted across the surface using Gaussian kernels. For all voxels we determine the distance to their 3D-splatted point origins. (d) The agreement λ is the extent to which this distance and the length of the 3D-splatted vector $\vec{v}$ correspond with one another.

and therefore we assign a high confidence. For each smoothed surface point, the point origin, the vector to the point origin and the confidence are stored.

The smoothed surface is voxelised using 3-D splatting: For each surface point, a Gaussian kernel (standard deviation 1.5, radius 5 voxels), weighted by the confidence γ for the point, is centred on the closest voxel position for that point. The point's stored information is additively spread to surrounding voxels via the confidence weighted kernel. After all surface points have been traversed, the voxelisation is normalised with the per-voxel accumulated confidence. The per-voxel accumulated confidence is separately normalised by the maximum per-voxel accumulated confidence.

For every voxel an agreement value λ is determined, defined as the extent to which the voxel location is in agreement with the Hough surface determined by the neighbouring voxels (see Figure 2.6).

2.2.5 Iterative refinement

In this step, the slice-by-slice separation contours are iteratively recalculated in accordance with the Hough feature volume. The resulting slice-by-slice separation contours form the final segmentation.

As shown in Figure 2.2, after their initial execution, stages 2.2.2 Joint Separation Loop and 2.2.3 Slice-by-slice Separation Contour are repeated until a sufficiently accurate set of separation contours are produced. With each iteration, new contours are calculated based on the Hough feature volume of the previous iteration, and based on these a new Hough feature volume is derived. The cost function C^T, shown in equation 2.3 and used in all repeated iterations is a modified version of the cost function C^H used in the initial iteration. Whereas C^H takes into account only the variations in volume intensity along the contour, C^T takes into account the agreement value λ described in Section 2.2.4 as well.

$$C^T = \sum_{k=1}^{N} \gamma_k \times \lambda_k + (1 - \gamma_k) \times \min(1, \frac{||H_k - H_{k-1}||}{100}) \tag{2.3}$$

More specifically, if confidence γ is low, i.e. a point is not close to the Hough surface, its cost is primarily determined by its intensity variation. However, if confidence γ is high, i.e. the point is close to the Hough surface, the agreement λ of a point contributes more heavily to the cost: High agreement leads to low cost and vice versa. With this, we ensure that contours run through surface points that are located close to the Hough surface and are in agreement with their neighbours as to the location of that surface.

The algorithm is iterated until convergence. The criterion for this is that two consecutive steps produce the same segmentation result. Inspection showed that for most of the datasets four iterations of the algorithm are sufficient for convergence. After the last iteration the joint separation lines are used to separate the two bones and create two distinct volume masks.

2.2.6 Evaluation

We have evaluated our technique on ten shoulder CT-datasets. The datasets we used for testing were acquired from the hospital PACS and were performed over a period as part of the standard treatment workflow. As such, CT parameters vary (see Table 2.1). All shoulders were diagnosed by an orthopaedic surgeon and rated as the highest level (level 5) of rheumatoid arthritis using the Larsen-score.
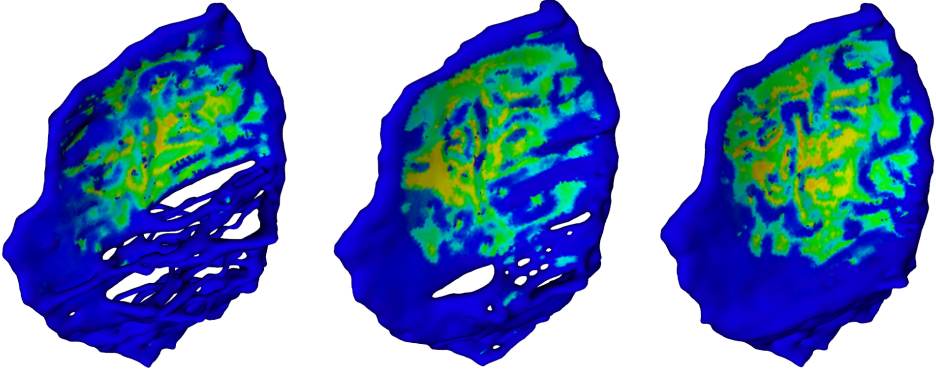
Figure 2.7: Three iterations of the segmentation algorithm. The colour mapping equals that of Figure 2.5. With each iteration, the smoothly curved surfaces influence the cost-function of neighbouring areas by evaluating whether a separation contour is in agreement with nearby parts of the Hough surface.

Table 2.1: Scan parameters of the evaluation scans.

Dataset	X-Ray Tube Current	Exposure Time	Spatial Resolution
1	120	1000	$0.900 \times 0.900 \times 1.000$
2	160	500	$0.900 \times 0.900 \times 1.000$
3	160	600	$0.858 \times 0.858 \times 1.000$
4	339	500	$0.970 \times 0.970 \times 1.000$
5	500	500	$0.488 \times 0.488 \times 1.000$
6	339	500	$0.970 \times 0.970 \times 1.000$
7	376	500	$0.885 \times 0.885 \times 2.000$
8	70	500	$0.412 \times 0.412 \times 1.000$
9	410	500	$0.934 \times 0.934 \times 2.000$
10	158	500	$0.919 \times 0.919 \times 1.000$

2.3 Results

To determine the accuracy of the algorithm, we compared the resulting segmented voxel masks with voxel masks that were obtained with manual segmentation. The voxel masks consisted of separate humeral (upper-arm bone) and scapular (shoulder blade) volumes. Manual segmentation was performed by an expert orthopaedic surgeon. We extracted a volume of interest which contained the glenohumeral joint plus an additional 10% of its size in all directions.

Table 2.2: Validation results of 10 shoulder CT datasets. The first column shows the id of the CT dataset. The second column shows the Dice coefficient of the voxel mask as created by manual segmentations and as created by our technique. Column three shows the Hausdorff distances.

Humerus		
Dataset	Dice coefficient [%]	Hausdorff distance [mm]
1	98.88	1.84
2	98.59	2.45
3	98.99	3.17
4	99.13	2.45
5	94.28	5.59
6	94.8	3.04
7	93.93	5.55
8	99.58	3.07
9	99.53	1.69
10	99.04	3.67

Scapula		
Dataset	Dice coefficient [%]	Hausdorff distance [mm]
1	98.28	2.11
2	98.6	4.52
3	99.18	9.28
4	98.34	1.52
5	98.47	4.75
6	97.05	2.97
7	97.84	4.83
8	99.53	9.19
9	99.53	1.26
10	99.25	3.30

For quantitative evaluation we calculated the Dice coefficient between all manual segmentations and the segmentations derived by our technique. The Dice coefficient P_{vo}, expressed as a percentage for convenience, is defined as follows:

$$P_{vo} = \frac{2 \times |S \cap R|}{|S| + |R|} \times 100\% \qquad (2.4)$$

where S and R refer to the two segmented volumes that are being compared. A voxel-perfect segmentation results in a Dice coefficient of 100%.

Table 2.2 shows the Dice coefficient for all datasets for both the scapula and the humerus. For the humerus, the median Dice coefficient was 98.9% with an interquartile range (IQR) of 95.8% to 99.4%. For the scapula, the median Dice coefficient was 98.5% with an IQR of 98.3% to 99.2%.

The extent of the volumes was limited to the volume of interest as used for the segmentation steps, i.e. the joint gap. This entails that a small segmentation error will have a significant effect on the Dice coefficient. However, because we also wanted to have a qualitative measure independent of the size of the volume masks, we calculated the Hausdorff distances using Mesh 1.13 (Aspert et al., 2002). The Hausdorff distance is the maximum distance of a volume to the nearest point in the other volume and thus reflects the largest segmentation error. As a frame of reference, please note that the average diameter of proximal humeri is approximately 46 mm (Boileau and Walch, 1997). For the humerus, the median Hausdorff distance was 3.06 mm with an IQR of 2.30 mm to 4.14 mm. For the scapula, the median Hausdorff distance was 3.92 mm with an IQR of 1.96 mm to 5.92 mm. The Hausdorff distances were added to Table 2.2.

The results of an evaluation dataset together with its manual segmentation can be seen in Figure 2.8. The Dice coefficients for the initial segmentation and three iterations are 56.32%, 84.12%, 97.30% and 98.88% for the humerus model and 69.02%, 87.99%, 96.78% and 98.28% for the scapula model. These are typical increments of accuracy that we see for other datasets.

In all cases, the complete segmentation process completed in under two minutes on a 2 GHz Core T2500 laptop processor. The time needed to find the joint separation loop ranged from about five to about ten seconds.

2.4 Discussion

2.4.1 Limitations

For datasets 5 and 7 the humerus volume mask differed considerably from the ground truth segmentation. Also, the Hausdorff distances of the scapulae of datasets 3 and 8 were relatively large. Upon closer inspection we noticed that osteophytes, i.e. bone deformations, at the edge of the glenohumeral joint had been included in the automatically segmented volumes, while they had been excluded from the manual segmentations. Because the density of these osteophytes varies heavily, subtle segmentation differences may influence whether an osteophyte is included in the segmented volume. A possible improvement would be to highlight the osteophytes and allow the user to explicitly make these segmentation decisions.
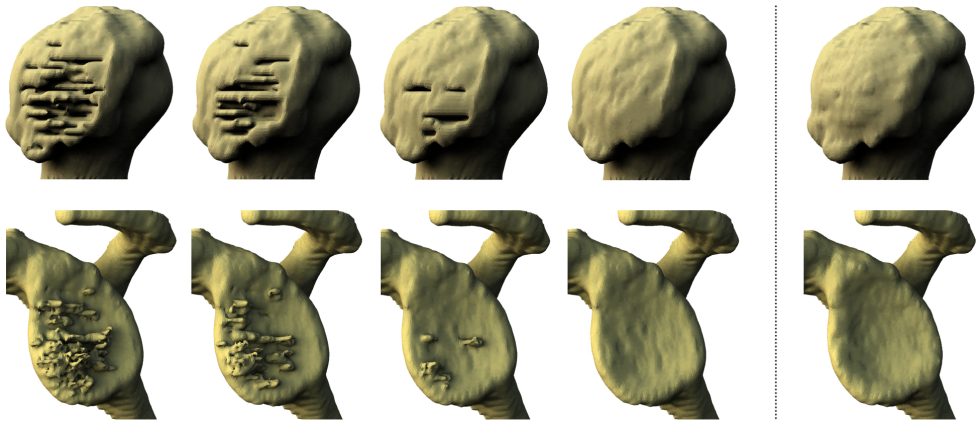
Figure 2.8: The scapula and humerus model of an evaluation dataset after the initial slice-by-slice segmentation and three subsequent iterations. The most right image shows the manual segmentation that was used to evaluate the quality of our segmentation.

Figure 2.8 and the corresponding Dice coefficients point out that the segmentation quality improves considerably during the first iterations. A side effect of our approach is that when slice-by-slice separation contours of adjacent slices follow a smooth curve, the Hough feature volume will pick up this smooth area and force the slice-by-slice separation contours in subsequent iterations in the same erroneous direction, never improving the segmentation quality for these specific parts. In general, the erroneous parts of the slice-by-slice separation contours do not follow smooth curves, because they run through the pathological bone area rather than through the joint space. Consequently, this distortion has limited effect on the segmentation accuracy of our approach, as shown by the evaluation results.

The criterions used for determining and closing the joint separation loop perform very well for the evaluation datasets. It is conceivable that one of the criterions is not met, although we have not experienced this for any of the 10 evaluation datasets. In this case, no joint separation loop will be returned and the surgeon has to reselect the joint to retry. As demonstrated by Chambers et al. the complexity of finding the shortest separating loop is a NP-hard problem (Chambers et al., 2008). The criterions we use to find the joint separation loop (i.e. evaluation of the minimum curvature of the surface and prevention of sharp inflections) are useful exploits, reducing this problem to a routine that, at least for the 10 evaluation datasets we used, returns a joint separation loop within ten seconds. One can think of ways to improve this algorithm, for example by using more selection points, adding to the robustness of

the algorithm.

Another limitation of this study that the quality of the evaluation data differed due to the varying acquisition parameters and subject variability. For example, the contralateral shoulder of subject 6 contained a prosthesis, producing scattering effects in the CT-scan. Although the visible scatter in the segmented shoulder was limited, this additional noise may affect the segmentation routine. A future phantom study would be interesting to systematically assess the sensitivity of our algorithm to noise. However, the large variation in our data suggests that the technique is relatively robust and thus applicable to CT scans with different noise levels.

2.4.2   Conclusion

In this chapter we have presented a novel segmentation technique that combines surface and volume processing to provide fast and accurate segmentation of arthritic glenohumeral joints from CT data. From the evaluation we conclude that our technique is sufficiently accurate for the segmentation of heavily deteriorated glenohumeral joints.

The segmentation results of our data collection of ten shoulders were compared to the manual segmentation as performed by an expert surgeon. The Dice coefficients and Hausdorff distances indicate that our technique yields highly accurate results compared to manual segmentation. Our technique was sufficiently robust to extract accurate segmentations from the datasets in spite of their pathological nature, as indicated by the Larsen-score level 5, the varying bone density and small joint space, and in spite of varying acquisition parameters.

To our knowledge, no other segmentation techniques exist that have been shown to cope with arthritic shoulder joints. As discussed in the introduction, Botha has shown that level-sets and watershed segmentation have limited success, in the course of which setting the parameters is a time-consuming process not suitable for clinical practise (Botha, 2005). Although Zoroofi et al. successfully segmented arthritic hip joints, they were less successful for arthritic hips with Larsen-score 4 and 5 (Zoroofi et al., 2003). The lack of fast segmentation techniques capable of segmenting arthritic shoulder joints was our motivation for the research described in this work. The technique is currently applied to a pre-operative planning application used in our clinic and will serve as a basis for surface-based orthopaedic applications that involve arthritic shoulder joints. The high accuracy together with the short time required for the segmentation process make this technique a good approach for the segmentation of glenohumeral joints in a clinical environment.

In future work we will test algorithm performance on other pathological joints, such as the hip and knee joint. Because these joints normally have a highly curved

surface like the glenohumeral joint, we expect that the algorithm may also work on these joints.

3

Interactive simulation and comparative visualisation of the bone-determined range of motion of the human shoulder

Peter R. Krekel[1],[2], Charl P. Botha[2], Paul W. de Bruin[1],
Edward R. Valstar[1], Piet M. Rozing[1], Frits H. Post[2]

[1]*Department of Orthopaedics, Leiden University Medical Centre*
[2]*Visualisation Group, Delft University of Technology*

Abstract

Pre-operative planning systems aid clinicians by giving insight into patient-specific issues before surgery is performed. The ability to perform a virtual shoulder replacement procedure enables the surgeon to explore the probable and plausible outcomes. Pre-operative planning software assists the surgeon in this complex decision-making process.

In our prototype pre-operative planning system for shoulder replacement, we create patient-specific bone-determined range of motion predictions based on collision detection using segmented CT-data. The gleno-humeral range of motion is visualised with motion envelopes, that indicate the maximum range of motion of the humerus in every direction. The prosthesis placement parameters can be adjusted interactively in our simulator, during which a novel visualisation technique depicts the differences between the current and previous range of motion.

In this chapter we present a fast and efficient method for highly interactive visualisation of collision detection based range of motion for the gleno-humeral joint. We are able to show in real-time the consequences of adjustments made to a planned shoulder prosthesis alignment by using geometry clipping-based optimisation, as well as precalculation and interpolation techniques.

3.1 Introduction

Osteoarthritis and rheumatoid arthritis, the two most common forms of arthritis, can lead to severe joint damage. The resulting pain and limited joint motion significantly restrict the patient in performing daily activities. In such cases, a joint replacement, i.e. a surgical procedure where parts of the joint are replaced with artificial components, may be indicated. A successful joint replacement leads to pain relief and improved joint mobility.

Replacement operations have a high success rate in the case of the hip or the knee joint. In the case of the shoulder, however, the procedure is often successful with regard to pain relief, but far less successful with regards to post-operative joint mobility or the durability of the implant. The extra complicating factors are the higher complexity of the shoulder joint and the limited field of view during surgery. Our primary motivation for developing a pre-operative planning system is to assist surgeons in performing the difficult shoulder replacement operation, and thereby helping to improve the success rate.

In a total shoulder replacement, the humeral head and the glenoid fossa are replaced with artificial components, as shown in Figure 3.1. The standard technique for planning a shoulder replacement is template-over-x-ray planning, which involves overlaying several transparent templates of different prostheses on radiographs of the shoulder to determine an appropriate prosthesis. However, the radiographs lack spatial information along the view direction, leading to visual ambiguities that complicate the planning. Our prototype shoulder replacement pre-operative planning system improves on this by allowing the surgeon to simulate the surgery in 3-D. Patient-specific information is extracted from a pre-operative CT scan. During the simulation, the system gives feedback on the surgeon's virtual surgery with regards to the predicted outcome of the operation.

An important aspect of this feedback is the interactive simulation and visualisation of the post-operative bone-determined range of motion (ROM) of the patient's shoulder. This functionality allows the surgeon to experiment with different prosthesis implantation possibilities and see, in real-time, what the effect of the changes would be on the post-operative bone-determined ROM. The interactive patient-specific ROM simulation and visualisation is the main subject and contribution of this chapter.

The remainder of this chapter is organised as follows: In section 2 we discuss existing work in the area of pre-operative arthroplasty simulation. Section 3 describes the simulation of bone-determined ROM for the gleno-humeral joint, followed by section 4 where visualisation of ROM envelopes and comparative ROM visualisation is discussed. In section 5 we explain the techniques we apply to enable fast updates of the comparative ROM visualisation, which greatly improves the interactivity of
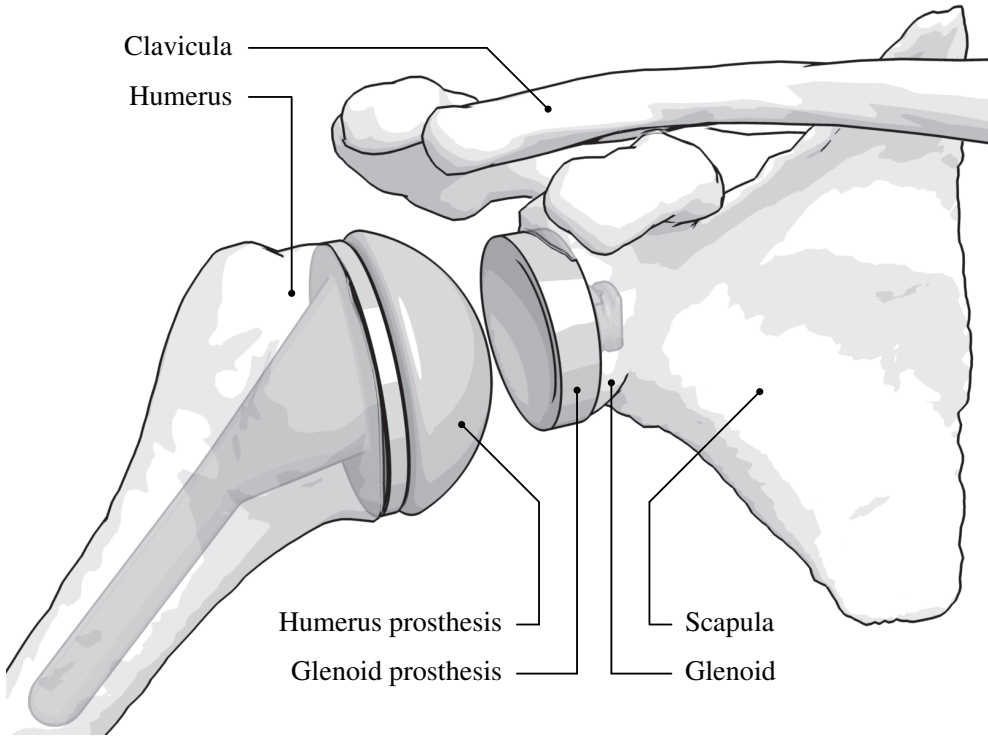
Figure 3.1: Illustration of a shoulder joint after total shoulder replacement.

our simulator. We present our results in section 6, followed by our conclusions and discussion of future work in section 7.

3.2 Related Work

A wide range of pre-operative planning systems exist, for example Hip-Op (Lattanzi et al., 2002), HipNav (Simon et al., 1997) and BrainLAB's VectorVision[1]. However, to our knowledge no such specific planning system for the shoulder joint is available at this time. Probable factors here are the complexity and the relatively lower number of replacements of the shoulder joint.

Some research has been done on pre-operative ROM estimation for the hip joint. Jamaraz et al. use analytical modelling of the properties of implants to estimate both the ROM and the chance of dislocation, with bony impingement hardly playing a

---

[1]http://www.brainlab.com/

part (Jaramaz et al., 1997). The approach of Richolt et al. resembles our approach more closely, by applying collision detection to the 3D problem of bony impingement (Richolt et al., 1998). Their system is designed for osteotomy rather than joint replacement and only determines ROM for joint rotation along a single user-defined axis.

The goal of the Comprehensive Human Animation Resource Model (CHARM) project was "modelling a 3D solid human body part with its interior details and having physically based simulation of movements and deformations" (Maurel et al., 2002). The emphasis of this project was on animation, rather than patient-specific ROM prediction (Maurel, 1999).

Lastly, the Delft Shoulder and Elbow Model (DSEM) is a complete musculoskeletal model of the shoulder and elbow joint that mainly focuses on muscle function and the involved forces and energy (Van der Helm, 1994). However, the DSEM is not patient-specific and therefore not yet usable for pre-operative planning.

3.3   ROM simulation

In order to calculate the ROM using a segmented CT dataset, we implemented a simplified bio-mechanical model of the gleno-humeral joint. A generally accepted hypothesis is that the gleno-humeral joint can be approximated by a ball-joint (Meskers et al., 1998, Van der Glas et al., 2002). We combined this model with collision-detection on surface models of the skeletal structures in the patient's shoulder.

The surface models are extracted from CT data using the segmentation techniques described in chapter 2. With this approach, it is possible to extract accurate and topologically correct surfaces describing the skeletal structures of the shoulder from CT data. The techniques are also able to cope with arthritic shoulders where joint space narrowing has occurred or the bone density has been affected. Conventional techniques, such as double thresholding followed by region growing, do not work in such cases. Shoulder replacement patients often suffer from both these symptoms.

During interactive simulation, we do not take into account rotation around the medial axis of the humerus, i.e. endo/exorotation, thereby reducing the number of degrees of freedom from three to two and greatly speeding up the simulation. This is a reasonable simplification for the following reasons:

- For a healthy joint, the amount of ROM gained as a result of endorotation and exorotation is only discernible in the upper extremes of the gleno-humeral joint. During abductive arm movements, exorotation of the humerus is a common response to be able to reach higher, though most of that particular ROM increase is coming from the scapulo-thoracic joint.
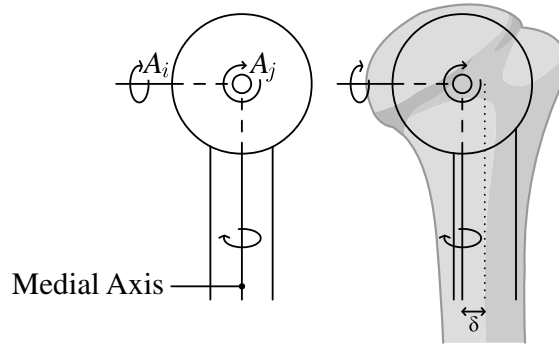
Figure 3.2: A schematic representation of the humerus and its rotational axes. As can be seen in this image, the additional ROM as the result of endo/exorotation is related to δ, the distance between the medial axis of the humerus and the vertical axis through the centre of rotation.

- The maximum achievable ROM increase due to exorotation is relatively small. It is related to the offset of the medial axis of the humerus in relation to the centre of rotation, as can be seen in Figure 3.2.

- Our simulation gives a conservative estimate of the shoulder ROM.

For testing purposes, we have included functionality in our simulator to determine and visualise the extra ROM gained by a single, adjustable exorotation angle. This enabled us to confirm the above-stated assumptions.

The centre of rotation of the gleno-humeral joint is defined by the diameter of the humeral prosthesis, which has a spherical head. Therefore, adjustments made to the prosthesis also affect the centre of rotation. For initial placement of the humeral prosthesis, we have implemented a sphere-fitting method. This entails that a sphere is fit over the humeral head to approximate the ideal centre of rotation, while continuously giving feedback on how much of the sphere surface is near or touching the humerus surface.

Additionally, our simulator is capable of handling hemi-prostheses, which is a prosthesis without a glenoid component, and reversed prostheses, where the spherical component is placed at the glenoid. For the latter, the centre of rotation is situated more inward.

For all prostheses, the ROM envelopes are constructed in the following way. The humerus is aligned with an initial orientation, which will be the starting alignment for all iterations. The simulation consists of two nested iterations. During the outer iteration, the humerus is rotated around the axis marked with A_i in Figure 3.2. Note

that axis A_j rotates along with A_i. At each rotation, the maximum possible orientation of the humerus around axis A_j is found by making use of a binary search. By repeatedly dividing the search interval in half, our ROM determination executes in $O(\log n)$, where n relates to the effective resolution of the end result of the binary search. Whenever colliding polygons are detected, we reverse the search direction. After an evaluation of available collision detection libraries we selected the Optimised Collision Detection library, or OPCODE (Krekel, 2005, Terdiman, 2001). OPCODE is a fast and accurate collision detection library based on memory-optimised bounding-volume hierarchies and most suitable for our particular problem domain. The pseudo-code version of the ROM determination procedure can be seen in Algorithm 3.1. The algorithm is also explained in Figure 3.3. For every change in the planning, the complete ROM has to be recalculated.

For hemi-prostheses an extra step is required. The humeral head should make contact with the glenoid at all times. Therefore, the humerus has an additional binary search iterator for a translational component as well, rather than just for the rotational extremes. This is not necessary for total shoulder prostheses, as we are targeting conformal prostheses, where the diameters of the glenoid and humerus components are equal. However, using the hemi-prosthesis modelling functionality, our system should be able to simulate non-conformal prostheses as well.

3.4 Visualisation

Once all directions of our ROM envelope have been probed for their maximum angles, we can begin constructing the ROM visualisation. We draw lines between the centre of rotation and an arbitrary point within the end of the shaft of the humerus, and then transform these lines according to their respective maximum angles. The resulting envelope is shown in Figure 3.4.

For each change made to the virtual prosthesis placement by the surgeon, a new ROM envelope is calculated. This enables the surgeon to visualise directly the complete shoulder ROM for a particular set of operational parameters. Being able to see the envelope update in real-time as changes are being made, helps the surgeon to investigate the effect of even small changes to the planned operation.

Several parameters that define the placement of the humerus prosthesis can be adjusted during the interaction. First of all, the cutting plane at the humeral head can be translated along its normal, as well as rotated around two axes perpendicular to the normal. Also, the position of the humerus prosthesis relative to the humerus can have a small offset in any direction within the cutting plane. These adjustments are also illustrated in Figure 3.6.
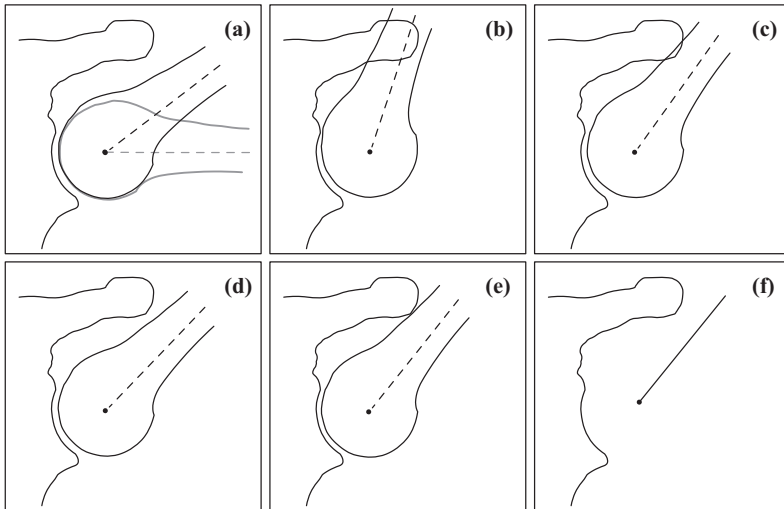
Figure 3.3: Binary search algorithm for one line of the ROM envelope. The horizontal humerus (a) represents the initial orientation. At each iteration, the increment is added to the previous angle (a, d, e) and halved. If colliding polygons are detected, the increment is preceded by a negation (b, c). If the increment is smaller than a certain threshold, the line is added to the envelope (f).
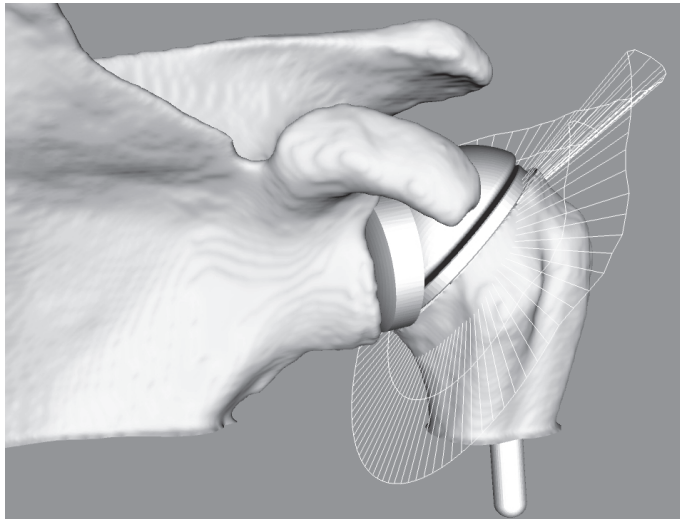

Figure 3.4: The visualisation of ROM by means of envelopes.

Algorithm 3.1 The ROM determination algorithm.

---

  function DetermineROM(resolution, angle, angle_increment)
  $i \leftarrow 0$
  while $i < 360$ **do**
    t_angle ← *angle*
    t_angle_increment ← *angle_increment*
    while (abs(*t_angle_increment*)$> e$) **do**   *// e is a threshold for t_angle_increment*
      SetOrientation(0,0,0)   *// Set the humerus to an initial orientation*
      RotateZ((*i/resolution*) * 360)
      RotateY(*t_angle*)
      RotateZ(-(*i/resolution*) * 360)
      if CDQuery()> 0 **then**   *// There are colliding polygons*
        t_angle_increment ← -abs(*t_angle_increment*) *// Make the increment negative*
      else
        t_angle_increment ← abs(*t_angle_increment*)   *// Make the increment positive*
      end if
      t_angle_increment ← *t_angle_increment* $\times 0.5$ *// Cut increment in half*
      t_angle ← *t_angle*+*t_angle_increment* *// Add the increment to the previous angle*
    end while
    AddToArray(*t_angle*)
    $i \leftarrow i + 360/resolution$ *// Proceed to the next direction*
  end while

The ROM determination algorithm. The auxiliary function *CDQuery* returns the number of colliding polygons. The parameters *resolution*, *angle* and *angle_increment* are adjustable and define the number of envelope lines, the initial angle we use for our simulation and the increment we add to the previous angle at each iteration, respectively. Also, the search range depends on these three parameters.

Placement of the glenoid prosthesis is performed according to a method described by Botha (Botha, 2005). It is quite strictly constrained by the quality and the geometry of the scapula. Therefore, we focused on the alignment of the humeral prosthesis.

In order to facilitate this important investigation of the increase or decrease in ROM that results from a particular change in the planning, we have implemented comparative visualisation functionality whereby the difference between two ROM envelopes can be explicitly visualised. The comparative visualisation is also updated in real-time as the surgeon interacts with the planning.

For two consecutive envelopes we depict improvements and deteriorations by connecting the lines with colored polygons. A red polygon denotes that the most recent envelope has a more limited ROM in that particular direction than the reference envelope, while a green polygon states the opposite. Additionally, the end points of the
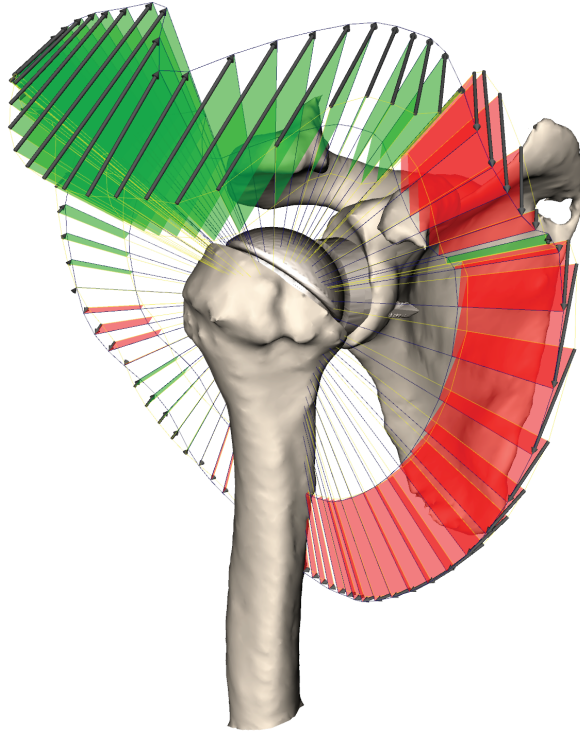
Figure 3.5: Comparative visualisation of two ROM envelopes. The first envelope is a previously determined ROM which was set as a reference envelope by the user. The second envelope is continuously updated for every adjustment applied to the prosthesis placement parameters.

lines are connected with arrows, pointing towards the most recent envelope. The resulting visualisation is shown in Figure 3.5. The reference envelope can be set to the current or any previously determined ROM envelope at all times.

3.5 Optimisation

To support the interactive usage of our system, we focused on decreasing the time required to display consecutive ROM envelopes during prosthesis placement adjustments. We have implemented two kinds of optimisations. Only one optimisation should be picked, depending on the intentions of the user. The first optimisation is based on precalculation and aims at a thorough exploration of the ROM for a single
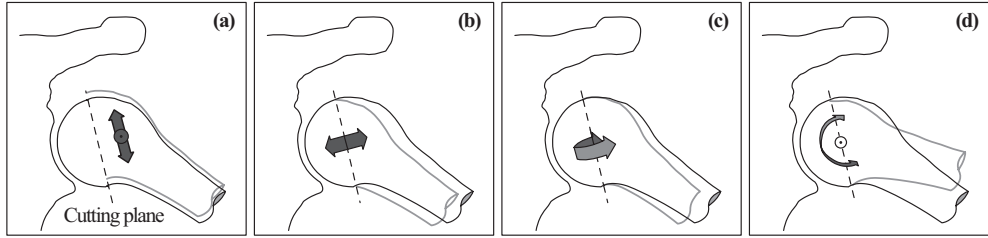
Figure 3.6: These are the possible placement adjustments, that are also systematically modified during precalculation. In (a) we see the humerus, which can be translated along the cutting plane. In (b) it is translated along the normal of the cutting plane. In (c) and (d) we see the two axes used for orientation changes. Note that all adjustments are applied to the humerus only, thereby changing its position relative to the prosthesis.

prosthesis. The second optimisation is based on geometry clipping and more suitable for comparison of the ROM of different prosthesis types. When no time is available for precalculation, this optimisation should be selected.

We describe both these optimisation methods in the following two subsections. In section 3.6, we show the results of performance and accuracy measurements on our simulator with and without optimisation.

3.5.1 Precalculation and interpolation

To ensure a satisfactory frame-rate, we optimised the simulation through precalculation and interpolation techniques. During the initialisation phase, a variable number of ROM envelopes are pre-calculated. Depending on the resolution and ranges, this number can vary from 400 to as much as 2000. For a single orientation of the humerus prosthesis, we start by pre-calculating envelopes for translational adjustments along the cutting plane (see Figure 3.6a). This is then repeated for translational adjustments along the normal of the cutting plane (Figure 3.6b). Finally, the previous two steps are repeated for variations of the prosthesis orientation (Figure 3.6c and d).

Now that we have completed the precalculation step we can interpolate the ROM predictions at a high frame-rate, with only little accuracy loss. When the CPU is idle, the accurate ROM envelope can be calculated and replace the interpolated envelope with a smooth transition.

The drawback of this approach is that the pre-calculations only hold for a single type and size of a prosthesis. When the surgeon wants to compare the ROM of various

prostheses for a particular dataset, precalculation will have to be done for each of those prostheses.

3.5.2 Collision Clipping

For the concept of collision clipping, we differentiate between placement adjustments that require geometry adaptation (GA) and those that do not. Geometry adaptation is necessary for prosthesis placement adjustments that redefine the cutting plane, relative to the humerus (see Figure 3.6b, c & d).

A problem with geometry adaptation is that the bounding boxes hierarchy, which is used by the collision detection library, becomes outdated and needs to be rebuilt. This can take up to 3 seconds for high-density models, slowing down the simulation unacceptably.

Instead of performing collision detection queries on the clipped model of the humerus, we use the unclipped model. Thus, our collision detection queries may return collisions of polygons that would normally have been clipped. By adding an additional query to the algorithm, we can find out on which side of the cutting plane the colliding polygons are located. If they are on the same side of the cutting plane as the prosthesis, the collisions are ignored. Otherwise, the algorithm can terminate, since we only need one admissible collision to identify an unacceptable humerus alignment.

Another slow down is caused by the clipping of the humerus model itself. Because we have now separated the graphical representation from the collision detection algorithm, the humerus model does not necessarily have to be clipped, other than for graphical representation purposes. Therefore, we use a much faster graphics hardware geometry cutting plane instead of an accurate clipping algorithm.

3.6 Results

So far, the prototype system we developed has been tested on two in-vivo shoulder CT datasets of patients requiring total shoulder replacements, with more tests being planned. However, due to the consistent results generated by the specialised segmentation techniques, we do not expect much deviation from these results for other datasets.

An orthopaedic surgeon used our simulator and these datasets for prosthesis placement analysis and stated that the presented ROM estimations correlated with anticipated behaviour. We received positive feedback on the interactively updated comparative visualisations, which was experienced as both fast and intuitive.

Table 3.1: Speed of simulation and rendering in updates per second. *no-opt*, *coll-clip* and *interp* are short for "no optimisation", "collision clipping" and "interpolation" respectively. *Collision clipping* refers to the measure documented in section 3.5.2. *Interpolation* refers to the measure documented in section 3.5.1. *GA* refers to "geometric adaptation" (see section 3.5.2). All performance figures are specified as updates per second, figures in parentheses refer to speedups relative to "no optimisation" performance.

	With rendering		Without rendering	
	no GA	GA	no GA	GA
no-opt	1.79	0.27	1.93	0.30
coll-clip	2.38 (×1.33)	2.22 (×8.22)	2.70 (×1.40)	2.69 (×8.97)
interp	19.23 (×10.74)	10.81 (×40.04)	388.7 (×201.4)	374.4 (×1248)

The accuracy of the interpolation is dependent on the variable density of precalculated ROM envelopes. For this specific benchmark, we calculated the deviation between various different ROM envelopes that were calculated with and without optimisation. In total, the deviation was measured for 5000 ROM angles. The median deviation was $0°$, the inter-quartile range (IQR) was $0.15°$ $(0° - 0.15°)$ and the maximum absolute deviation was $2.67°$. This deviation is small enough to be justified by the significant interactive speed-increase gained through the optimisation.

We benchmarked the precalculation process as well as the interactive performance of our simulator on a Pentium 4 running at 2.66 GHz with 512 MB of RAM. The humerus model consisted of 50.000 polygons, while the scapula consisted of 155.000 polygons. Precalculation of 1782 complete ROM envelopes took 22 minutes. This has to be performed once per patient shoulder and can be integrated with the CT acquisition workflow.

Performance figures for the interactive ROM simulation are listed in Table 3.1. As can be seen, the speed increase due to collision clipping varies from a factor of 1.33 to 8.22 for normal usage of the simulator. The speed increase due to interpolation varies from a factor of 10.74 to 40.04. If we discard the graphical representation, the speed increase by interpolation gets as high as a factor of 1248. From these results we draw the following conclusions:

First, when no optimisation takes place, adjustments that require the geometry to be modified have a much lower update rate than other adjustments. This originates in the problem of geometry adaptation (described in section 3.5.2) and results in an update rate of 0.27 updates/s.

Second, the frame-rates of the aforementioned adjustments are substantially hig-

her when we apply the collision clipping optimisation. This optimisation enables interactive usage of our simulator without any form of precalculation. Consequently, we can use this technique to explore and compare the ROM estimations for multiple types and sizes of prostheses.

Third, the speed increase for interpolated ROM envelopes without graphical feedback is extremely large. This can be ascribed to the interpolation process, which is far less computationally expensive than the accurate determination of a single ROM envelope. For unoptimised ROM calculations and collision clipping, hardly anything of the routine is changed when graphical feedback is disabled, explaining the poor speed increase for these categories.

We conclude from these results that both optimisations are very effective. Compared to interpolated ROM estimations, the frame-rate for real-time exploration with collision clipping is on the low side. Perhaps additional speed increase is possible if we use heavily decimated models or limit the search range to areas where problems are likely to occur. Nevertheless, the fact that collision clipping does not require precalculation steps, makes it a good alternative for pre-calculated ROM predictions.

3.7 Conclusions and Future Work

In this chapter we presented a practical technique for the calculation and visualisation of shoulder ROM envelopes. We designed an extensive precalculation and interpolation scheme that enables the exploration of a shoulder replacement planning in real-time. For every change made by the surgeon during the pre-operative planning, the resulting ROM can be interactively visualised. We also employ the graphics hardware clipping plane to achieve interactivity at a lower frame-rate, without the requirement of precalculation.

Because comparing different ROM envelopes is crucial for the evaluation of different pre-operative choices, we implemented a comparative visualisation for ROM envelopes. The comparative visualisation can also be updated interactively and explicitly shows differences in mobility that result from the surgeon's actions during the pre-operative planning.

We performed measurements to show that the difference between interpolated and calculated ROM envelopes is relatively small. Speed measurements showed that the simulator is highly interactive when we apply precalculation and interpolation techniques.

The system we describe in this chapter concerns bone-determined ROM, which provides feedback on the risk of impingement. We plan to extend this with information on the presence of muscle tissue, ligaments and cartilage. Alternatively, a model

of these aspects could be used, such as the DSEM, described in section 3.2. While the model would greatly complement our impingement-based ROM system, it is not yet patient-specific (Van der Helm, 1994). Still, integration of the DSEM is under consideration for future work.

Our simulator is an important component of a pre-operative arthroplasty planning system for the shoulder joint (Botha, 2005). However, the presented techniques are generic and applicable to other joints as well, such as the hip and knee joint. With regard to the simulator, we will continue to add new functionality and refine existing features to better fit clinical practise, for example expansion of the prostheses database and improvement of user interface elements.

Finally, we plan to perform a validation study on cadaver shoulders, where motion limitation should correspond to the ROM estimations of our simulator.

4

Evaluation of bone impingement prediction in pre-operative planning for shoulder arthroplasty

Peter R. Krekel[1], Paul W. de Bruin[1], Edward R. Valstar[1],
Piet M. Rozing[1], Frits H. Post[2], Charl P. Botha[2],

[1]*Computer Graphics, Delft University of Technology*
[2]*Department of Orthopaedics, Leiden University Medical Centre*

Abstract

In shoulder arthroplasty, malpositioning of prostheses often leads to reduced post-operative range of motion and complications such as impingement, loosening and dislocation. Furthermore, the risk of impingement complications increases when reverse total prostheses are used. For this purpose a pre-operative planning system was developed that enables surgeons to perform a virtual shoulder replacement procedure. Our pre-operative planning system simulates patient-specific bone-determined range of motion, meant to reduce the risk of impingement complications and to improve the range of motion of patients undergoing shoulder replacement surgery. This chapter describes a validation experiment with the purpose of ratifying the clinical applicability and usefulness of the range of motion simulation module for shoulder replacement surgery.

Our experiment was performed on cadaveric shoulders. We have set up a data connection between our software environment and an existing intra-operative guidance system to track the relative positions of the bones. This allowed us to visualise the patient-specific surface models within our software to the position and alignment of the tracked bones. For both shoulders range of motion measurements were recorded and tagged with relevant information such as the type of prosthesis and the type of movement that was performed. The observed range of motion and occurrences of impingement were compared to the simulated equivalents. The median deviation between observed impingement angles and simulated impingement angles was -0.30° with an interquartile range of 5.20° (-3.40° - 1.80°). We conclude that the range of motion simulator is sufficiently accurate to fulfil its role as a supportive instrument for orthopaedic surgeons during shoulder replacement surgery.

4.1   Introduction

Shoulder arthroplasty aims to provide pain relief and to restore joint mobility. However, success rates in shoulder replacements are considerably lower than in knee and hip replacements (Hasan et al., 2001). This can be partially ascribed to the complexity of the shoulder joint. The surgical exposure provides little room for manoeuvring the instruments and causes the field of view for the surgeon to be limited. This frequently results in malalignment of prostheses (Hasan et al., 2002). Malalignment of shoulder prostheses leads to a diverse range of complications, for example increased wear, reduced stability of the glenohumeral joint, limited range of motion (ROM) and impingement (Iannotti et al., 2005, Dines et al., 2001). Long term consequences of impingement are abrasion of bone, loosening of the prosthesis and increased risk for the necessity of revision surgery (Williams et al., 2001).

Impingement complications are frequently seen with reverse shoulder prostheses, a type of prosthesis usually indicated for patients who suffer from a severely impaired rotator cuff (Grammont et al., 1987, Guery et al., 2006, Rockwood, 2007). Scapular notching refers to impingement of the humeral cup with the glenoid neck and is the type of impingement that is most common for reverse shoulder prostheses. Sirveaux et al. carried out a multi-centre study consisting of 80 shoulders, that showed scapular notching in 51 cases (Sirveaux et al., 2004). A similar study by Juvenspan et al. showed scapular notching in 39 of 55 cases (Juvenspan et al., 2005). Conversely, several studies show that careful planning greatly reduces the risk on scapular notching (Frankle et al., 2005, Nyffeler et al., 2005, Simovitch et al., 2007). Anticipating the frequent occurrence of impingement and the clear need to prevent it, we have developed a pre-operative planning system for shoulder replacements that interactively simulates bone-determined ROM. The system was described in detail in Chapter 3 of this thesis. We have included a short summary of the system in Section 4.2.1.

This chapter describes an experiment for the validation of the ROM simulations. The purpose of the experiment was to determine the accuracy of the ROM simulator. In addition, we have evaluated the ability of the system to predict impingement complications such as scapular notching. The prediction of bone impingement enables the surgeon to set up a plan that explicitly avoids this type of complications.

4.2   Methods

4.2.1   Description of the pre-operative planning system

Our pre-operative planning system loads CT-data and extracts surface models of the scapula and humerus. Subsequently, the surgeon can place prosthesis models on the

bone models. Currently, the system only supports total glenohumeral prostheses, i.e. both a cup and a ball component have to be placed. The system does support total reverse prostheses.

The system automatically calculates the position of well-known landmarks on the bone models. Planes are moved through the object to find the most extreme points on the models. The centre of rotation of the glenoid is determined by applying a Hough-transform to the surface models. The landmarks can also be selected manually. Using the landmark positions, a predefined pre-operative plan is transformed to the patient-specific case. Subsequently, prostheses can be dragged to different positions, thereby altering the plan.

In order to calculate ROM, we have implemented a bio-mechanical model of the gleno-humeral joint. A generally accepted hypothesis is that the gleno-humeral joint can be approximated by a ball-joint (Van der Glas et al., 2002, Meskers et al., 1998). No displacement is taken into account. We used the scapula coordinate system as described in the recommendations of the International Society of Biomechanics (Wu et al., 2005). The coordinate system is depicted in Figure 4.1. In this chapter, clinical terms are used to describe motion. Anteflexion refers to elevation parallel to the sagittal plane along the Z-axis, abduction refers to elevation in the coronal plane along the X-axis and endorotation refers to axial rotation along the humeral shaft or Y-axis.

Bone-determined ROM is automatically determined by systematically reorienting the humerus with placed humeral component in all directions, starting from an initial abduction of 45, while checking for collisions with a collision detection algorithm (Terdiman, 2001). During alterations of a pre-operative plan, ROM is continuously being calculated and visualised with a specialised visualisation technique. If ROM in a certain direction deteriorates, this is depicted with red surfaces. If it improves, this is depicted with green surfaces. This provides an intuitive user interface for the surgeon to optimise a plan with regards to ROM. Automatic optimisation is not yet incorporated, mainly because ROM is not the only aspect that plays a part in determining the most optimal alignment. For instance, fixation of the prosthesis is optimal when the screws are inserted through thick cortical bone. Also, the orientation of the components determines the post-operative stability of the joint (Iannotti et al., 2005).

Future work includes the implementation of an intra-operative guidance system, enabling the surgeon to carry out the operation in accordance with the pre-operative plan.
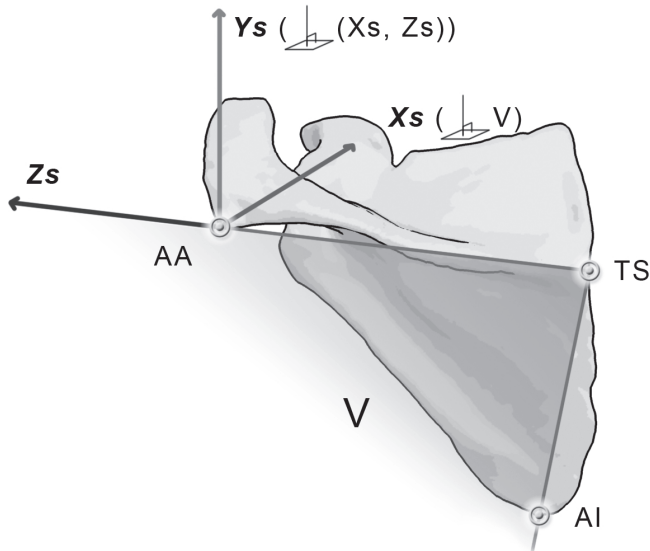
Figure 4.1: Definition of the scapula coordinate system. AA = Angulus Acromialis, TS = Trigonum Spinae Scapulae, AI = Angulus Inferior. Os: The origin coincident with AA. Zs: The line connecting TS and AA, pointing to AA. Xs: The line perpendicular to the plane formed by AI, AA, and TS, pointing forward. Ys: The common line perpendicular to the Xs- and Zs-axis, pointing upward.

4.2.2 Validation Experiment

The outline of the experiment is depicted in Figure 4.2. For this experiment we have used the intact shoulders of a cadaver. The cadaver had been specially embalmed to maintain flexibility of the extremities (Complucad ANATOMIC, Complucad International S.A.).

First, a series of axial CT-scans was made using clinical shoulder protocols (Toshiba Aquilion CT Scanner, Toshiba Medical Systems, Otawara, Japan). The scan data were reconstructed at 512 512 541 voxels, with spatial dimensions 0.54 0.54 1.0 mm. The CT-scans of both shoulders were segmented using the DeVIDE visualisation platform (Botha, 2005). Following segmentation, surface models of the scapulae and humeri were created.

Shoulder replacement procedures were performed on both shoulders of the cadaver. We have used the modular ESKA Multiplex shoulder prosthesis (ESKA Implants GmbH & Co, Lübeck, Germany), which consists of two base platforms for the scapula
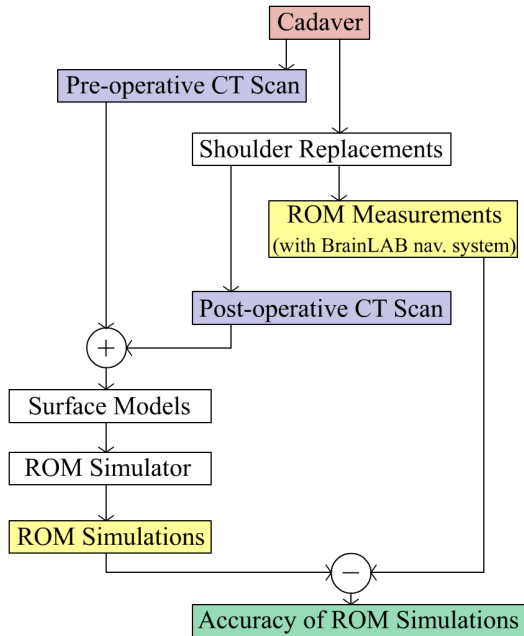
Figure 4.2: This diagram shows the outline of the validation experiment. First, a pre-operative CT-scan was made. Shoulder replacements were performed on both shoulders. A post-operative CT-scan was made and this data was combined with the pre-operative plan to repair faults as a result of scattering caused by the prostheses. This data was converted to surface models and used for ROM simulations. We also performed ROM measurements on the cadaver with an optical tracking system. These observations were compared with the ROM estimations of our ROM simulator.

and the humerus. The prosthesis can be tailor-fitted to the patient using different components that are attached to the base platforms (see Figure 4.3). This allows us to analyse multiple configurations of types (normal and reversed) and sizes, just as our pre-operative planning environment allows for quick interchanging of prostheses. To vary the set of impingement angles, the base platform of the left humerus was deliberately positioned with a different inclination and more distally than the base platform of the right shoulder.

A computer navigation system (BrainLAB VectorVision, BrainLAB AG, München, Germany) was used for real-time tracking of shoulder motion. The navigation sys-
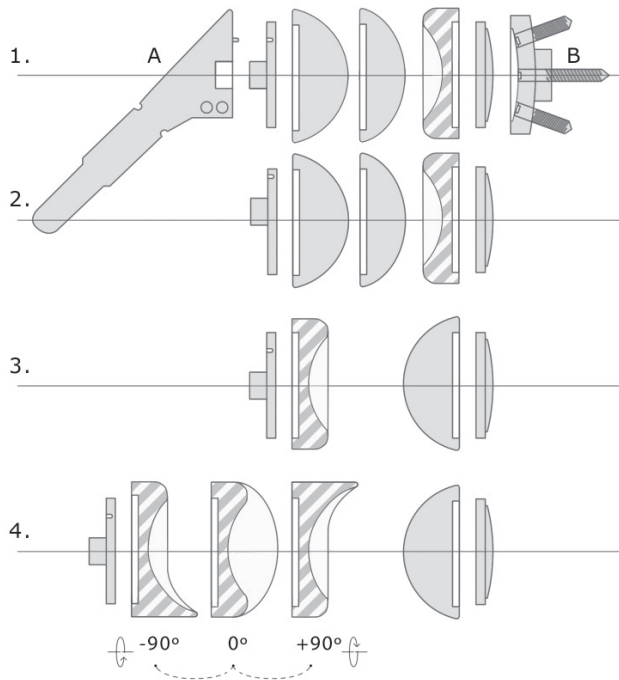
Figure 4.3: An overview of the modular ESKA Multiplex shoulder prosthesis. A is the humeral base component, with detachable stem. B is the glenoid base component. Line 1 to 4 show the different configurations used during the experiment: 1) a normal total shoulder prosthesis with an 18 mm spherical head, 2) a normal total shoulder prosthesis with eccentric humeral components with 14 and 18 mm spherical heads, 3) a reversed total shoulder prosthesis and 4) a reversed total shoulder prosthesis with three orientations of a polyethylene cup with slope for the humeral side.

tem uses two infra-red cameras and retro-reflective markers on the instruments and marker trees. This system is used in our hospital for various orthopaedic surgery procedures (spine, knee, and hip replacements). At the time of writing, no shoulder specific module was available. To enable motion tracking of the shoulder bones, basic registration and tracking functionality was implemented as described below. Communication with the navigation system was accomplished by using a research software library (VectorVision Link, BrainLAB AG, München, Germany).

A marker tree consists of three retro-reflective markers that are attached to a metal Y- or T-frame. Different configurations of the markers allow the navigation system to identify specific marker trees and instruments. The marker trees are attached to

Figure 4.4: After attachment of the marker tree various landmarks on the scapula are indicated percutaneoulsy. The markers on the sharp pointer, the scapula reference frame and on the humeral tracker are visible.

guidewires with a diameter of 3 mm, which are drilled into the bone. This fixation is important, because any relative movement between the marker tree and the bone will be misinterpreted as movement of the bone.

After fixation, the surgeon registers each marker tree to its corresponding bone (see Figure 4.4). Using a sharp pointer device with retro-reflective markers, a number of specific landmarks are indicated on the bone. The same landmarks are indicated in the intra-operative planning module, after which the registration matrix can be calculated.

The marker tree that is attached to the scapula is used as the reference coordinate system. The pointing device and the marker tree attached to the humerus report their position and orientation in this coordinate system. After registration of the scapula and the humerus, our intra-operative tracking system is able to interactively visualise the patient-specific models and their current relative position and alignment

Figure 4.5: Real-time motion tracking. Marker trees are attached to each bone, and these are tracked by the infra-red guidance system. The intra-operative tracking system on the laptop shows the real-time position and orientation of the tracked bones.

(see Figure 4.5).

For both shoulders, we measured the motion limitations of eight different prosthesis types and sizes. The prosthesis configurations were chosen so that a diverse set of impingement occurrences were observed. Any occurrence of impingement during motion tracking was specifically noted in the motion tracking logs (see Figure 4.6). All motions were recorded as a time series of transformation matrices, tagged with prosthesis type and measurement information and then exported to a database.

The motions consisted of arm movement from $0°$ to maximum anteflexion, from $0°$ to maximum abduction and finally from maximum exorotation to maximum endorotation at maximal elevation in the scapular plane. Occasionally, motion was limited by the presence of soft tissue, but when possible bone impingement was forced and
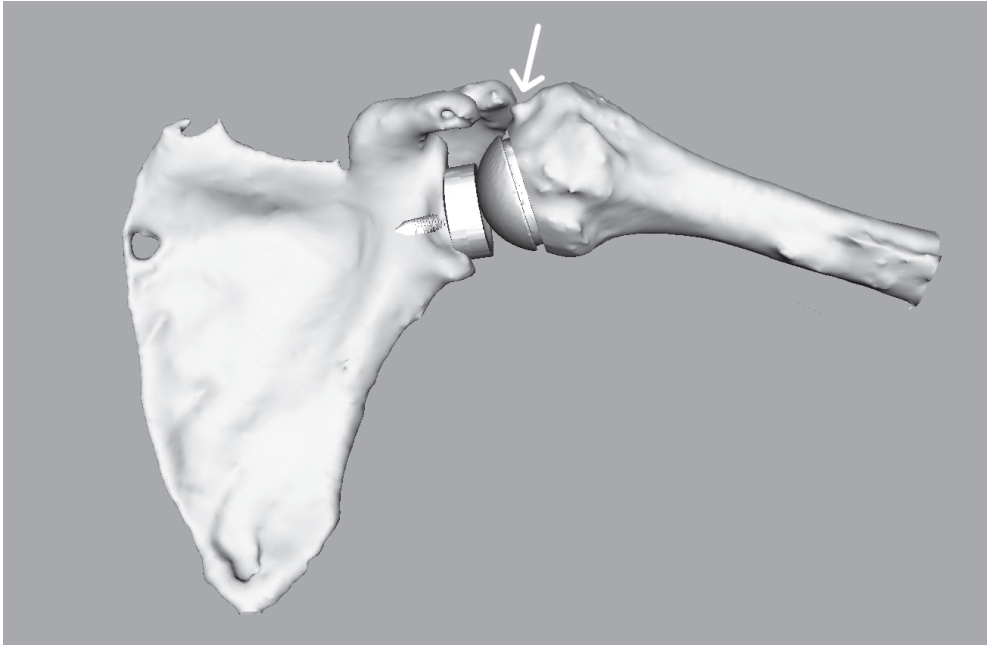
Figure 4.6: Motion recording, showing impingement between the tuberculum majus on the humeral side and the acromion on the scapular side. The location of impingement is indicated by a white arrow.

noted for later comparison with the ROM simulations. The orthopaedic surgeon performing the arm motion visually determined whether a limitation was caused by bone impingement or by soft tissue. To evaluate the repeatability of the motions, four of the measurements were recorded twice.

Both shoulders with base plates were CT-scanned post-operatively, using the same protocols as for the pre-operative scans. This data was then segmented. To avoid artifacts as a result of scattering, we combined the post-operative models with the pre-operative models by manually overlaying them (see Figure 4.7). Thus we obtained accurate bone models that have the prosthesis base platforms installed. These models were loaded into our pre-operative planning system. The motions were simulated by the ROM simulator of our pre-operative planning system and the resulting impingement angles were noted. The advantage of using scanned post-operative models rather than virtually planning the operation is that the models used for our ROM simulations more accurately represent the geometry of the measured cadaver shoulders. Using the pre-operative planning functionality would introduce additional
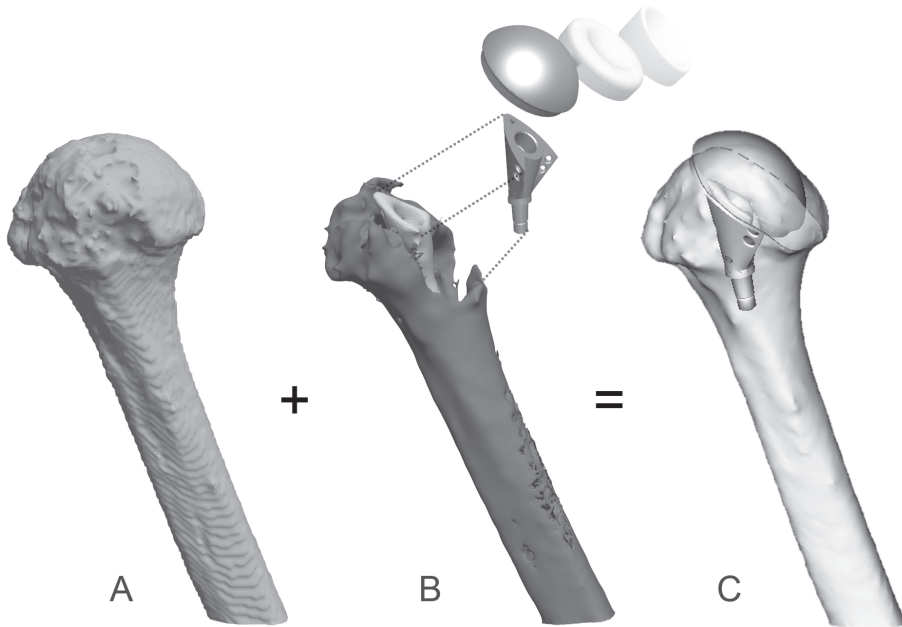
Figure 4.7: Pre-operative (A) and post-operative (B) surface models. Scattering caused by the prosthesis prevents complete segmentation of the CT-data. However, by overlaying the two scans, the prosthesis position and alignment can be reconstructed (C). The resulting models were used as input for our ROM simulations.

errors. Please note that the goal of this experiment is to validate the ROM simulations rather than the pre-operative planning system as a whole.

We compared the impingement angles as observed during the experiment with the impingement angles as determined by our ROM simulator. The median deviation, the interquartile range and maximum absolute deviation were calculated for the three separate motions as well as the complete set of measurements. For these calculations the measurements of the left and right shoulder were combined.

4.3   Results

The ROM simulations and experimental observations are listed in Table 1. The observed limitations were sometimes caused by soft tissue not capable of extending any further as a result of tension. These limitations are also given for reasons of com-

Table 4.1: Results of the motion recordings and ROM simulations for the left shoulder. The ball and cup prosthesis components have a radius of 22 mm. If applicable, 'h' gives the height of the component at its centre line in mm. When a value is printed in *italics*, this means that the motion limitation was caused by soft tissue. Motion limitations that were not measured during the experiment are indicated by the word 'no'. To facilitate comparison, the observed impingement angles are printed **bold**, together with their simulated counter parts. Two of the values are highlighted to demonstrate how the values should be compared. Statistical results are given in the main text.

| Prosthesis configuration | | Motion | Left shoulder | | | |
| | | | Simulated impingement | | Observed limitation | |
Humerus	Glenoid		Begin	End	Begin	End
Ball (h=14)	Cup	abduction	0	84	no	*63.5*
		endorotation	-28	**71**	*16.6*	**69.2**
		anteflexion	0	90	no	*61.6*
Ball (h=18)	Cup	abduction	0	91	no	*62.7*
		endorotation	-27	**72**	*27.3*	**69.6**
		anteflexion	0	87	no	*67.5*
Ball (h=14) eccentric	Cup	abduction	2	85	no	*64.5*
		endorotation	-16	**52**	*16.4*	**59.1**
		anteflexion	4	**79**	no	**70.7**
Ball (h=18) eccentric	Cup	abduction	3	84	no	*56.2*
		endorotation	-13	**39**	*6.5*	**42.8**
		anteflexion	3	82	no	*66.1*
Cup eccentric	Ball (h=14)	abduction	21	**75**	no	**72.5**
		endorotation	**16**	69	**11.6**	71.5
		anteflexion	17	**56**	no	**62.7**
Cup prox. slope	Ball (h=14)	abduction	19	**71**	no	**68.5**
		endorotation	**-5**	44	**-2.2**	48.9
		anteflexion	**23**	61	**25.1**	58.8
Cup ant. slope	Ball (h=14)	abduction	18	**68**	no	**68.3**
		endorotation	**18**	70	**15.0**	72.1
		anteflexion	23	**61**	no	**60.0**
Cup dist. slope	Ball (h=14)	abduction	**33**	73	**31.5**	68.4
		endorotation	**-1**	57	**-2.6**	63.9
		anteflexion	28	59	no	*56.9*

Table 4.2: Results of the motion recordings and ROM simulations for the right shoulder. The ball and cup prosthesis components have a radius of 22 mm. If applicable, 'h' gives the height of the component at its centre line in mm. When a value is printed in *italics*, this means that the motion limitation was caused by soft tissue. Motion limitations that were not measured during the experiment are indicated by the word 'no'. To facilitate comparison, the observed impingement angles are printed **bold**, together with their simulated counter parts. Two of the values are highlighted to demonstrate how the values should be compared. Statistical results are given in the main text.

| Prosthesis configuration | | Motion | Right shoulder | | | |
| | | | Simulated impingement | | Observed limitation | |
Humerus	Glenoid		Begin	End	Begin	End
Ball (h=14)	Cup	abduction	-6	56	no	*52.9*
		endorotation	**-3.3**	**94**	**-5.5**	**95.7**
		anteflexion	-33	112	no	*42.1*
Ball (h=18)	Cup	abduction	-6	56	no	*52.8*
		endorotation	-43	**101**	*-3.2*	**98.6**
		anteflexion	-35	111	no	*43.2*
Ball (h=14) eccentric	Cup	abduction	-4	54	no	*52.7*
		endorotation	-18	**105**	*9.7*	**111.8**
		anteflexion	-30	112	no	*41.0*
Ball (h=18) eccentric	Cup	abduction	-5	53	no	*49.5*
		endorotation	-39	**94**	*13.7*	**96.0**
		anteflexion	-28	112	no	*36.6*
Cup eccentric	Ball (h=14)	abduction	7	**49**	no	**55.3**
		endorotation	**-8**	**63**	**-6.5**	**62.2**
		anteflexion	7	88	no	*37.2*
Cup prox. slope	Ball (h=14)	abduction	**7**	47	**6.1**	**46.1**
		endorotation	**-10**	**63**	**-6.9**	**67.4**
		anteflexion	**7**	55	**10.4**	*41.0*
Cup ant. slope	Ball (h=14)	abduction	**11**	**50**	**10.0**	**52.6**
		endorotation	-14	**46**	*-2.9*	**49.9**
		anteflexion	**18**	66	**19.5**	*36.4*
Cup dist. slope	Ball (h=14)	abduction	**26**	**51**	**26.2**	**49.7**
		endorotation	-7	**63**	*-9.2*	**70.8**
		anteflexion	**26**	75	**25.7**	*39.3*

Table 4.3: Statistics summary of Tables 4.1 and 4.2.

Motion	Median	Interquartile Range	Max. Abs. Deviation
abduction	0.95°	2.53° (-0.28° – 2.25°)	7.25°
endorotiation	-2.10°	6.20° (-4.40° – 1.80°)	6.50°
anteflexion	-0.60°	4.98° (-3.08° – 1,90°)	8.90°
all	-0.30°	5.20° (-3.40° – 1.80°)	8.60°

pleteness. The accuracy of the ROM simulations can be determined by examining the difference between the measurements of the cadaver experiment and the simulations. Motions that were recorded twice were very similar with almost identical motion limitations (difference $< 0.5°$) and are therefore not listed.

As Table 2 points out, the observed impingement angles of the cadaver experiment correspond to the impingement predictions of our system. The median deviation is limited to a few degrees for all motions. To determine the statistical significance the Spearman Rank Correlation Coefficient was calculated, resulting in a correlation of 0.982 with a significance of $p < 0.005$.

The ROM of the left shoulder differed from the ROM of the right shoulder due to the different alignment of the base platforms. For both shoulders impingement was observed more frequently for reverse prostheses than for normal prostheses. Impingement with the upper structures of the scapula (the acromion and coracoid process) occurred frequently during anteflexion and abduction, due to the more medial location of the centre of rotation. In addition, scapular notching was seen for almost all motion recordings of reverse prosthesis configurations.

Inaccuracy as a result of the hardware limitations of the BrainLAB VectorVision system was also determined during this experiment (De Bruin et al., 2007). The mean translational error for locating a marker was 0.1 mm, 0.05 mm and 0.25 mm in the x, y, and z directions respectively. Because the scapula and humerus marker trees are approximately 30 cm apart, the maximal angular error introduced by hardware limitations is smaller than 0.1°. This error is acceptable for our experiment.

To determine how accurately the post-operative models where overlaid with the pre-operative models, minimum distances between the models were calculated on a per-vertex base. Because the post-operative models were different near the replaced regions, we only used a clipped half of each of the models. The mean error was 0.41 mm with a standard deviation of 0.23 mm. Increasing the accuracy of the models does not lead to substantially different ROM simulation results.

4.4 Discussion

In this chapter we have described an experiment for the evaluation of the accuracy of our ROM simulation module. We have developed a CT-based navigation system, with which passive cadaveric joint motion was tracked. Subsequently, the recorded motions were compared with ROM simulations in order to validate the latter.

Literature reports on the use of ROM simulations and impingement prediction for total hip replacement procedures. Jaramaz et al. and Yoshimine et al. analytically determined ROM as imposed by the prosthesis geometry (Jaramaz et al., 1997, Yoshimine and Ginbayashi, 2002). Sato et al. studied the advantages of impingement prediction for the hip joint, using both the prosthesis geometry and surface data of the bone (Sato et al., 2000). Their simulations were also clinically validated using optical tracking. To our knowledge, no publications exist describing validated simulation of bone-determined ROM for shoulder replacement surgery, even though the occurrence of impingement complications after shoulder replacement surgery is a frequently seen problem.

There are limitations to this study. The number of two shoulders is relatively low to make claims on the accuracy of our ROM simulator. However, the utilisation of different prosthesis configurations leads to a larger number of unique impingement cases that can be used for validation of the ROM simulator.

Optical tracking systems are known to have some inaccuracy due to the registration step, which requires the surgeon to indicate the exact same points on the physical bones as on the virtual bones. Differences between these locations result in a registration error. However, for the measurements in this experiment we have only used the rotational information as provided by the optical tracking system. This information relies on the relative movement of the marker trees rather than absolute positions. If registered landmarks are close to each other this may introduce a small error in the rotation axis. Because the medial and lateral epicondyles are relatively close to one another we expect to have introduced a small registration error in the axis used for endorotation. Based on visual inspection of the registration we suspect that this error was limited. However, for definition of the axes used to measure abduction and anteflexion the selected landmarks are sufficiently far apart. In future a possible solution to this problem is the utilisation of fiducial markers that are inserted before acquisition of the pre-operative CT scan and can later be used to ensure a correct registration.

Our ROM simulator uses CT data as acquired by the standard scanning protocol for shoulders. However, the time required to manually segment the data is approximately one hour. This may complicate clinical applicability of the system. We are currently working on new techniques and algorithms to speed up this segmentation process.

From our results we conclude that the impingement predictions of the system generally correspond to the actual incidence of impingement during recorded shoulder motion. However, a number of observed ranges of motion were smaller than their simulated counter parts. This was expected and can be explained by the movement restrictions as imposed by the presence of soft tissue. Because soft tissue is not incorporated into the ROM simulations, the simulations are restricted to predict motion limitations as imposed by bony impingement. This already is quite helpful to the surgeon, as it alerts the surgeon to possible impingement complications.

Our simulations confirm that the humeral component of a reverse prosthesis frequently impinges with either the glenoid component or with the glenoid. As discussed in the introduction, this may cause early loosening of the glenoid prosthesis and leads to bone damage, further complicating revision surgery. Subacromial and subcoracoid impingement was also observed for most of the total reverse shoulder configurations. The accuracy of the ROM simulations is well within range to predict these impingement complications beforehand, allowing the surgeon to adapt the pre-operative plan. Future work will include the implementation of an intra-operative guidance system, based on the optical tracking system described in this chapter. The intra-operative guidance system will ensure that the actual surgery corresponds to the pre-operative plan as defined by the surgeon with our pre-operative planning system.

If surgery is conducted according to the pre-operative plan as composed in our pre-operative planning system, it is plausible that the post-operative bone-determined ROM corresponds to the ROM as predicted pre-operatively by our system. Moreover, all of the observed occurrences of impingement during the described experiment were predicted by the system. We therefore recommend to comply with the ROM predictions of the system during the planning stage of a shoulder replacement procedure, keeping in mind other aspects such as prosthesis fixation and the presence of soft tissue. Finally, from the results of this experiment we conclude that the system is particularly useful for non-anatomical prosthetic designs such as reverse prostheses, because they entail an increased risk of impingement complications.

5

Effects of proximal humeral fracture morphology on glenohumeral range of motion

Peter R. Krekel[1,2], Addie Majed[3], Angelo Tardugno[4],
Charl P. Botha[1,2], Rob G.H.H. Nelissen[1], Roger J. Emery[3]

[1] *Department of Orthopaedics, Leiden University Medical Centre*
[2] *Computer Graphics, Delft University of Technology*
[3] *Department of Orthopaedics, St. Mary's Hospital London*
[4] *Department of Bioengineering, Imperial College London*

Abstract

The morphology of proximal humerus fractures varies greatly, ranging from non-displaced 2-part fractures to 4-part fractures with inclined articular surfaces and displaced tuberosities. Existing classification systems attempt to formalise these features and relate them to clinical results. The repeatability of these classification systems has been shown to be poor, giving rise to the question whether a more objective measure entails improved predictability of outcome.

Using a system that simulates bone-determined range of motion of spheroidal joints such as the shoulder joint we categorically analysed a series of 79 proximal humerus fractures. Morphological properties of the proximal humerus fractures were related to simulated bone-determined range of motion.

The interobserver variability of range of motion assessment using our system showed excellent agreement (0.798). Maximal glenohumeral abduction and forward flexion of intra-articular fractures were 34.3$\pm$6.6 SE and 60.7$\pm$12.4 SE degrees. For fractures with a displaced tuberculum major they were 75.0$\pm$5.9 SE and 118.2$\pm$4.9 SE degrees, for fractures where both tuberosities had been displaced they were 60.0$\pm$10.9 SE and 69.6$\pm$13.4 SE degrees. For non-intra articular fractures without displaced tuberosities they were 89.3$\pm$3.3 SE and 122.6$\pm$3.4 SE degrees. The head inclination angle was positively correlated with maximum abduction (0.362, $p = 0.014$). Offset was negatively correlated with maximum abduction, but not statistically significant (0.834, $p = 0.087$).

We conclude that intra-articular fractures generally have the worst prognosis with regards to bone-determined range of motion. Fractures with displaced tuberosities show more motion limitations for abduction than for forward flexion. A reduced head inclination angle is a strong predictor of limited bone-determined range of motion for all types of proximal humerus fractures. No correlations were found between the maximum forward flexion range and the measured morphological parameters, indicating that it is difficult to predict range of motion based on morphological parameters only and that extensive range of motion simulation is required to predict outcome.

5.1 Introduction

Proximal humerus fractures (PHFs) often occur in the elderly population as a result of falling from standing height and are often osteoporosis related. The treatment options include conservative treatment and surgical intervention, the latter ranging from percutaneous wire fixation or open reduction and internal fixation to hemi-arthroplasty. The treatment decision is based on patient age, assessment of image modalities such as radiographs and computed tomography (CT), as well as the application of fracture classification systems found in the literature. However, the classification systems have been much disputed for their reproducibility and effectiveness in predicting outcome.

The first PHF classification system was published by Codman, who differentiated between the humeral head, the humeral shaft and the tuberosities (Codman, 1934). An extension of Codman's classification system, and the most frequently used classification system, is the classification system by Neer (Neer, 1970). The Neer classification system differentiates between 2-, 3- and 4-part fractures as well as the dislocation of fragments. In recent years the notion has occurred that second order effects such as vascularity must be taken into account when assessing PHFs, leading to the classification system proposed by the Arbeitsgemeinschaft für Osteosynthesefragen (AO) (Müller et al., 1994). Recently, Hertel developed a binary fracture description based on fracture planes rather than the number of fragments and found correlations between the classification and restriction of blood supply (Hertel et al., 2004).

In the literature, the intra-observer repeatability and interobserver reliability for Neer classification has been proven to be fair or poor, with Kappa values ranging between 0.40 to 0.60 (Bernstein et al., 1996, Kristiansen et al., 1988, Sidor et al., 1993, Siebenrock and Gerber, 1993). Simplification of the classification system subdividing the fractures into fewer categories did not significantly improve these values (Sidor et al., 1993). As demonstrated by Majed et al., removing imaging subjectivity in the production of prototype models of the fracture did not improve the reliability for Neer and AO PHF classification systems (Majed et al., 2011a). This persisting subjectivity of the PHF classification systems in combination with the severe implications of treatment decisions encouraged us to assess the possibilities of a computerised assessment rather than a subjective classification.

There are many aspects involved in the evaluation process that precede the treatment decision of a PHF. However, the morphology of the glenohumeral joint and loss of smooth articular congruency may be a significant cause of loss of motion. Indeed, fracture fragment deflection has been argued to cause vascular insult (Müller et al., 1994). Displacement is affected by tendon attachment points (Neer, 1970), while passive range of motion (ROM) is affected by impingement of rigid structures and displacement of the articular surface of the humeral head (Edelson et al., 2004). In

this article we assess impingement and interrupted articulation using a computerised simulation model.

The main objective of this study is to define the relationship between three shape parameters of PHFs and the inherent bone-determined ROM in a dynamic simulation model. In addition we look at the simulated bone-determined ROM when a categorical approach is taken. The morphological properties of 79 cases of PHFs were determined using CT scans. The bone-determined ROM was independently estimated by two observers using a software package designed for this purpose. With this study we demonstrate that bone-determined ROM simulation of fractures may be a valuable supportive instrument in the decision-making process involved in the treatment of these fractures.

5.2 Methods

5.2.1 Data description

For this study a collection of 100 anonymised post-trauma CT scans of the shoulder area of PHF-patients was utilised. Exclusion criteria were poor image quality and the presence of abnormalities such as recurrent fractures or prosthetic materials. After application of the exclusion criteria 79 datasets remained. The remaining CT scans were segmented and converted to surface models using Mimics (Materialise NV, Leuven, Belgium). For each dataset a scapula model and humerus model were obtained.

5.2.2 Shape classification

To investigate the implications of different fracture patterns we have categorised our data into four groups. The groups are illustrated by Figure 5.1 and had the following characteristics: 1) Intra-articular fractures, 2) fractures with a displaced tuberculum major, 3) fractures with a displaced tuberculum minor and major, also known as a 'shield', and 4) all other fractures that do not belong to the former groups and do not satisfy the exclusion criteria. A fragment was considered displaced when a step was present on the surface. It was hypothesised that each of the groups would have ROM limitations characteristic of the distinctive morphological properties.

Head inclination, sagittal head angulation and offset were measured in accordance with a process described by Majed et al. (Majed et al., 2011b). Each model underwent a process of endosteal and periosteal morphological assessment (see Figure 5.2). Proximal ellipse fitting defines a distal major and minor axis whilst an intramedullary axis is determined. The centre of the humeral head is determined after sphere fitting to the articular surface, whilst an ellipse is fitted to the articular
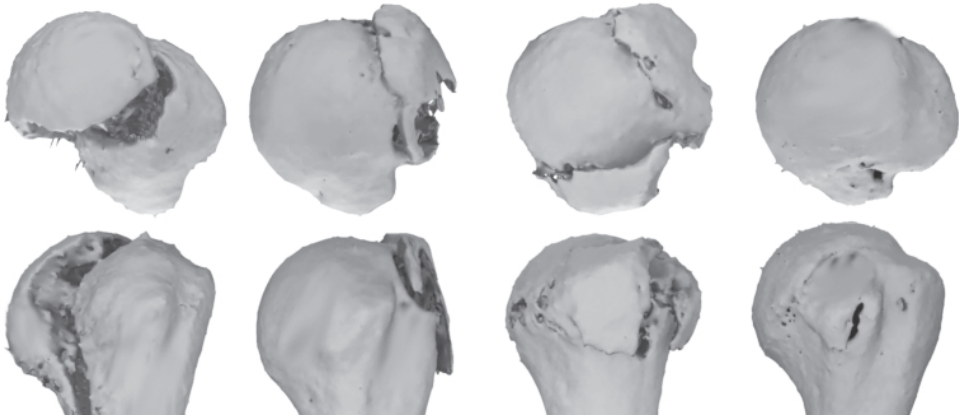
Figure 5.1: The four categories we adopted for our data. 1) Intra-articular fractures, 2) fractures with a displaced tuberculum major, 3) fractures with a displaced tuberculum minor and major and 4) all other fractures that do not belong to the former groups and do not satisfy the exclusion criteria.

margin to determine the anatomical neck plane. A customised algorithm allowed the determination of head inclination and of sagittal head angulation (in the lateral plane) whilst the medial and posterior offsets were also determined.

5.2.3 Range of motion simulation

ROM simulation was performed using a previously described system with minor modifications (Clinical Graphics, Den Haag, The Netherlands). The system was originally developed for pre-operative planning of shoulder arthroplasty (Krekel et al., 2006). In a cadaveric study we demonstrated that the error margin of the predicted angles of impingement lies within a range of 5 degrees (Krekel et al., 2009). For this study we have adapted the system to support geometry of PHF cases. Adaptations involved skipping the prosthesis placement functionality and implementing minor modifications of the bio-mechanical model to accommodate for the non-conformity of the glenoid fossa and humeral head, as described below.

The simulation routine is initiated by importing 3-D models of the scapula and humerus. Subsequently, the system calculates the position of well-known landmarks. Planes are moved through the object to find the most extreme points on the models. The centre of rotation of the glenoid is determined by applying a Hough-transform to the surface models. Landmarks can also be selected manually. For this study, landmarks were calculated automatically and verified by an orthopaedic surgeon.
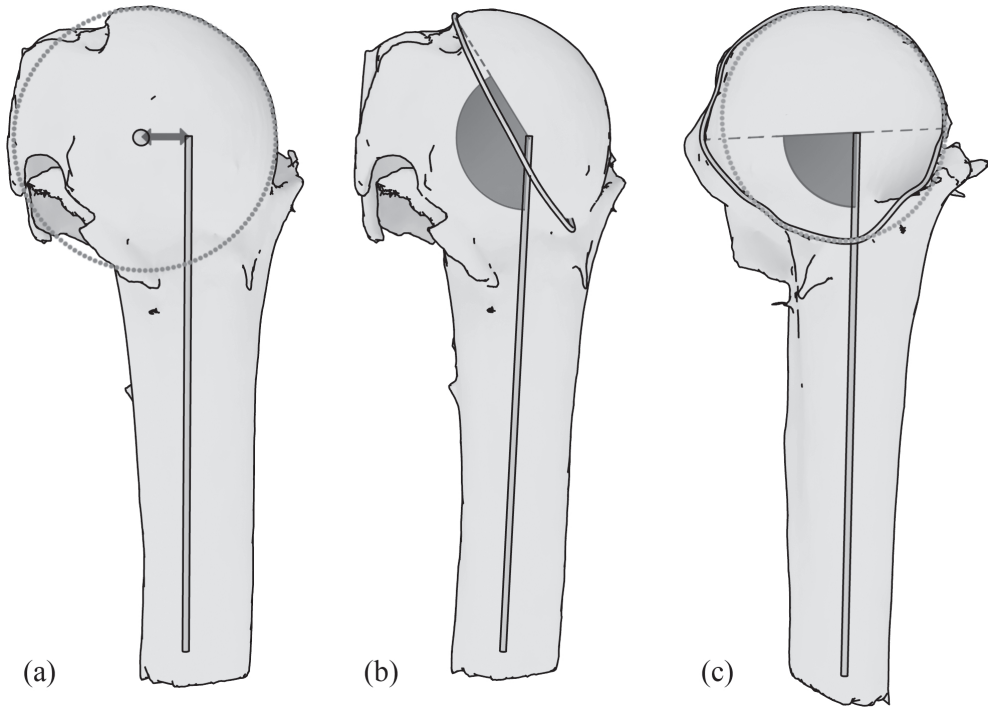
Figure 5.2: Measured morphological parameters. The centre of the head is determined by sphere fitting to the articular surface and defines the offset with respect to the intramedullary axis (a). Head inclination is determined by the intramedullary axis of the humeral shaft and the long axis of an ellipse fitted to the articular margin (b). Sagittal head angulation is determined by the intramedullary axis of the humeral shaft and the short axis of an ellipse fitted to the articular margin (c).

To dynamically simulate bone-determined ROM, we have implemented a biomechanical model of the gleno-humeral joint. A generally accepted hypothesis is that the gleno-humeral joint can be approximated by a ball-joint (Van der Glas et al., 2002, Meskers et al., 1998). When the humeral head is fractured, joint articulation may be affected, thereby jeopardising this hypothesis. Displacements of the articular surface with respect to the glenoid are taken into account by considering motion of the humerus invalid when the articular surface loses contact with the glenoid fossa.

Joint stabilising forces normally provided by the rotator cuff during arm motion are simulated by applying a translation of the humerus towards the glenoid surface. When the humeral head reaches the glenoid, further translation is halted. This enforces contact between the glenoid fossa and the humeral head.
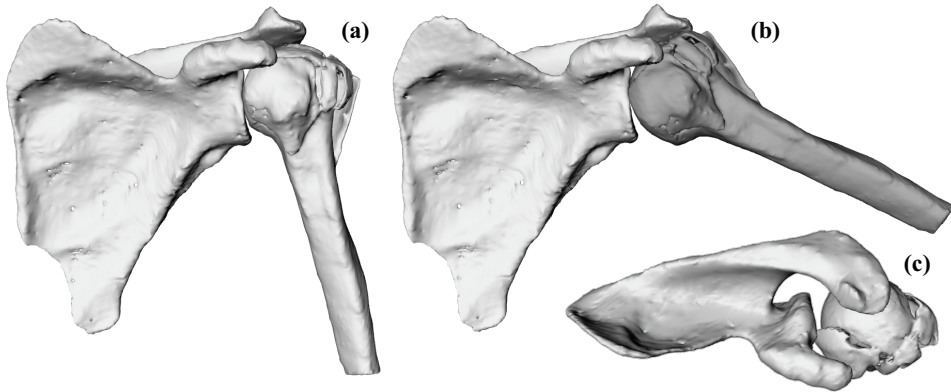
Figure 5.3: The ROM simulator. A kinematic model is applied to surface models of the scapula and humerus **(a)**. When impingement is detected by a collision detection algorithm the bone is coloured red **(b)**. Interrupted articulation of the joint is not detected automatically and therefore two observers analysed the series of fractures **(c)**.

We used the scapula coordinate system as described in the recommendations of the International Society of Biomechanics (Wu et al., 2005). In this chapter, clinical terms are used to describe motion. Forward flexion refers to elevation parallel to the sagittal plane. Abduction refers to elevation in the coronal plane and internal rotation refers to axial rotation along the humeral shaft.

After initialisation, the posture of the humerus can be manually adjusted. While the posture is adjusted, a collision detection algorithm evaluates whether geometric objects are intersecting (Terdiman, 2001). If impingement is detected, the humerus is coloured red, alerting the user that the given posture is invalid (see Figure 5.3). Interrupted articulation of the humeral head on the glenoid is visible in the simulations but not automatically detected. For this reason two observers operated the system manually.

To quantify the ROM of the individual PHF cases, the maximum range of forward flexion and abduction was determined. Because the scanned arm position and orientation was not controlled at the time of data acquisition, the neutral orientations of the humeri were indeterminable. To account for this, we performed the ROM measurements for different degrees of axial rotation. Maximum abduction and maximum elevation were measured in 40 degrees and 20 degrees of internal rotation, in the neutral (scanned) position, and in 20, 40, 60 and 70 degrees of external rotation. Generally, when lying down in the CT scanner, patients will have their arm moderately

internally rotated to minimise pain. Therefore we chose to evaluate a larger range of external rotation than internal rotation. In total an axial rotation range of 110 degrees was analysed. The findings of both observers were compared to evaluate the interobserver variability. To obtain the final values for maximum forward flexion and abduction of each of the fractures the measurements of the observers were averaged. The results were statistically compared to the shape parameters of the models.

5.2.4   Statistical Analysis

For statistical analysis the SPSS software package was used (SPSS Inc., version 17.0, Chicago, Illinois). The interobserver variability of our measurements was assessed using the Pearson product-moment correlation coefficient (PMCC). For interpretation, the criteria formulated by Cichetti and Sparrow were used: 0.00 to 0.39, poor; 0.40 to 0.59, fair; 0.60 to 0.74, good; or 0.75 to 1.00, excellent (Cicchetti and Sparrow, 1981). General linear models were used to determine correlation between morphological parameters and ROM. Statistical results were considered statistically significant when $p < 0.05$.

5.3   Results

We studied the standard error of the mean of the ROM measurements (see Figure 5.4). The ROM measurements indicate that intra-articular fractures have the smallest range for abduction and forward flexion (34.3 ± 6.6 SE and 60.7 ± 12.4 SE), followed by shield-type fractures (60.0 ± 10.9 SE and 69.6 ± 13.4 SE). Fractures with just a displaced tuberculum major show limitations for abduction, but not for forward flexion (75.0 ± 5.9 SE and 118.2 ± 4.9 SE). This can be explained by the displaced tuberosity, colliding with the acromial arch. Finally, non-intra-articular fractures that do not have displaced tuberosities have ROM that is comparable to that of healthy subjects (89.3 ± 3.3 SE and 122.6 ± 3.4 SE versus 102.3 ± 2.8 SE and 96.2 ± 3.8 SE).

No correlation was found for head inclination versus maximum forward flexion for any of the groups. This also holds for sagittal head angulation versus maximum forward flexion and offset versus maximum forward flexion. However, for all groups head inclination correlated with the maximal abduction range (see Figure 5.5). With multiple linear regression it was determined that the slope of each of the categories was similar ($p = 0.941$). The slope of the head inclination versus maximal abduction was approximately 0.362, meaning that for every degree of head inclination the bone-determined abduction range increases with 0.362 degrees. The correlation coefficient was 0.482, indicating a moderate correlation. This result was statistically significant
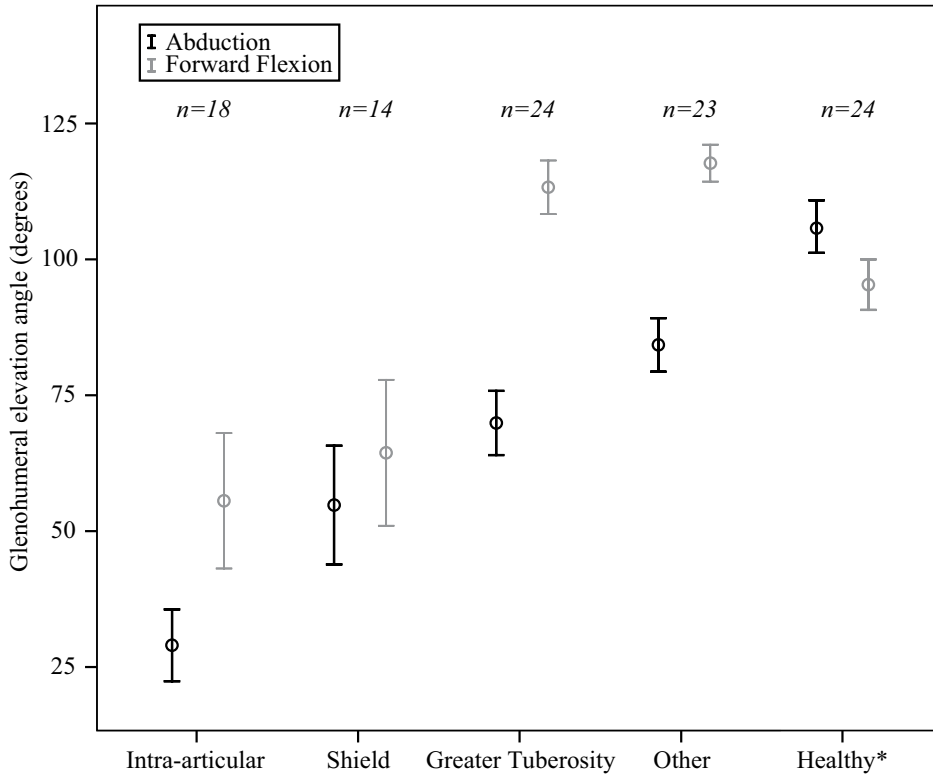
Figure 5.4: Maximal angles relative to the scapula. Displayed are the mean±SE. Shield type fractures have a displaced tuberculum major and minor. Other type fractures do not belong to the other three categories. For the reference of the ROM of healthy subjects (marked *) we used the information from the study by Magermans et al. (Magermans et al., 2005). In contrast to the four preceding categories these data consist of actual recorded ROM in 24 healthy subjects.

($p = 0.014$). The intercepts cover a range of 56.5 degrees, showing clear distinctions between the groups. The low intercept of intra-articular fractures indicates that these fractures have the worst prognosis to start with. Regardless these fractures show a similar improvement with increased head inclination angle in comparison to other groups.

Maximum abduction did not correlate with sagittal head angulation (-0.070, $p = 0.303$). It did correlate negatively with offset with a slope of -0.834, but this correlation was not statistically significant ($p = 0.087$, see Figure 5.6).

The interobserver variability of the ROM measurements was 0.798, showing ex-
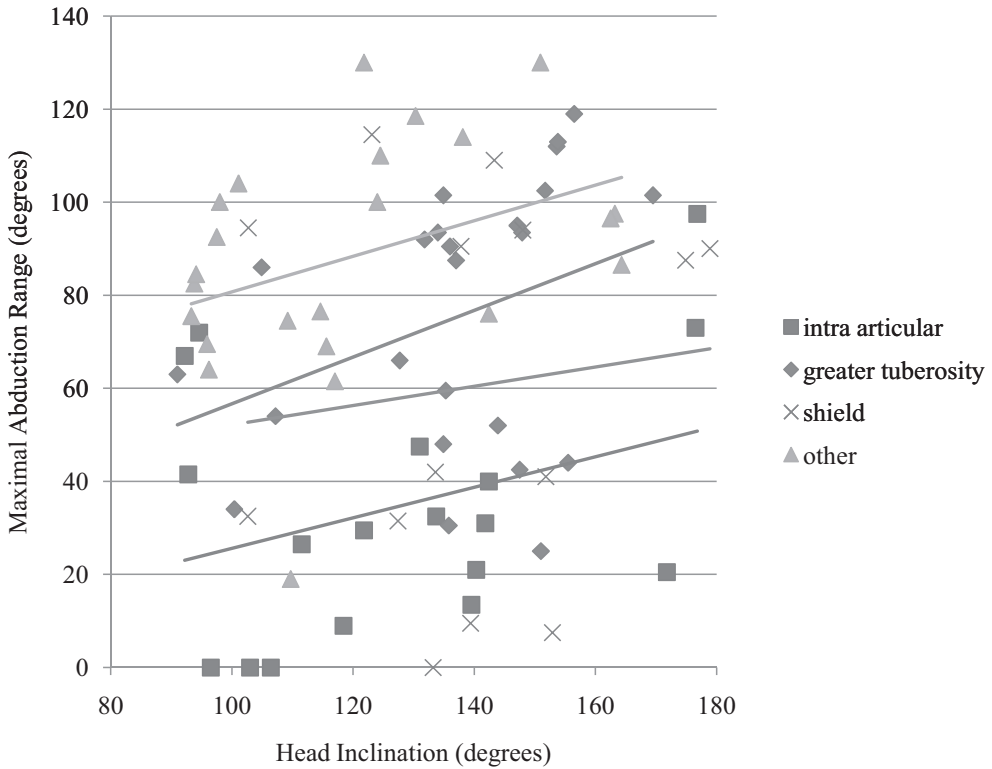
Figure 5.5: Maximal abduction versus the measured head inclination angle. The linear regression lines of all groups are increasing with respect to the head inclination angle. This indicates that a reduced head inclination angle is a strong predictor of limited ROM. This figure also shows that intra-articular fractures generally have a lower abduction range than other types.

cellent agreement.

5.4 Discussion

In this chapter we described a ROM simulation system used to quantify the bone-determined ROM of 79 cases of PHFs and related the results to fracture morphology. From this study it can be concluded that intra-articular fractures generally have the worst prognosis with regards to bone-determined ROM. During forward flexion but even more so during abduction the articulation of the glenohumeral joint is jeopar-
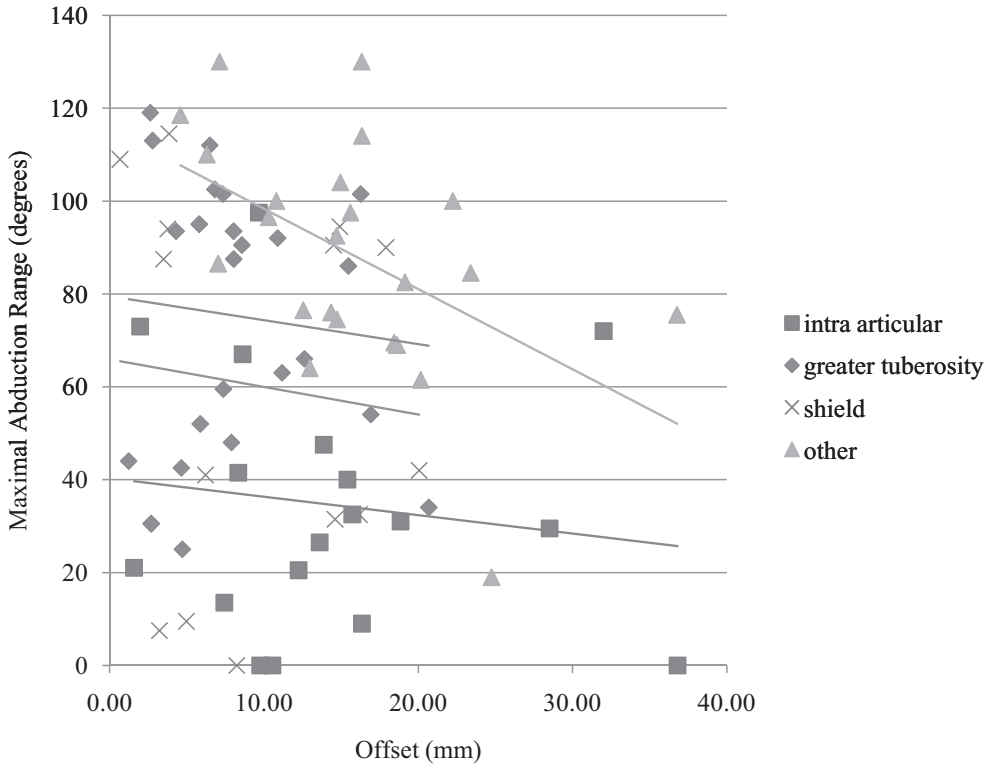
Figure 5.6: Maximal abduction versus the measured offset.

dised, preventing further motion. Fractures with displaced tuberosities show more motion limitations for abduction than for forward flexion. However, when the tuberculum minor is still attached, forward flexion is generally not problematic with regards to impingement. Only when both the tuberculum major and the tuberculum minor displace the maximum bone-determined forward flexion range is reduced.

Interestingly none of the morphological measurements, other than the categorisation of our data, had a predictive value with regards to the maximum forward flexion range for any of the groups. This as opposed to the maximum abduction range where some correlations were found with morphological measurements. Conclusions that follow from the data are that reduced head inclination angle is a relatively strong predictor of a limited abduction range for all types of proximal humerus fractures. Sagittal head angulation was not correlated with the maximum abduction range. Finally, offset of the articular fragment with regards to the intra-medularry axis correlated with the maximum abduction range, but not statistically significant. With the
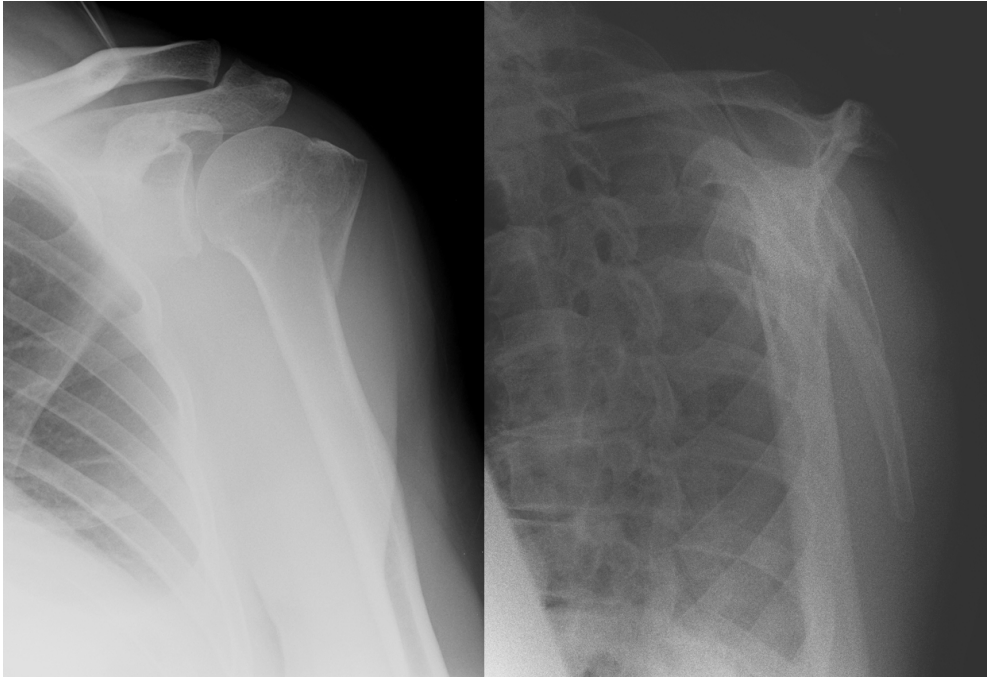
Figure 5.7: AP and lateral radiographs of the proximal humerus fracture also depicted in Figure 5.3. With these radiographs it is difficult to distinguish between the different fragments of the fracture and to predict their influence on the bone-determined ROM.

relatively low p-value of 0.087, we are cautiously optimistic about the results that could be achieved testing with a larger number of CT scans.

Interrupted articulation at the glenohumeral joint as a result of displaced fragments is difficult to detect using traditional radiographs. As an example we have included the AP and lateral radiographs of the fracture that was depicted in Figure 3 (see Figure 5.7). The displaced tuberculum minor causing interrupted articulation in subfigure 3 is not distinguishable at these radiographs. A CT-scan reveals the displaced tuberculum minor. The described ROM simulations of the fracture answer clinically relevant questions and add to the conclusiveness of the assessment.

There are limitations to this study. The humeral epicondyles were not included in the CT scans. Therefore we were unable to measure retroversion of the humeral head. Additionally, we were unable to measure the absolute axial rotation of the humerus. To account for this, we performed ROM measurements for a large range

of elevation planes and used the maximum value as an indicator of mobility. In our opinion, this is a justified metric because patient treatment decisions are based on achievable functional results. A large elevation angle, regardless of the exorotation of the humerus, can be considered a desirable result.

The ROM simulation system does not incorporate soft tissues in the simulations. This entails that the true ROM of the patient will be smaller than the conservative estimate as determined by the simulations. However, the simulator detects collisions of rigid structures and these will also limit the active ROM of patients. In future work we wish to relate the ROM simulations to function.

Zyto et al. demonstrated that conservative treatment of complex proximal humeral fractures is arguably favourable relative to Neer's doctrine of surgical intervention (Zyto et al., 1995, Zyto et al., 1997, Zyto, 1998). Furthermore, Nanidis et al. have demonstrated that outcome and complication rates are similar when treating 3 and 4 part fractures conservatively and operatively (Nanidis et al., 2010). However, being able to predict at least bony functional ROM has not been possible or described in the literature. The results up to now seem to point out that the determination of functional movement using our algorithms could positively augment the decision-making process.

5.5 Conclusion

We hypothesised that computer assisted assessment of bone-determined ROM may be a valuable addition to fracture classification systems. To this extent a study on the effects of fracture morphology on the bone-determined ROM was conducted using a ROM simulator based on CT. The interobserver agreement of two observers using the ROM simulator was excellent. This indicates that, when compared to the interobserver agreement of existing classification systems, patient-specific ROM simulations may be a good alternative in the support of treatment decisions for PHF.

From this study we conclude that intra-articular fractures have the worst prognosis with regards to bone-determined ROM. Fractures with displaced tuberosities show more motion limitations for abduction than for forward flexion. It was shown that a reduced head inclination angle is a strong predictor of limited ROM for all types of proximal humerus fractures. The possible relation between offset and maximum abduction range was not statistically significant. Finally, the measured morphological parameters do not seem to have predictive value for the maximum forward flexion range.

Motion simulation results of the adopted categories are clustered. This suggests that, besides a measure to predict function, the system may also be used to support

classification of PHFs. It seems likely that a combination of a classification system and dynamic patient-specific simulations will result in improved results with respect to outcome prediction. In future work this claim must be validated with a large prospective study that includes a 1-year follow-up and the assessment of function.

6

Visual analysis of multi-joint kinematic data

Peter R. Krekel[1,2], Edward R. Valstar[1,5], Jurriaan de Groot[3],
Frits H. Post[2], Rob G.H.H. Nelissen[1], Charl P. Botha[2,4]

[1] *Biomechanics and Imaging Group, Leiden University Medical Center*
[2] *Computer Graphics, Delft University of Technology*
[3] *Department of Rehabilitation Medicine, Leiden University Medical Center*
[4] *Divison of Image Processing, Leiden University Medical Center*
[5] *Biomechanical Engineering, Delft University of Technology*

Abstract

Kinematics is the analysis of motions without regarding forces or inertial effects, with the purpose of understanding joint behaviour. Kinematic data of linked joints, for example the upper extremity, i.e. the shoulder and arm joints, contains many related degrees of freedom that complicate numerical analysis. Visualisation techniques enhance the analysis process, thus improving the effectiveness of kinematic experiments.

This chapter describes a new visualisation system specifically designed for the analysis of multi-joint kinematic data of the upper extremity. The challenge inherent in the data is that the upper extremity is comprised of five cooperating joints with a total of fifteen degrees of freedom. The ROM may be affected by subtle deficiencies of individual joints that are difficult to pinpoint. To highlight these subtleties our approach combines interactive filtering and multiple visualisation techniques.

Our system is further differentiated by the fact that it integrates simultaneous acquisition and visual analysis of bio-kinematic data. Also, to facilitate complex queries, we have designed a visual query interface with visualisation and interaction elements that are based on the domain-specific anatomical representation of the data. The combination of these techniques form an effective approach specifically tailored for the investigation and comparison of large collections of kinematic data. This claim is supported by an evaluation experiment where the technique was used to inspect the kinematics of the left and right arm of a patient with a healed proximal humerus fracture, i.e. a healed shoulder fracture.
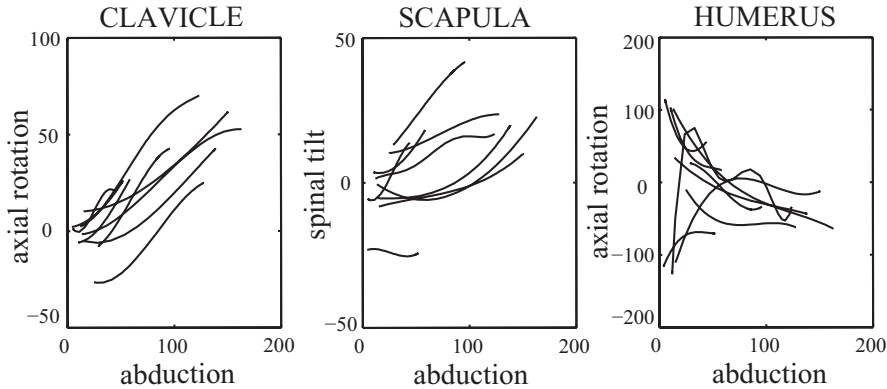
Figure 6.1: An example of three angle-angle plots. These plots show the relation between elevation of the arm (abduction) and other angles of three joints of nine subjects. Image courtesy of Frans Steenbrink.

6.1 Introduction

Kinematic data describes the movement of limbs and is used in biology, sports, orthopaedics and rehabilitation medicine. The data is generally acquired using motion tracking systems, imaging systems or computer simulation. Examples of motion tracking systems are Optotrak (Northern Digital Inc., Waterloo, Canada), which uses optical sensors, and Flock of Birds (Ascension Technology Coorporation, Burlington, USA), which uses electromagnetic sensors. The acquired kinematic data is used to monitor surgical interventions or to help answer fundamental research questions on kinematic behaviour.

Despite the widespread use of kinematic analysis methodologies, creating visual representations of motion data that support clinically relevant conclusions is challenging. The most common method for depicting kinematic output is the angle-angle plot. This is a two-dimensional plot that displays how a certain joint angle relates to another joint angle. See Figure 6.1 for an example of a series of standard angle-angle plots. Angle-angle plots are limited to depicting two parameters, even though joint kinematics are often correlated in three or more dimensions. For complex research questions this may result in a large number of angle-angle plots. For example, one publication by De Groot et al. includes a total of 27 angle-angle plots (De Groot, 1997). In our opinion these plots are functional when exact numerical values and relations are required. However, for the exploration of kinematic data alternative representations may be more informative.

This inspired us to create a system for the analysis of complex, multi-joint kinema-

tic data that gives insight in relationships between joint angles that would otherwise require a predetermined hypothesis. In order to assist this process, we have employed both forward and inverse visual query techniques in our framework. With the former, researchers can inspect the range of motion (ROM) of multiple joints and find the relationships between the available degrees of freedom (DOFs). With the latter, the joint configurations that were used to reach a queried location are extracted, functionality that is useful in investigating for example compensatory kinematics in pathological joints. We believe that this system could eventually lead to new observations and different focus with respect to kinematic coupling of DOFs.

The contribution of this work is a comprehensive new approach to the visual analysis of complex multi-joint kinematic data. To the best of our knowledge, visual analysis techniques have not yet been proposed for this type of kinematic data. Novel characteristics of this approach include the following:

- Our system integrates real-time visualisation and acquisition. In other words, the visualisation process starts during data acquisition, enabling the operator to steer the acquisition process, guided by conclusions drawn from the visual analysis.

- Our forward visual query interface combines interaction and visual feedback in an integrated anatomical representation, allowing users to perform complex queries in a recognisable and therefore straightforward manner.

- We demonstrate the utility of our work on the kinematic data acquired of a proximal humerus fracture patient.

Supporting our main technical contributions, the complete implementation of this approach is available as open source at the following URL:

`http://fobvis.googlecode.com.`

The remainder of this chapter is structured as follows: in Section 6.2 we discuss existing literature on kinematic data visualisation. In the subsequent section we describe our visualisation framework, including the kinematic model and filtering mechanisms that we apply. In Section 2.2.6 we describe an evaluation experiment. For this experiment we recorded the motion patterns of a subject with a healed shoulder fracture and demonstrate that the visualisation framework enables researchers to analyse the recorded motion patterns in great detail. Lastly, we discuss the contributions and limitations of our system and conclude with a prospect on future work.

6.2 Related Work

Much of the research on kinematic analysis finds its origins in gait analysis, the study of locomotion (Whittle, 2006). Many improvements to the standard angle-angle plot originate from this field. For example, by adding a third dimension to the plots, an additional parameter can be visualised (Manal et al., 2005). In addition, by colour coding the graphs, another parameter can be added, resulting in a total of four parameters of a motion recording that can be visualised (Manal and Stanhope, 2004). The drawback of these approaches is that the straight-forward addition of the third dimension unnecessarily complicates the interpretation of the data. Also, using colour to represent a continuous parameter is ill-advised, especially if this channel could later be useful for example to distinguish between patient measurements, a categorical parameter (Mackinlay, 1986).

The work most related to our research is that of Keefe et al. (Keefe et al., 2009). Their visualisation system is an excellent example of how a multiple-view approach effectively shows relationships within kinematic data. Using small multiples they visualise cycles of motion of pig jaws during eating. Although many parallels exist between their and our work, their visualisation technique is specifically targeting sequential data, whereas in our data we are interested in visualising the relationships between multiple connected joints. Similarly, Chen et al. used the approach of small multiples for the cyclic patterns of bat wings during flight (Chen et al., 2007). Although they use many markers on the bats' wings, there is no joint decomposition with subsequent analysis of a multi-joint kinematic model.

With regards to ROM visualisation for the upper extremity there are several examples of applied visualisation techniques. A basic approach is presented by Ct et al., who use 2-D projected stick figures to show the kinematic results of a hammering task (Côté et al., 2005). This visualisation suffices when looking at joint height, but does not reveal the kinematic relationships.

In previous work we presented a technique for visualising ROM of the shoulder joint (Krekel et al., 2006). The described pre-operative planning system visualises the simulated ROM of the glenohumeral joint with a movable prosthesis. Although the comparative visualisation techniques are effective for the glenohumeral joint, these techniques do not hold for the analysis of a multi-joint kinematic chain. The main reason for this is that most joints do not function as ball-and-socket joints.

Van Sint Jan et al. presented an interesting system that visualises the kinematics of multi-joints (Van Sint Jan et al., 1998) . Their work uses computed tomography along with kinematic recordings to link bone morphology of the fingers to kinematics. Their visualisation method is limited to 3-D playback of the kinematics using patient-specific surface models.

Analogue to path planning techniques in robotics, a multi-joint chain can be described in configuration space (Barraquand and Latombe, 1991, Lozano-Pérez, 1990). The term *configuration* refers to a single pose of the chain of joints. The individual joints have a local ROM that determine the total set of possible configurations, i.e. the configuration space. Our system is built around this concept, with separate views and filtering mechanisms for the DOFs of the joints and for the total ROM of the limb.

In the literature, similar visualisation approaches exist, for example Abdel-Malek et al. (Abdel-Malek et al., 2004) and Lenarčič et al. (Lenarčič and Klopčar, 2006), who describe multi-joint kinematic models with accompanying visualisations of the configuration space or reachable arm space. An interesting supplement to these references dates back to 1955, where a similar ROM visualisation technique was used to design aeroplane cockpits (Dempster, 1955). Although these visualisations give insight in the reachable arm space, they do not disclose the underlying kinematic dependencies. To our knowledge, no technique exists that visualises both the DOFs of a kinematic model and the resulting functional ROM.

6.3 Methods

6.3.1 Requirements Analysis

To catalogue the requirements of an improved approach to visualising ROM measurements, we used the Delphi method (Rowe and Wright, 1999). Two human movement scientists and four orthopaedic surgeons of different clinical institutions, reflecting our target audience, were questioned using a list of propositions and a number of example visualisations. The complexity of the propositions varied, ranging from 'Quantifying measurements is more important than visualising them' to propositions as 'I can use this example visualisation to track the progression of a muscular deficiency'.

Important conclusions that followed from this questionnaire were the following:

- Clinicians prefer more intuitive visualisations, whereas human movement scientists prefer visualisations that give access to more quantitative information, regardless of the additional clutter that comes with this information. All of the clinicians indicated that they were willing to use only the most simple visualisation in their conversations with patients, fearing that any visualisation other than a simple shoulder picture would be too difficult to understand for the average patient. To accommodate this requirement, a clear distinction is made throughout this work between visualising a subject's function and visualising the ROM of individual joints.
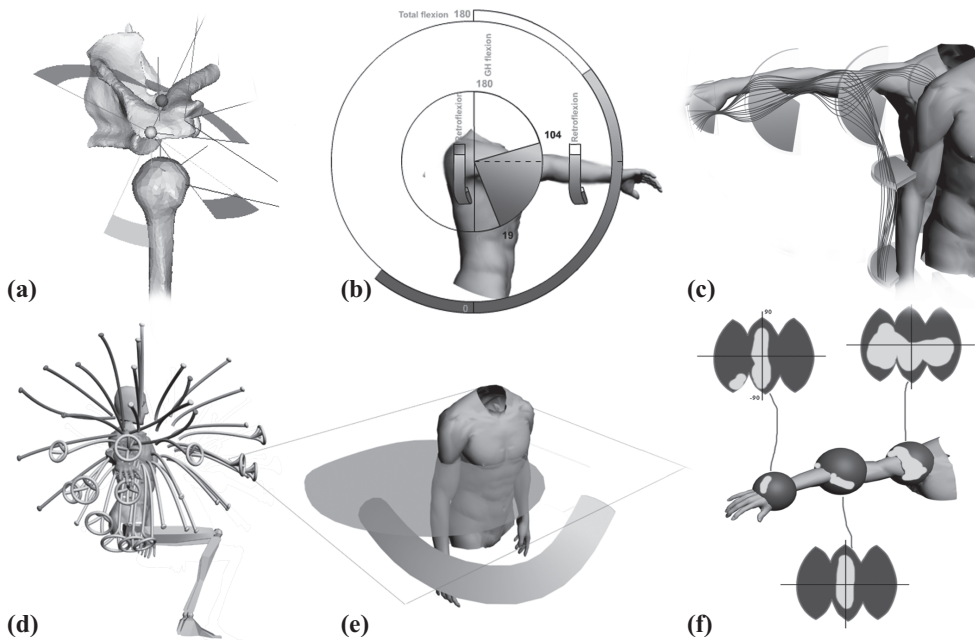
Figure 6.2: Visualisation concepts that were presented to the participants of the questionnaire. Participants were asked to rate several aspects with regards to clarity and usefulness before and after an explanation was given. See Section 6.3.1 for a description of the subfigures.

- With respect to the possible benefits of a new visual analysis system, participants indicated that assessment of pathology, follow-up of patients and communication with colleagues were of foremost importance.

- Due to time constraints, clinicians would be willing to spend only a few minutes analysing the kinematic data. This introduces the requirement that a kinematic visualisation technique has to be fast and intuitive.

- The reachable arm space visualisation by Lenarčič et al. (see Section 6.2), used as an example visualisation, was thought to be very useful. A similar visualisation disclosing more details on the separate joints was expected to fulfil most of the requirements.

Figure 6.2 shows some of the visualisation concepts presented to the participants of our questionnaire. The proposed visualisations were the following (see figure):

a. An integration of the DOF values with the animated bone model representation. We have implemented this technique and discovered that occlusion and continuously changing coordinate systems make this visualisation counterintuitive.

b. A schematic 2-D plot of the various parameters. This concept was eventually extended and implemented in our 3-D Pose View (see Section 6.3.5).

c. Integration of the parallel coordinates plot with the spatial location of the joints. Although this would make the semantics of the plot more intuitive, it was expected that the anatomical location would complicate the visual representation and hence understanding of relations between angles.

d. A segment visualisation with various types of endpoints to depict parameters. This view merges the visualisation of individual joint angles and the total functional ROM. We consider this undesirable because each answers a different set of research questions.

e. Volume visualisation with a slice-viewer and visualisation method to depict trajectories. For this specific application, volume rendering would not contribute any specific advantages. Furthermore, the conversion to volumes would unnecessarily complicate the interactivity of our system.

f. A spherical representation of the joint, mapped to a 2-D plot. Not all joints are spherical joints, making it hard to defend this visual encoding. In addition, this representation only allows for two degrees of freedom (DOFs) per joint.

Although these visualisation techniques were not used, various aspects were extracted and incorporated in the final visualisation system described herein.

6.3.2 Software

The software used to record shoulder motion is FobVis, a package developed by our institution. FobVis is currently built for the Flock of Birds electromagnetic system, but the generic design facilitates the use of other motion tracking systems, for example Optotrak. It has been implemented as a state machine, the transitions between states reflecting the motion tracking procedure described below. Figure 6.3 shows a screenshot of FobVis.

The work described in this article is implemented as a module in the FobVis software and directly uses the recorded data as input for kinematic analysis. Both the FobVis software and the visual analysis module are available as open source.
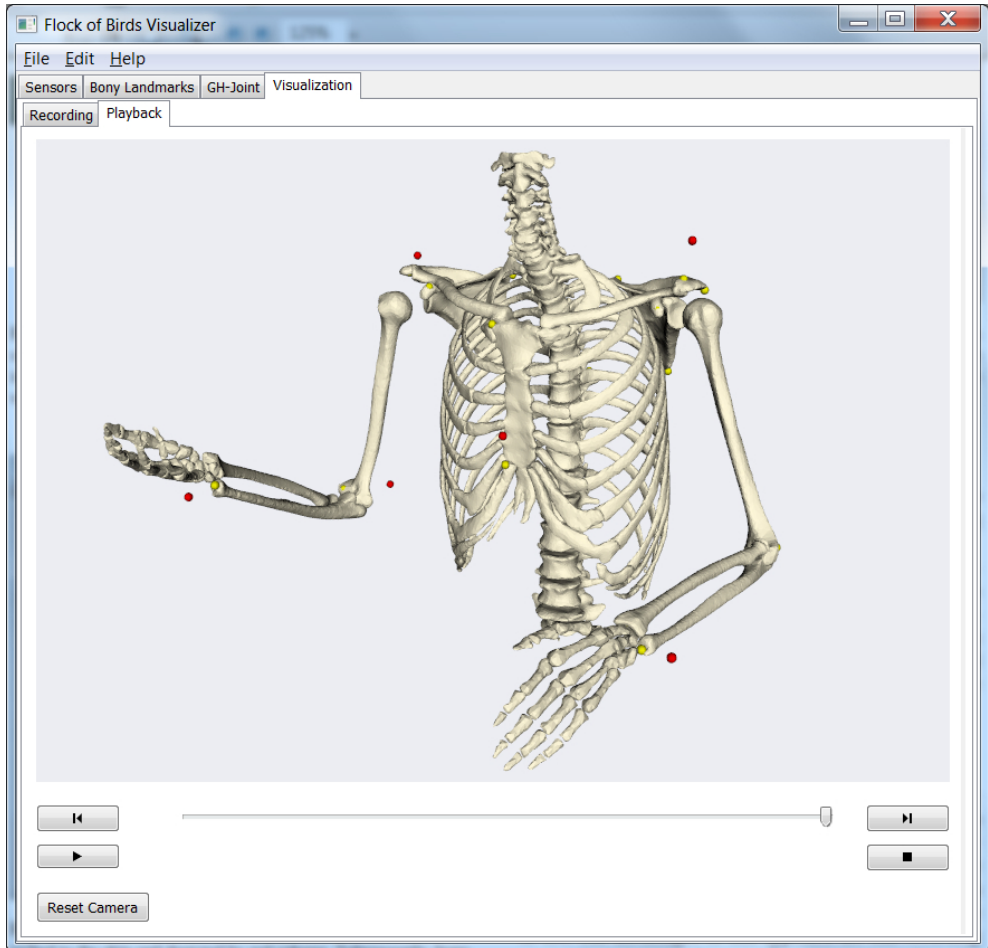
Figure 6.3: The FobVis motion tracking software. Sensors are attached to the skin and depicted by red spheres. Subsequently, bony landmarks are registered relative to these sensors and depicted by yellow spheres. The surface models are rigidly transformed in accordance with the sensors and their respective bony landmarks.

6.3.3 Motion Tracking

Motion tracking was performed using the Flock of Birds motion tracking system. The workflow for recording motion is in accordance with Kontaxis et al. (Kontaxis et al., 2009) and consists of the following steps:

1. Sensors are attached to the body of the subject.

2. The positions of prominent bony landmarks relative to the sensors are registered using a motion tracked pointing device.

3. The subject follows the movement instructions of the researcher, during which the positions and rotations of the sensors are recorded. In combination with the bony landmark positions relative to the sensors this gives sufficient information to track motion of the bones, with a small error due to the sensors being attached to the skin rather than to the bones.

In common motion recording protocols, the subject is instructed to make specific movements that are expected to answer the research questions under investigation. Our technique is based on the principle that as much data should be collected as possible. The acquisition process is closely monitored by the operator, assisted by the real-time visualisations of our system. After the acquisition, the investigator can filter data and focus on the specific type of movements he would like to see. The advantages of this approach are that recording motion is not restricted to specific movements, making the recording procedure less error-prone. In addition, the investigator can pose additional research questions after doing the measurements, as a large collection of motion data is included in the visualisation.

The motion recording system is continuously updated at 25 frames per second, giving immediate feedback to the researcher. This allows the researcher to determine when enough data has been gathered by inspecting the visualisations.

6.3.4 Kinematic Model

Kinematic models of the human body usually consist of a hierarchical structure of kinematic chains. A kinematic chain is a series of linked rigid body segments connected by joints with one or more rotational degrees of freedom. The motion of a kinematic chain is defined by the link lengths and the variation of joint angles. The lengths are assumed to be constant for a given individual, so the postures and motions can be completely described by the joint angles.

Different kinematic models can be used to analyse motion data. We have defined our kinematic model in accordance with the authoritative work on upper extremity
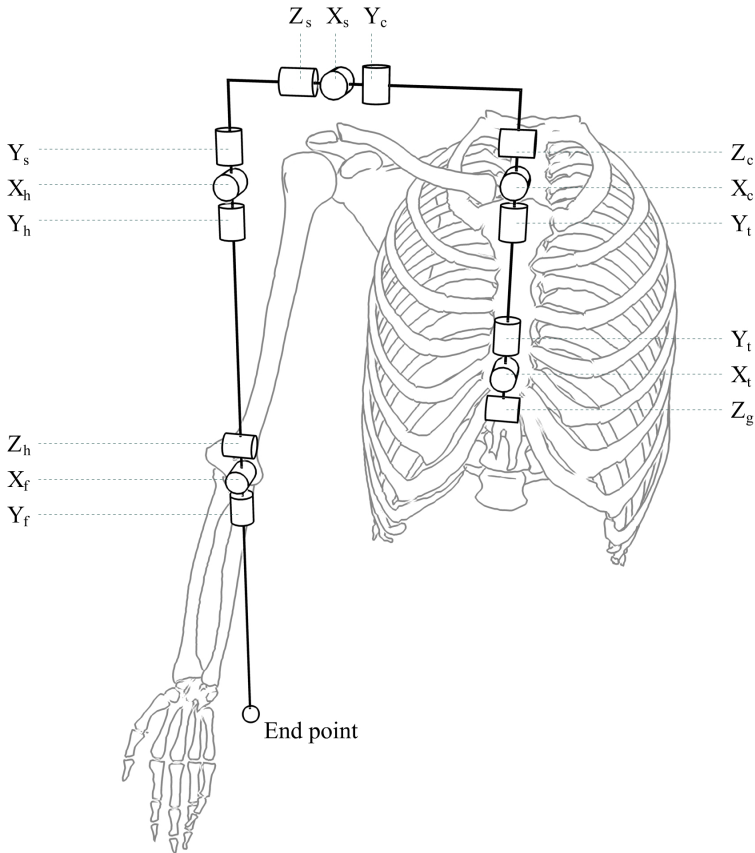
Figure 6.4: Kinematic model as used within our system. The chain of rotations along various axes begins at the spine and terminates at the hand. The character *g* refers to the global coordinate system; *t*, *c*, *s*, *h* and *f* refer to the thorax, clavicle, scapula, humerus and forearm coordinate system respectively. The model is completely described in Wu et al. (Wu et al., 2005).

kinematics by Wu et al. (Wu et al., 2005). The assembly and connectivity of the modelled joints is depicted in Figure 6.4, rotations starting at the first degree of freedom of the spine and terminating at the last degree of freedom of the elbow. Quantified angles are defined relative to the proximal (preceding) joint as well as relative to the global coordinate system. These angles are calculated in real-time as motion data is acquired.
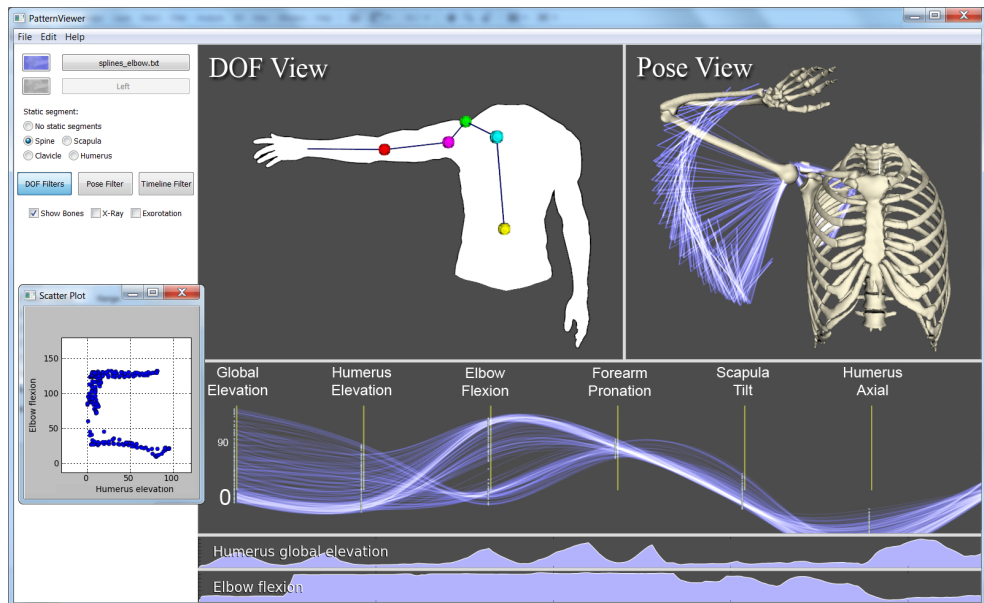
Figure 6.5: A screenshot of the system. The DOF View visualises the individual DOFs of the different joints on demand. The Pose View shows the recorded poses and thus visualises the functional ROM. The parallel coordinates plot visualises the interrelationships between DOFs. At the bottom of the interface 2D plots of data values over time can be added. Lastly, a number of scatter plots can be in visualised in a separate frame.

6.3.5 Visualisation and Filtering

Multiple linked views are used to analyse the kinematic data (see Figure 6.5). The degrees of freedom View, or DOF View, shows the local ROM of each of the DOFs of the individual joints. The Pose View is used to depict the total functional ROM of the multi-joint configuration, as well as spline curves to see a time window around poses. A parallel coordinates plot is used to quantify relationships between the parameters of the kinematic model. In addition, an unlimited number of 2D plots of data values over time can be added. Lastly, scatter plots can be generated. The different views are discussed below.

During acquisition all views are continuously updated, providing interactive feedback on the motion data acquired. Large differences in ROM are noticeable, but generally and especially when working with large datasets, the number of visible poses is too large to disclose valuable information. Visualisation and filtering form an

integrated system that allows the user to analyse and compare large collections of complex kinematic data.

To find interesting characteristics of the data the researcher may want to omit data outside of a given range of a specific DOF, inspect recordings that go through a point in space or select a certain time range of the recordings where something occurred that he found interesting. For this purpose a number of filters were implemented. Filters can be activated or deactivated, depending on the requirements of the intended task. The user interface components of each of the filters are integrated in the visualisation of the kinematic aspect the filter acts upon.

Two motion recordings can be loaded simultaneously, allowing for comparison of datasets. Examples are pre- and post-operative measurements, left and right shoulders or a (bundled) group of patients suffering from the same pathology, compared to an equally large group of healthy subjects. Motion recordings are assigned different colours and adjust their alpha blending in each of the views in accordance with the number of poses that are visible to optimise the amount of information shown.

In the following subsections, we discuss each of the views of our application, first focusing on the chosen visual representation and then detailing the filtering possibilities for that view.

DOF View

To determine how datasets are different from one another, researchers will generally be interested in how the DOFs vary in relationship to other DOFs. In the DOF View these ROM intervals are depicted in the form of joint widgets (see Figure 6.6). Joint widgets can be added by selecting a joint node and indicating which kinematic parameter is of interest via a pop-up menu. The widget shows the minimum and maximum value of the selected parameter for each of the active datasets. To prevent clutter, joint widgets can be collapsed by selecting their centre point.

Besides visualising the ROM of a DOF, joint widgets also function as the user interface element of DOF filters. These are used to hide kinematic data in the linked views, filtering the data based on a selected range of the concerning DOF. The joint widget contains an orange pie-shaped figure, its adjustable size modifying the filtered range. Interaction with the widget updates the linked views, showing only the kinematic data that passed *all* of the DOF filters.

Pose View

In the Pose View the recorded poses are displayed as simple line drawings (see top-right of Figure 6.5). Joints can be disabled, transforming the line drawings to take
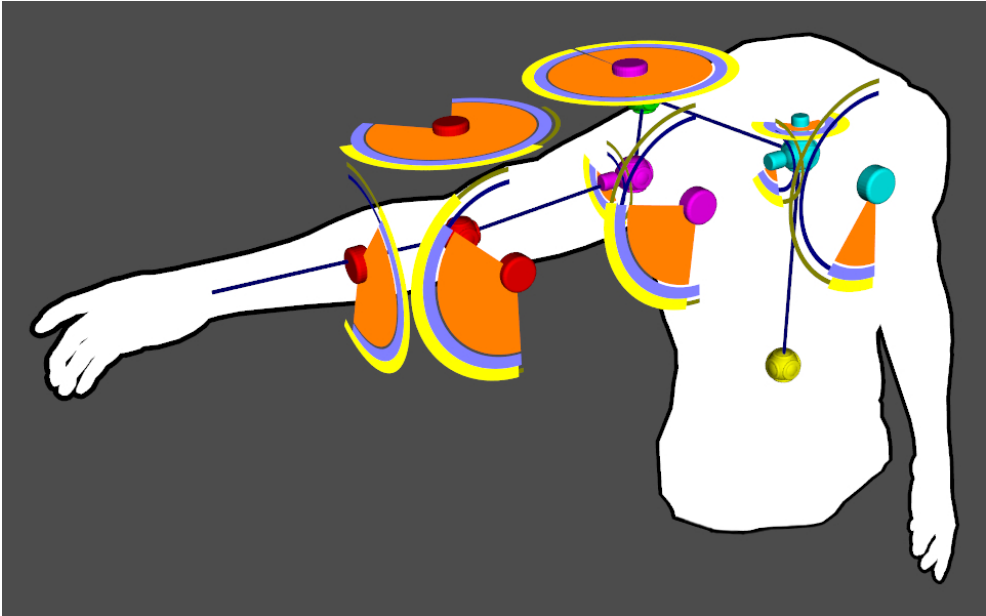
Figure 6.6: The DOF View. Initially this 3D view only displays the silhouette of a human torso with a schematic representation of the predefined connected joints. By selecting joints the user can add visual representations of the ROM of the DOFs as defined by the applied kinematic model. For each of these DOFs a joint widget is added that includes a blue and a yellow bar representing the ROM of two different datasets. The orange pie-shaped parts are DOF filters, used to display only a part of the data in the linked views. To prevent clutter joint widgets can be collapsed by selecting their centre point.

into account the disabled joint and its corresponding DOFs. This allows researchers to analyse what part of the functional ROM can be ascribed to the ROM of specific joints.

Axial rotation is an import kinematic parameter as it is often jeopardised in case of a pathology. Because each pose is represented by a collection of simple lines, the basic visualisation is not capable of visualising the axial rotation of a segment. Optionally, the researcher can visualise axial rotation by replacing the line segments with corkscrew representations that rotate either inward or outward, depending on the sign and magnitude of the axial rotation (see Figure 6.8).

Alternatively, users can choose to visualise the poses as interpolated spline curves. Spline curves originate from a selectable set of joints, their length depending on the size of the adjustable time window. The benefit of spline curves is that they are time
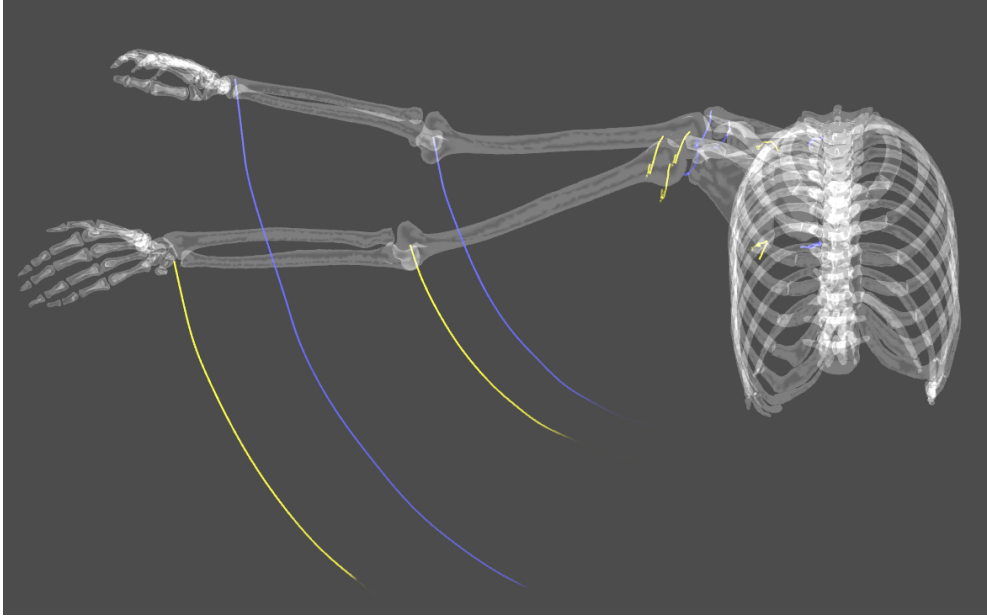
Figure 6.7: Spline curve visualisation. This visualisation can be used to inspect a time window around a specific pose. An advantage of this visualisation method is that it shows how a subject reached for a specific area.
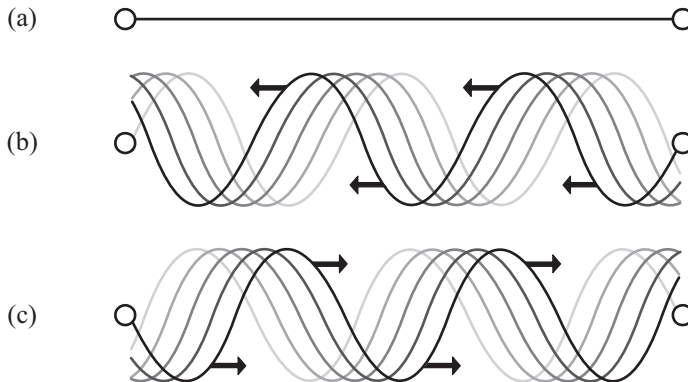
Figure 6.8: Axial rotation visualisation. (a) Segments that consist of a single line, for example the upper arm, have axial rotation that is not visible using the standard line drawing. (b, c) Optionally these segments can be replaced by corkscrew lines, spiralling inward or outward depending on the sign and magnitude of the axial rotation. See Figure 6.9 for an example of this visualisation.

Figure 6.9: The Pose View filter. The hand can be dragged to a position in space. This position is then used for an inverse query to determine how a subject reached for that position. Note that the subject of the yellow dataset reached for the point in a different manner compared to the subject of the blue dataset. Also notice that the blue lines of the upper arm are showing a larger amplitude, indicating that the axial rotation of the upper arm of this subject had a greater magnitude.
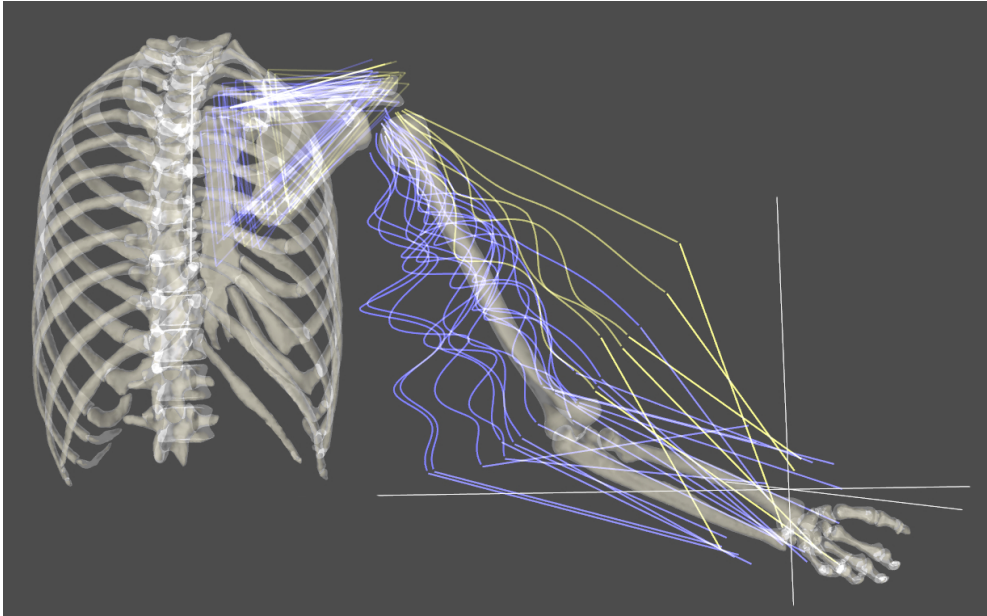
dependent and can therefore be used to analyse the time window around a specific pose. A disadvantage of this visualisation technique is that the view becomes cluttered when using large time windows for large quantities of data.

In the Pose View a skeleton surface model represents an individual pose when required. This includes the visualisation of newly acquired poses during recording and poses that have been selected in the parallel coordinates plot.

The Pose View includes a pose filter that uses the position of the hand of the skeleton surface model. By dragging the hand to different positions, recorded poses that do not come within a scalable sphere around the hand are occluded. In this way the filter can be used to visualise functional information, showing how a subject reached for a specific area. See Figure 6.9 for an example of this filter.

While the hand is dragged to different locations the skeleton surface model snaps to the closest pose that passes the filter. If none of the recorded poses pass the fil-

ter, a simple inverse kinematics model is used to determine the arm position for the new location of the hand. The inverse kinematics model determines the gradient of each of the DOFs and applies weighted rotations in accordance with these gradients. The individual DOFs are limited to the ROM interval as determined from the motion recordings. The inverse kinematics model is only used for real-time visual feedback during interaction.

Parallel Coordinates Plot

The parallel coordinates plot serves as a quantitative confirmation tool for motion patterns found in the DOF View and Pose View. Each recorded pose is represented by a single spline (see Figure 6.10). The view can be configured to accommodate the researcher's requirements, plotting any of the parameters in sequence. The selection and ordering of parameters depends on the research question and aspects of interest found in the DOF View or Pose View.

We adopted curved (cardinal) splines to distinguish multiple splines going through the same values, as was proposed by Graham et al. (Graham and Kennedy, 2003). In combination with alpha blending this enables us to display a large number of poses without losing the focus on relationships between multiple DOFs of the kinematic data. Optionally, the user can switch to linear splines, as these may reveal linear relationships that are not visible when using cardinal splines.

The parallel coordinates view is linked to the other views. Selection of a specific spline will update the Pose View to show the selected pose. In turn, when any of the filters in the DOF View or Pose View are modified, the parallel coordinates view is updated.

2D Plots

In addition to the above views, 2D plots of data values over time can be added (see Figure 6.10). Besides the informative aspect of these 2D plots, the researcher can use them as a timeline filter. Highlighting a range in one of the 2D plots causes the data outside of this range to be hidden. In practise this filter is frequently used complementary to a DOF filter. The latter filters a selection range of the DOFs, whereas the timeline filter allows selection of one of the intervals that passed the DOF filter.

Scatter Plots

Scatter plots can be generated by right-clicking between two axes of the parallel coordinates plot. All scatter plots are continuously updated, thereby only showing the recordings that have passed the active filters. Scatter plots are capable of revealing
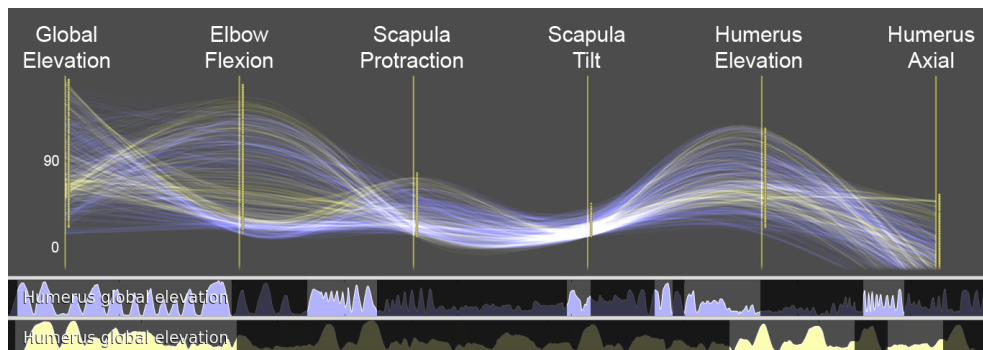
Figure 6.10: Parallel coordinates plot for two sets of motion recordings. The plotted parameters can be customised. Below the parallel coordinates plot are two 2D plots of a specific parameter, in this case global elevation, over time for each dataset.

more complex relationships than possible with the parallel coordinates plot. The disadvantage of using scatter plots is that they can only show two parameters at once. As such, a scatter plot is comparable to angle-angle plots.

6.4 Evaluation

An evaluation experiment was performed with a patient who suffered a proximal humerus fracture injury. This is a complex fracture where the shoulder part of the upper arm shatters into multiple parts, each connected to a tendon of the different muscles of the rotator cuff, i.e. the muscles that provide shoulder stability. After the fracture occurred the shoulder was operated on to reconstruct the normal anatomy. The patient was seen eight months after trauma. In this time period the formerly fractured shoulder regained similar ROM as compared to the healthy opposite side.

To demonstrate how our system can be employed to analyse the kinematics of these fractures we used the Flock of Birds system and instructed the patient to perform multiple elevation tasks in various manners. This included a crouched and extended attitude, forward elevation (flexion) and sideways elevation (abduction). Subsequently, the resulting motion recordings were analysed using our system.

No literature is available describing the kinematic changes for this specific type of injury. However, in normal shoulder kinematics the scapula (the shoulder blade) moves in unison with the humerus (the upper arm bone) during an elevation task. This is called the scapulo-humeral rhythm. In healthy subjects this is a near linear relationship where for every degree of elevation the scapula upward rotation increases
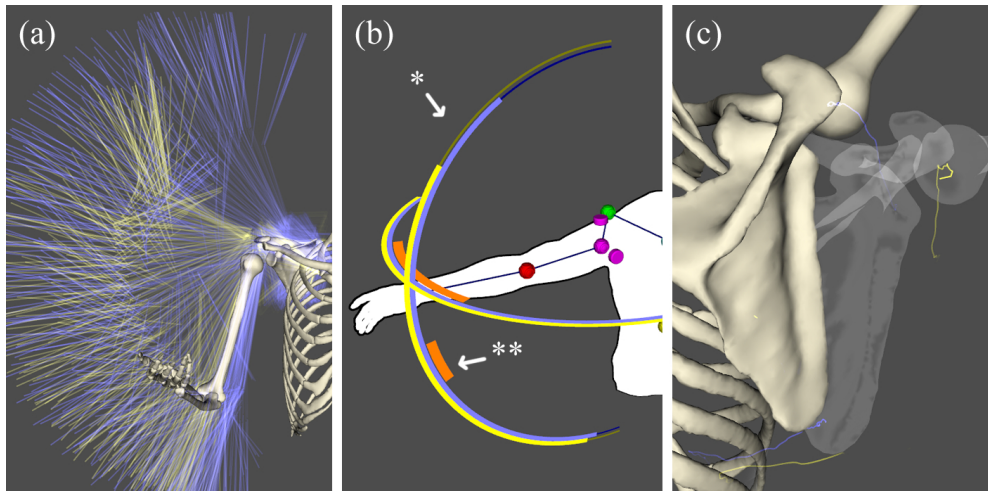
Figure 6.11: Approach to answering the research questions, further explained in Section 6.4.

with ±0.5 degrees (Ebaugh et al., 2005). With this experiment we wanted to assess whether this relationship still holds for the healed shoulder.

In summary, the research questions were:

1. Is there an impairment, and if so, where is it located?

2. Has the scapulo-humeral rhythm of the formerly fractured side changed?

The steps followed to find the answers to the research questions are depicted in Figure 6.11. The Pose View (Figure 6.11a) demonstrates that the ROM of the healthy side is larger than the ROM of the formerly fractured side. The difference in ROM is also evident from the DOF-view (Figure 6.11b, *-mark). Using the DOF filters we adjust the visible elevation interval (marked **) and restrict our data to a specific elevation plane to allow for comparison of the two recordings. Subsequently, the different scapulo-humeral rhythm becomes visible, both by means of the surface models and by means of spline curves. To quantify the difference we inspect the parallel coordinates plot seen in Figure 6.12.

From this analysis we conclude that there is indeed an impairment. Interestingly, the deficiency does not just find its origins in the formerly fractured humerus, but also in the mobility of the shoulder blade. A possible reason for this can be the experience of pain or increased muscle tension.

Secondary to the above, the visualisation demonstrates that the scapula of the formerly fractured side does not move in unison with the humerus. Specifically, we
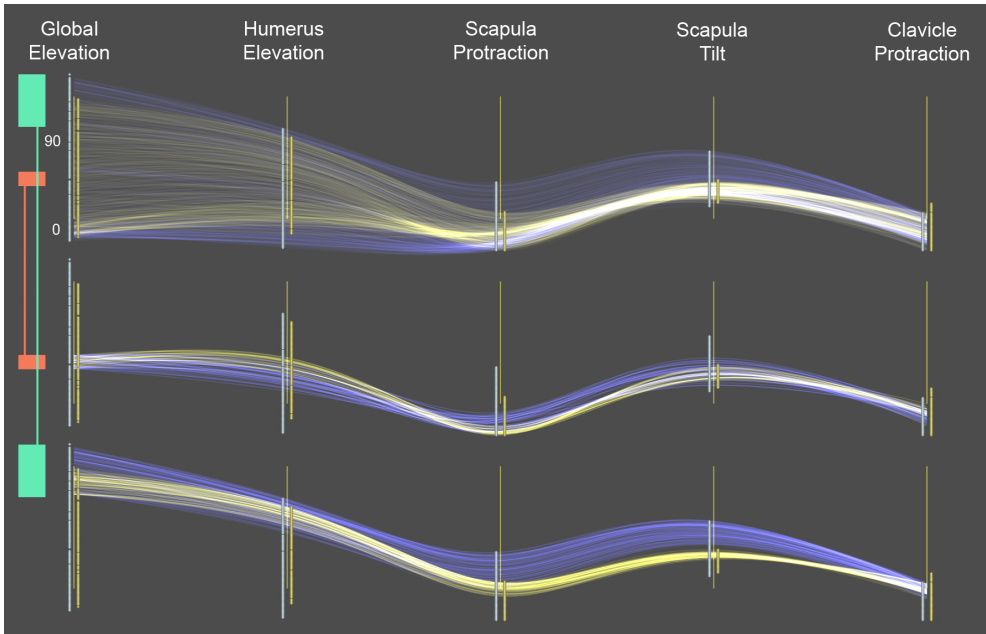
Figure 6.12: Parallel coordinates plot of the mirrored formerly fractured shoulder (yellow) and the healthy shoulder (blue). The top subfigure shows the complete collection of splines, each one representing a recorded pose. The remaining subfigures show the same plot with different DOF filters for the global elevation parameter. The filters are visible on the left of the image. Notice the different values of scapula protraction and tilt at different global elevation angles, indicating that the scapula hardly compensates for the loss of humeral ROM.

conclude that the scapulo-thoracic rhythm of the right shoulder deviates from that of the left shoulder in that scapula protraction and tilt lag behind of humeral elevation.

A limitation we encountered during this experiment is that the limited accuracy of bony landmark registration may result in an offset for the coordinate systems or segment lengths. As was shown by Karduna et al. (Karduna et al., 2001), this inaccuracy does not prevent analysis of motion patterns of individual datasets. However, when comparing multiple datasets as we did in this evaluation experiment, inaccuracy may lead to a relative offset in the coordinate systems used for kinematic analysis.

An involved orthopaedic surgeon later stated that he was impressed with the visualisation and speed of the system. His feedback was valuable for the continuation of this research.

6.5 Conclusions and Future Work

In this chapter we have presented a novel visualisation system for the analysis of kinematic recordings for the upper extremity in combination with a new method of data sampling. The system currently supports six visualisation techniques that are collectively used to filter motion data and inspect relationships between the various DOFs. Although designed for the upper extremity, the presented techniques can be applied to other multi-joint chains.

The benefit of our visualisation system is that users can analyse kinematic recordings without predetermined hypotheses. It allows users to find interesting patterns that could otherwise only be found through a large number of angle-angle plots. Using the step-by-step approach described in our evaluation experiment the majority of kinematic research questions can be answered.

As was shown in the evaluation experiment, the visual analysis technique is effective for comparison of two recordings, bearing in mind that inaccuracy of the motion recordings may lead to incorrect representations. We are aware that these inaccuracies affect the kinematic analysis, but wish to emphasise that this problem also holds for conventional kinematic analysis. In addition, we have shown that our visualisation system is robust to these errors to a certain extent.

An interesting extension of the system would be to incorporate acquisition hints based on an automatic comparison of the acquired data with a collection of kinematic measurements. In this way the kinematic measurements themselves can zoom in on interesting characteristics, thereby not only relying on the assessments of the researcher.

An important message of this work is that kinematic behaviour requires a combination of visualisation and filtering techniques, as was demonstrated with our system. The modular design of our system allows for the implementation of additional filters and visualisation methods and raises the question whether this work should be taken one step further. It is conceivable that modular approaches commonly seen in image processing may be applicable for kinematic data, even though image data and kinematic data are of a very different nature. Future work includes the development of a data-flow network editor where filtering and visualisation modules can be connected to produce a specific kinematic visualisation.

7

Clinical applications

Peter R. Krekel[1,2], Anne J.H. Vochteloo[1], Michiel A.J. van de Sande[1],
Jochem Nagels[1], Rolf M. Bloem[3], Rob G.H.H. Nelissen[1]

[1] *Department of Orthopaedics, Leiden University Medical Center, The Netherlands*
[2] *Computer Graphics, Delft University of Technology, The Netherlands*
[3] *Department of Orthopaedics, Reinier de Graaf Gasthuis, The Netherlands*

Abstract

This chapter describes the application of the range of motion simulation system presented in Chapter 3, 4 and 5 to three orthopaedic problems. Three case reports are presented, followed by a general discussion. The case reports demonstrate the applicability of the simulation system in orthopaedic decision-making.

The first case concerns a 58-year old female patient who reported in the Emergency Department with a Neer 3-part proximal humerus fracture. Using the range of motion simulation system and a CT scan we analysed the fracture and calculated the correction required to prevent impingement. The fracture was reduced and stabilised by a locking plate, realigning the medialised and internally rotated humeral shaft. Range of motion limitations due to bony impingement visible in the simulations of the pre-operative CT scan had mostly disappeared in the simulations of a post-operative CT scan.

The second case report concerns a 62-year old female patient who had undergone total hip replacement surgery. Eight months after the operation she reported with pain, a constant feel of instability of her replaced hip joint and a 'clicking'-sound that she heard during movement patterns that included a large abduction angle. Analysis of a CT-scan using the range of motion simulation system revealed that the acetabular cup component was malaligned and caused impingement with respect to the femoral neck, resulting in subluxation. The patient preferred not to undergo revision surgery, but rather prevent the extreme movements she made. She indicated that the range of motion simulations helped her to better understand the problem and to avoid the motion patterns that lead to the subluxation and subsequent discomfort.

The last case report in this chapter describes the technical and clinical results of two consecutive arthroscopic shavings of an osseous cam protrusion in a 50-year old male patient with complaints of femoroacetabular impingement. Twelve weeks after the first arthroscopic shaving, the patient still experienced groin pain. Using the range of motion simulation system the kinematics of the hip joint were analysed. Bone impinging at the hip joint during the range of motion simulations was was removed in a second arthroscopic procedure. Six months post-operatively the patient is almost pain free and has regained range of motion to a functional level.

7.1 Case report 1: Range of motion implications of a proximal humerus fracture

7.1.1 Introduction

Proximal humerus fractures (PHF) have an incidence rate of approximately 73 in 100.000 and are more prevalent in elderly (Lind et al., 1989, Van Staa et al., 2001). Depending on the severity of the fracture, several treatment options are proposed, ranging from conservative treatment to shoulder arthroplasty. The decision is often based on factors such as age and patient expectations, on assessment of radiographs or computed tomography (CT), as well as on the application of different fracture classification systems presented in the literature (Codman, 1934, Neer, 1970, Hertel et al., 2004). However, the classification systems have been much disputed for their reproducibility and effectiveness in predicting outcome (Sidor et al., 1993, Siebenrock and Gerber, 1993).

The implications of treatment decisions, i.e. surgical or conservative treatment, in combination with the subjectivity of the PHF classification systems encouraged us to investigate whether or not a computerised dynamic assessment of the fracture adds to the decision-making process in the treatment of PHFs. A critical aspect in the prediction of outcome of PHFs is the altered (post-trauma) bony morphology, leading to a variety of conditions of which loss of Range of motion (ROM) and persistent pain are most relevant. Both can be related to impingement of bone at the shoulder joint. In this case report we demonstrate the clinical use of our dynamic ROM simulation system in a relative young patient with a Neer 3-part humerus fracture.

7.1.2 Case description

The patient was a 58 years-old, previously healthy woman that fell from her bike. She was presented at the Emergency Department of our hospital with a painful right shoulder. Physical examination revealed a painful, slightly swollen shoulder with ecchymosis. There was no apparent neurovascular injury. The X-ray of her shoulder (see Figure 7.1) showed a 3-part PHF. No other fractures or abnormalities were diagnosed.

In this case radiographs alone could potentially lead to misdiagnosing this fracture as a 2-part PHF with only slight medial displacement of the humeral shaft. The additional use of CT imaging revealed a 3-part fracture with significant medial displacement of the humeral shaft of 23 mm while it was also 38° internally rotated with respect to the humeral head. Additionally, the CT data was loaded into the ROM simulation system that was described in detail in Chapter 3 of this thesis.
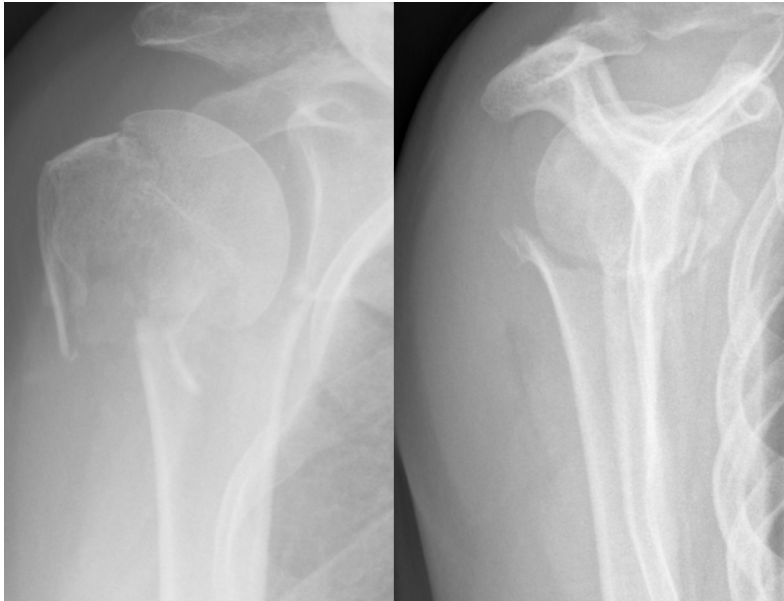
Figure 7.1: Pre-operative AP and lateral radiographs of right shoulder. Only with the use of a CT-scan the 3-part PHF could be fully appreciated.

Pre-operative simulation of ROM, assuming the fracture would have healed in post-traumatic configuration, indicated that the available range of external rotation in 0° of adduction would be limited to only 4° due to the medialisation and rotation of the humeral shaft. According to the ROM simulations the limitation of external rotation would decrease to 0° beyond 45° of abduction, giving rise to the question whether this limitation would create blockade for external rotation. The ROM simulations did not show risk of impingement between the greater tuberosity and the acromial arch (see Figure 7.2).

Initially, it was decided to treat this fracture conservatively, because the predicted deficiency in ROM would not limit activities of daily living. At radiological follow-up, after the first week of immobilisation, secondary displacement of fracture occurred, with further medialisation of the humeral shaft. This deterioration was probably due to muscle pull at the fracture elements by teres minor and pectoralis major muscles. After the secondary fracture displacement it was decided to perform open reduction and internal fixation, using an angular stable locking plate.

Using a deltopectoral approach, the greater tuberosity was reduced and the medialisation and rotation of the humeral shaft were corrected. The reduced fracture
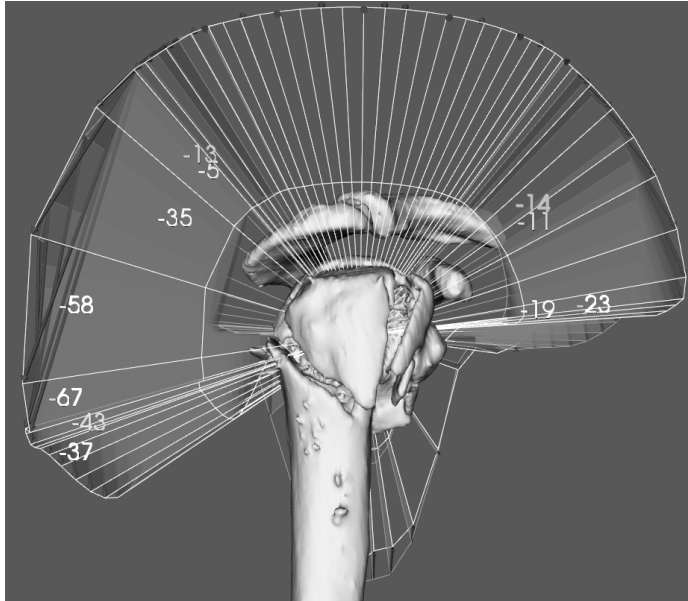
Figure 7.2: Bone-determined ROM simulation using the pre-operative CT data. A comparison is made with ROM simulations of a healthy subject (coloured surfaces and number of degrees). Using this simulation we found a large ROM deficiency for external rotation and a relatively small deficiency for forward flexion. There is no impingement of the tuberosities with the acromial arch.

was fixed with a angular stable locking plate (Litos Tifix, Hamburg, Germany) (see Figure 7.3).

Assisted active forward flexion and circumduction of the shoulder was initiated immediately after surgery. After 2 weeks active physiotherapy was allowed with a maximum forward flexion of $90°$ and maximum external rotation of $20°$. After 6 weeks unrestricted active shoulder training was started.

7.1.3 Results

Post-operatively, ROM simulations indicated that external rotation in $0°$ of adduction was now limited to $20°$. Beyond $20°$ of abduction no limitation of external rotation was observed. This is shown in Figure 7.4. In accordance with the pre-operative simulations, no impingement of the greater tuberosity occurred in this simulation. Follow-up of fracture healing with plain X-rays showed normal fracture healing without secondary displacement or early signs of avascular necrosis.

Figure 7.3: Post-operative AP and lateral radiographs of right shoulder. Reduction of the greater tuberosity and correction of the medialisation and rotational displacement of the humeral shaft was achieved using an angular stable locking plate.

Twelve weeks post-operatively the following ROM was obtained: active forward flexion was $110°$, external rotation in $0°$ of adduction was $15°$ and external rotation in $90°$ of abduction was $30°$. Passive ROM revealed no differences in joint mobility between the sound and the healed shoulder.

7.2   Case report 2: Hip prosthesis luxation analysis

7.2.1   Introduction

Dislocation of total hip prostheses is a relatively common complication in total hip arthroplasty. In a study by Phillips et al. the incidence of hip dislocation after primary hip replacement was reported to be 3.9% (Phillips et al., 2003). The risk of dislocation is highest within the first three months and is reduced over a period of one year (Lindberg et al., 1982).

When a dislocation of prosthesis components occurs this may be attributed to the alignment of the prosthesis components, but also to other causes such as cognitive
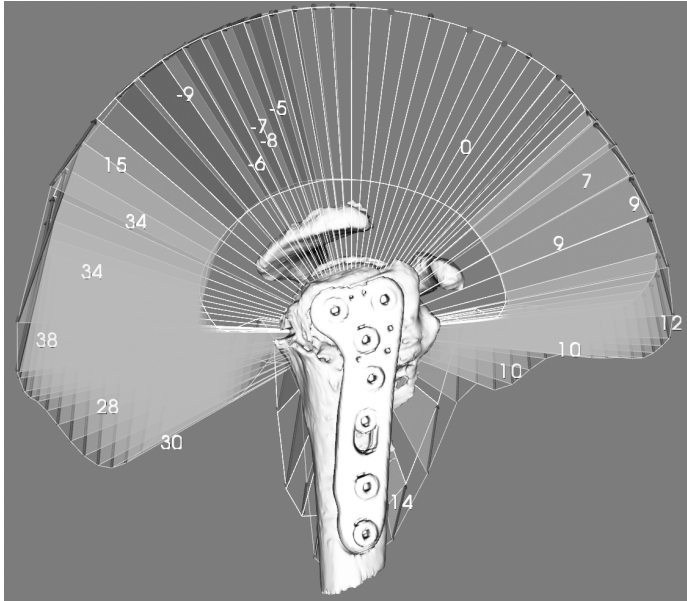
Figure 7.4: Bone-determined ROM simulation using the post-operative CT data. A comparison is made with the pre-operative ROM simulations. Many of the ROM limitations caused by the morphology of the fracture have been alleviated, as depicted by green surfaces. The change of bone-determined ROM ranged is 38° for backward flexion and 12° for forward flexion.

problems of the patient or soft tissue problems. Identification of the reason for dislocation is important, since only in the case of malalignment of prosthesis components a revision operation may prevent further dislocations.

Assessment of prosthesis alignment and its possible cause for hip dislocation is generally performed using static radiographs and CT-scans, even though the dislocation is a dynamic process. In this case report the ROM simulation system is used to dynamically evaluate the risk of dislocation of a hip joint with a total hip prosthesis.

7.2.2 Case description

A 61 -year old female patient reported with greater trochanter and groin pain and a clicking sensation in her artificial hip. She had a total hip replacement 8 months earlier, following the diagnosis of osteoarthritis. When she consulted the clinic she reported that the clicking sensation in the hip occurred spontaneously 6 months after surgery, and was present while rising from a chair, while walking with firms steps

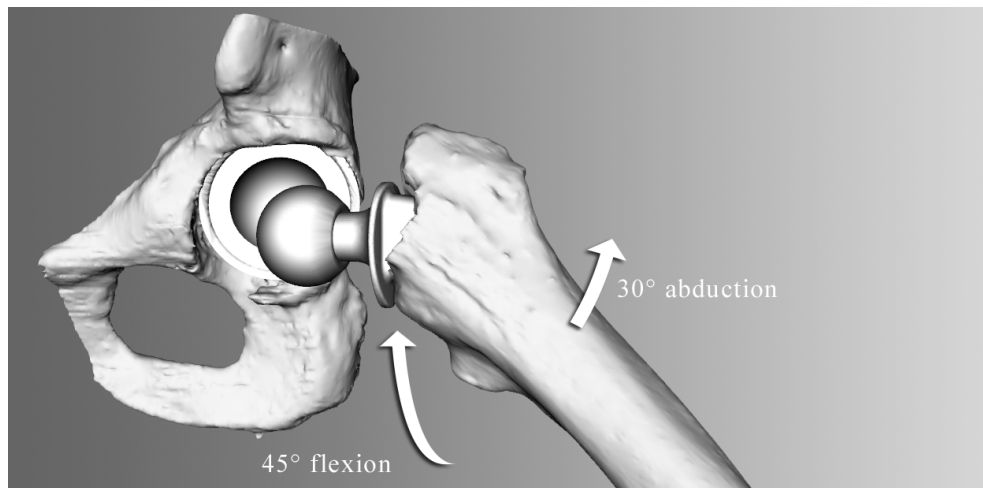**Figure 7.5:** ROM simulation of the hip joint. According to the simulations dislocation occurred a combined movement of 45° of flexion and 30° of abduction.

and while doing her Yoga exercises (especially during the Buddha sitting position). During this click, she had an uneasy feeling about her hip. She was active, could walk for an unlimited distance, if the painful clicking did not occur. Professionally, she worked as a teacher. At clinical examination her legs showed equal leg length. The hip excursions were extension / flexion 0° / 120°, abduction / adduction 40°/0°/30° external/ internal rotation 45°/0°/40° degrees respectively. The clicking sound could be reproduced in a combined flexion, abduction and external rotation movement. The patient did not have complaints regarding the contra-lateral joint.

Radiographic analysis using X-ray photographs and CT showed a cup inclination of 65° and 40° of cup anteversion. With the CT data ROM simulation was performed to further assess the risk of luxation of the prosthesis.

7.2.3 Results

Analysis of a post-operative CT-scan using the ROM simulation system confirmed that the acetabular cup prosthesis was malaligned and caused impingement at 45° of flexion and 30° of abduction (see Figure 7.5). The simulations predicted that posterior dislocation would occur beyond a combined movement of 30° of abduction and 45° of flexion.

Although the simulations indicated that some improvement could be gained by repositioning the acetabular cup, the patient did not prefer to have revision surgery.

However, the ROM simulations helped her to better understand the 'mechanical' hip problem, thus she could avoid making the motion patterns that lead to the subluxation of the hip (i.e. the clicking) discomfort.

7.3 Case report 3: Range of motion implications of femoroacetabular impingement

7.3.1 Introduction

In femoroacetabular impingement (FAI), deformations of the femoral head or the acetabular rim lead to bony impingement, resulting in limited hip motion, pain and progressive damage to the labrum. Recent work suggests that FAI may lead to osteoarthritis (Ganz et al., 2003). Although the etiology of FAI is still unclear, a variety of causes are described, such as excessive sporting activities and post-traumatic or congenital deformities (e.g. developmental dysplasia of the hip) (Leunig et al., 2005).

Two types of FAI are recognised; the cam type and the pincer type. When the acetabular rim shows deformations, this is referred to as a pincer type FAI. Cam type FAI refers to deformations of the femoral head. Cam and pincer individually reduce the space for movement and lead to FAI symptoms. The two types are reported to occur simultaneously in 86% of patients (Beck et al., 2005). However, recent evidence indicates that cam and pincer hips are distinct patho-anatomic entities (Cobb et al., 2010). Treatment options vary and include surgical dislocation and arthroscopic surgery. Satisfactory outcome is reported to range from 90% to 100% for arthroscopic management (Larson and Giveans, 2008, Philippon et al., 2009) and from 68% to 80% for open surgery (Beck et al., 2004, Krueger et al., 2007).

Multiple imaging modalities are used for diagnosis and assessment of FAI (Beall et al., 2005, Tannast et al., 2007b, Beaulé et al., 2005, Nötzli et al., 2002). However, these image modalities are static and therefore do not provide sufficient insight in the dynamic spatial relationship of the femoral head and acetabulum. Instead, a dynamic diagnostic approach should be used, such as presented by Tannast et al. (Tannast et al., 2007a).

In the case of a failed primary surgical correction of FAI, the decision whether to perform a second operation is based on considerations regarding the altered expectations of the patient in combination with the limited chance of improvement. In addition, the risk of further weakening the femoroacetabular joint must be assessed, as it has been shown that bone strength is greatly affected when large amounts of bone are removed from the femoral head (Mardones et al., 2005). If the outcome of primary management is unsatisfactorily, this is frequently due to persisting impinge-

Figure 7.6: Pre-operative AP and lateral radiographs.

ment (Philippon et al., 2007). Additional evaluation instruments may support further treatment decisions.

In this case report the ROM simulator is used to analyse the bone-determined ROM of a hip joint. From this analysis motion patterns that may lead to FAI symptoms for a particular patient can be determined.

7.3.2 Case description

The patient was a 50-year old male with a progressive painful right hip since the last 5 years. Work and sports activities were limited due to the hip pain. Limping became more apparent the last year and pain forced him to stop walking after 5 minutes.

Physical examination revealed pain with rotation in 90° of flexion. Flexion beyond 100° was not possible. Internal rotation was limited to 20°. External rotation was not impaired. The anterior impingement test was positive.

Radiographs unveiled a cam deformity at the medial side of the femoral head and mild degenerative changes on the acetabular side (see Figure 7.6 and 7.7). During arthroscopy the suspected cam lesion was seen, additionally we saw an intact labrum and mild degenerative changes of the cartilage of the antero-lateral part of the acetabulum, Outerbridge classification I-II (Outerbridge, 1961). The cam lesion was shaved off. Partial weight-bearing was allowed directly after surgery, followed by full weight bearing after 6 weeks.

The arthroscopic correction was only marginally successful as pain recurred 12 weeks after surgery. Minimal improvement in daily work and walking distance was
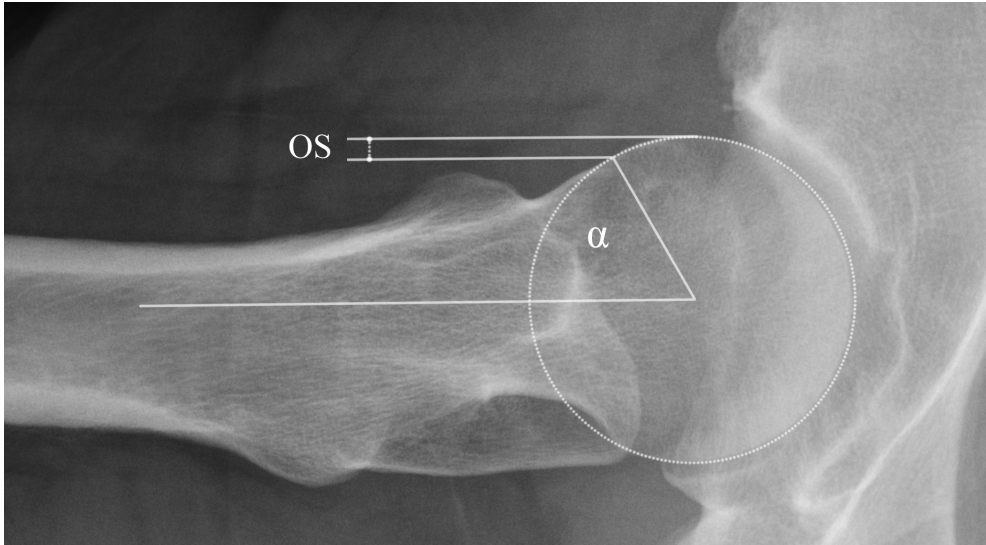
Figure 7.7: Axial view of the femur, showing an increased alpha angle (a = 62°) and decreased head-neck offset (OS).

seen. Using a regular CT scan we determined whether a sufficient portion of the cam protrusion had been shaved off. This seemed to be the case. Subsequently, it was decided to simulate the ROM of the patient in order to gain insight in the kinematics of the joint. Using the ROM simulation system the CT scan of the hip joint was analysed.

According to the simulations the risk of impingement was small in pure flexion and pure abduction. However, 45° of a combined flexion and abduction motion was predicted to lead to impingement (see Figure 7.8). The available range of internal rotation at 90° of flexion was 15°, compared to 35° (±12°) in healthy hip joints as found by Tannast et al.. (Tannast et al., 2007a).

A second arthroscopy of the affected hip was performed during which the remaining osseous rim on the femoral head was shaved off.

7.3.3 Results

Six months after the procedure, the patient is almost pain free and has regained a pain-free functional ROM. Limping had disappeared and he could walk pain-free. Informed consent for a CT scan was obtained for evaluation, in which the ROM simulations showed that impingement was absent (see Figure 7.9 and 7.10).
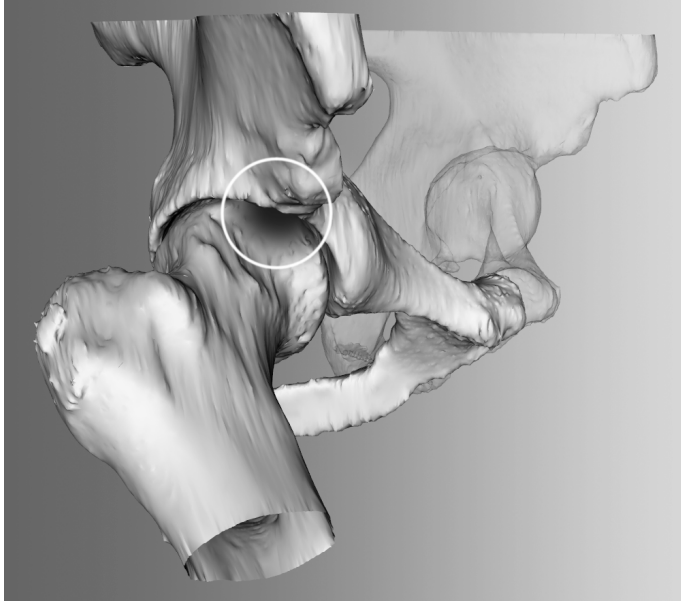
Figure 7.8: ROM simulations of the hip joint. The pose of the femur is adjustable. When impingement is detected, the femur is colored red.

7.4 Discussion

In this chapter, three applications of the ROM simulation system were described, demonstrating its potential as a dynamic assessment tool in orthopaedic decision-making. This new technique may provide the surgeon with a better tool to predict surgical success. Restoration of ROM, besides sufficient pain relief, should play a central role in choosing different treatment modalities. The ability to choose patients that may benefit from surgery in an early stage of the treatment protocol may not only improve functional outcome scores after surgically treated, but also provide for better informed consent.

There is an ongoing discussion whether or not to operate on three and four-part PHFs especially in the elderly patient as sufficient proof from large prospective randomised clinical trials is still lacking. Functional outcome and patient satisfaction varies greatly and depends on multiple parameters. Important parameters are the amount and direction of displacement and the necessary reduction of fragments during surgery. These are patient-specific parameters and are difficult to determine using static modalities such as radiographs and CT. The described dynamic diagnostic ROM simulation system helps in making the decision for conservative or surgical treatment
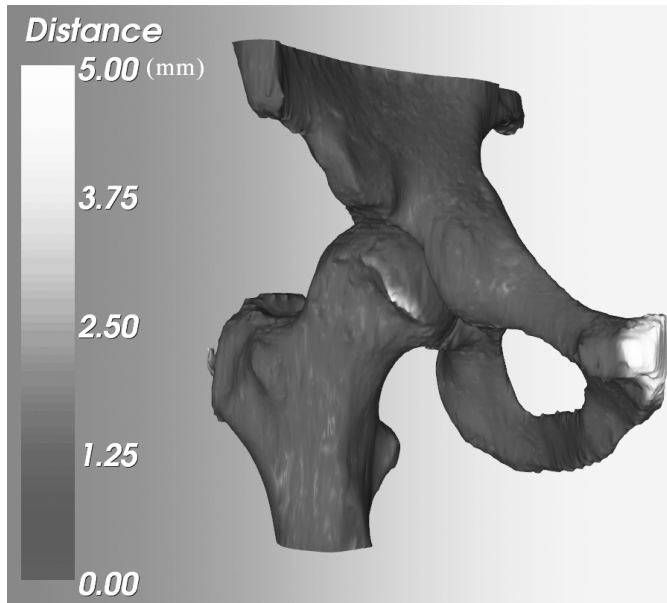
Figure 7.9: Difference in the bone models that are extracted from the CT data before and after the second arthroscopic shaving. This visualisation indicates which part of the femoral head has been shaved off during the second arthroscopy. Point distances are in millimetres. The pubis is highlighted because of a difference in the scanned area.

of a PHF. The simulation of post-trauma function was indicative of functional outcome and supports our claim that the system may be used to facilitate the treatment decision regarding these fractures.

In total hip replacements, revision surgery is demanding for the patient. The decision whether or not to revise a prosthesis should be carefully considered, especially in the case of dislocations where multiple causes can be discerned which are not always related to the interrelation between the femoral head and acetabular cup. In our case we were capable of demonstrating that the simulated risk of dislocation corresponded with the discomfort of the patient and the 'clicking'-sound that was heard during the physical examination. The patient opted not to undergo revision surgery. However, the visual representation of the dislocation was helpful for her and allowed her to understand what motion patterns were causing the discomfort. This indicates that besides supporting treatment decisions, the simulation system can also be used to explain clinical problems to patients.

Our case study on FAI demonstrates the relevance of dynamic assessment when
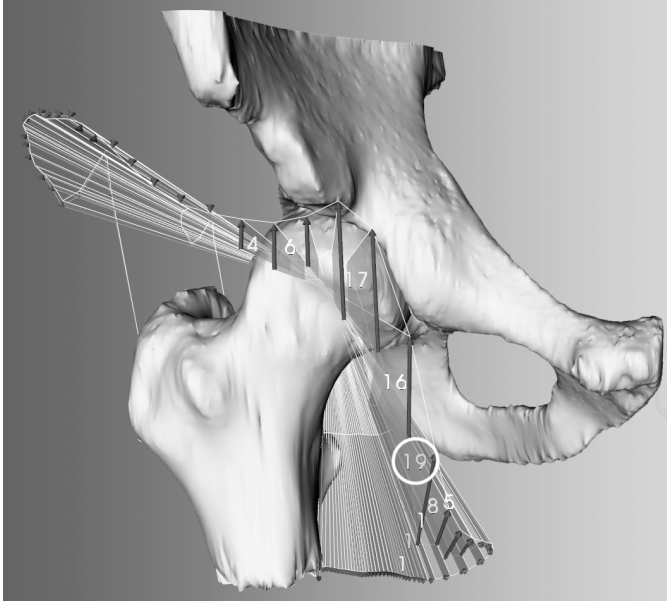
Figure 7.10: ROM simulation results using the post-operative CT scan. This visualisation depicts the outlines of the ROM as constrained by collision between the two bones. The numbers indicate the ROM improvement when compared to the bone models of the pre-operative CT scan. An additional $19°$ of ROM was gained by further shaving of the femoral head.

outcome of primary arthroscopic management is unsatisfactorily. The ROM simulations may aid clinicians in determining possible gain of a second operation. An important consideration in the decision for further treatment is that re-operation, whether arthoscopically or open, can cause considerable comorbility to a patient. Additional image modalities and simulation instruments that support and justify this decision are beneficial in this matter for both the surgeon and the patient. In the described case the use of simulation software to establish how osseous anatomy disturbs function of the hip joint seems effective.

In conclusion, we believe that the ROM simulations form a promising technique to predict the ROM of articular joints, assuming there is no additional pathology to muscles and nerves. The hypothesis is that it is a helpful tool for choosing between different treatment options. In the future this hypothesis should be tested using a case control study for each of the above applications.

8

General discussion

In this thesis we investigated the supportive role of medical visualisation in the making of orthopaedic treatment decisions that affect the ROM and articulation of spheroid joints. To this aim, we have studied medical visualisation applications in image processing, diagnosis, pre-operative planning and post-operative evaluation. In the following sections we will summarise and discuss our conclusions.

8.1   Image processing

In spite of the improved quality and resolution of modern scanning equipment, image data of pathological joints can be difficult to interpret by automated processes. This leads to challenging segmentation problems. One such segmentation problem is seen in shoulder replacement surgery for patients with rheumatoid arthritis, where the automated extraction of bone models is complicated as a result of the deteriorated state of the joint. The difficulty of this segmentation problem depends on the extent of joint space narrowing and the variations in bone density.

In the literature, optimal solutions to segmentation challenges often consist of a combination of several segmentation techniques (Van Ginneken et al., 2007, Metz et al., 2008). To solve our particular segmentation problem we have adopted volume and surface processing techniques and combined them with interactive visualisation. The applicability of Hough-transforms as a solution to segmentation tasks that involve curved shapes is well-known (Van der Glas et al., 2002, Illingworth and Kittler, 1988). However, the combination of a Hough-transform with visualisation of minimum-curvature is novel and appears to be effective for the segmentation of

severely arthritic shoulder joints. We have demonstrated that semi-automatic segmentation of rheumatoid joints in CT can be performed quickly and accurately, in spite of varying acquisition parameters.

8.2   Diagnosis & pre-operative planning

In orthopaedics, image data is commonly used to assess the state of joints. However, clinically relevant derivations of the data, e.g. the articulation of a joint or the volume of a muscle, are difficult to extract by merely depicting the data. In the assessment process clinicians will generally evaluate these parameters and base treatment decisions upon their expert judgement (Preim and Bartz, 2007). Many of these parameters can be accurately simulated by simulation models, provided that the underlying assumptions are validated. Examples of simulation models are finite element models to evaluate bone strength and musculoskeletal models to predict muscle function.

In this thesis we studied the simulation and visualisation of bone-determined ROM of spheroid joints such as the shoulder and hip joint. This is an important factor in the prediction of post-operative joint mobility.

The simulator was initially applied in a pre-operative planning system for shoulder replacement surgery. Interactivity of the system was realised by the development of two optimisation techniques that were presented in Chapter 3. Besides its application to shoulder replacement surgery, the simulator was used to analyse a series of 79 proximal humerus fractures (PHF) with two observers. The high inter-observer agreement found in this study is an indication that ROM simulation of PHFs is a promising approach that may substitute classification systems commonly used to decide on treatment. Conclusions that followed from this study are that a smaller retroversion angle leads to limited ROM for all types of PHFs and that intra-articular fractures generally have a worse prognosis with regards to bone-determined ROM.

The application of our system to PHFs demonstrates that the concept of ROM simulation is extensible to other pathologies. This claim is further supported by the case studies presented in Chapter 7, where the system was successfully applied to treat a patient with a PHF, a patient with a malaligned hip prosthesis that increased the risk on dislocation, and finally a patient with femoroacetabular impingement.

A currently unaddressed question is whether pre-operative planning has added value when no intra-operative guidance method is used to ascertain that the operation is carried out in accordance with the pre-operative plan. The purpose of pre-operative planning is to provide the surgeon with an accurate and complete mental image of the joint that he is going to operate on. This is exactly what a surgeon does when he uses conventional methods such as radiographs or CT to prepare for surgery. Simulations

and medical visualisation add to this image and support the surgeon in the decision-making process during surgery, also in the absence of coupled surgical guidance. This was confirmed by the case studies presented in Chapter 7.

Besides the support of diagnosis and pre-operative planning, visualisation systems can be used to train surgeons. In addition, they allow surgeons to explain to patients what pathology they have and how it should be treated. Improved understanding by the patient may result in better compliance with the chosen treatment and more correct expectations regarding the result of treatment.

8.3   Evaluation

In orthopaedic research and rehabilitation medicine, joint function in subjects is recorded to monitor disease progression and surgical intervention. The recordings assist in answering fundamental research questions on kinematic behaviour. The data that follows from motion recordings often consists of many parameters that vary over time. The most frequently used visualisation technique for this type of data is the angle-angle plot, which displays only two kinematic parameters. In the case of multi-joint kinematic data, more advanced techniques facilitate data analysis.

We investigated the clinical applicability of a series of new visualisation approaches in a Delphi study format (Rowe and Wright, 1999). The resulting visualisation technique was designed in accordance with the well-known Visual Information-Seeking mantra of Shneidermann (Shneiderman, 1996): *overview first, zoom and filter, then details-on-demand*. This principle can be used to guide the development of visual analysis applications that deal with large amounts of data. The challenge of these visualisation tasks lies in hiding excess data and emphasising data that is of interest to the researcher.

In solving this problem for kinematic data, a multi-view application was developed that allows users to visualise a large collection of visible recorded poses (*overview first*). The user adds filters to occlude data that is not informative in the context of the current research question (*zoom and filter*). By filtering and zooming in on interesting motion patterns, the visualisation becomes more clear and depicts the relationship that is under investigation. When interesting poses have been found, the user can select these poses and request details of that specific pose (*details-on-demand*). Examples are the individual joint angles and their respective 3-D representation. This can be further extended by incorporating more complex data derivations, such as limb speed, force measurements and musculoskeletal model simulations.

One of the observations following from this work is that kinematic data can be easily dealt with using a modular data-flow approach as is common for image pro-

cessing. This can be achieved by means of a network editor such as DeVIDE or ME-VISlab (Botha and Post, 2008, Koenig et al., 2006). Network editors represent data and the operations upon the data as blocks that can be connected with each other to derive modified versions of the data or to produce visual representations of the data. The advantage of choosing a network oriented approach for kinematic data would be that the kinematic model and the representation of the data can be easily adjusted to accommodate different users, as is often required in research on kinematics.

8.4   Conclusion

In this thesis we have demonstrated that medical visualisation can support several clinical decisions that affect the ROM of spheroid joints. In shoulder replacement surgery, the decision for a type, size and alignment of prosthesis was facilitated by demonstrating the effects of surgery on the bone-determined ROM of the glenohumeral joint. In proximal humerus fractures, the decision whether or not to operate was supported by simulating the bone-determined ROM and the articulation of the fractured joint, thereby indicating what fragments of the fracture should be reduced to avoid impingement complications and malarticulation. In femoroacetabular impingement, we demonstrated that our system can be used to support the decision on whether or not to operate and what part of the femoroacetabular joint should be shaved off to avoid further impingement.

8.5   Future Work

As the quality and resolution of existing scanning equipment improves and more image modalities become available, it is expected that decision-support systems will be capable of simulating additional aspects that are relevant for treatment. Examples are the analysis of vascularity around joints and finite element analysis of bones, prosthetic components and muscles. To further enhance the post-operative function prediction with soft-tissue influence, musculo-skeletal models such as the Delft Shoulder & Elbow Model should be integrated in a pre-operative planning system (Van der Helm, 1994), together with techniques to establish patient-specific parameters such as muscle volume from the image data.

In continuation of this research a new project has been initiated that will address intra-operative guidance for shoulder arthroplasty. The objective of this project will be the development of an adaptive surgical instrument that mechanically guides prosthesis placement. At the time of writing, no surgical guidance method for shoulder arthroplasty has been shown to be sufficiently accurate, fast and cost-efficient.

When we evaluate the course of medical visualisation research, two notions are of special interest. The first notion is that medical visualisation techniques often face difficulties in the introduction to clinical practise (Preim and Bartz, 2007). The added value of 3-D visualisations to common 2-D representations is sometimes disputable, especially since the conversion may occlude significant details in the data. With the development of new visualisation systems comes the responsibility to validate results. Clinicians, on the other hand, should keep in mind that all imaging modalities are supportive instruments that are sometimes inconclusive. Future medical visualisation solutions should assist clinicians in this, for example by visualisation of uncertainty (Pang et al., 1997).

A second interesting notion is that the academic value of medical visualisation is sometimes disputed (Van Wijk, 2005). Medical visualisation seldomly follows a scientific model that starts with a hypothesis other than the hypothesis that the clinical problem can be addressed with a visualisation system. In addition, there are often multiple solutions to the research question, the effectiveness of solutions being subjective.

One could argue that the scientific aspect of medical visualisation lies in its underlying principles and techniques. The Visual Information-Seeking mantra by Shneiderman is an example of such a principle, teaching us how to cope with large amounts of data when a visualisation method is built (Shneiderman, 1996). Other examples include research on colour coding (Christ, 1975), perception analysis (Tory and Möller, 2004) and visual encoding principles that deal with the applicability of visual channels (e.g. colour, size, shape, etc.) in conveying information (Mackinlay, 1986). Closely related are the effects of the human visual working memory on user performance regarding 2-D, 3-D and multi-view approaches (Plumlee and Ware, 2006). A last example is the work by Munzner, that deals with standardisation of visualisation grammar and the hierarchy of classes in visualisation research (Munzner, 2009). This provides researchers with a framework that allows them to more accurately describe their contribution to visualisation research.

The described fundamentals also apply to medical visualisation applications. It is conceivable that the data characteristics in combination with our perception and working habits imply that certain approaches are to be preferred above others, depending on the visualisation problem. Future research includes the study of systematic approaches in solving these visualisation problems, for example, by means of a decision tree. In this way, applied medical visualisation benefits from fundamental research, allowing clinical problems to be solved even more effectively.

Bibliography

[Abdel-Malek et al., 2004] Abdel-Malek, K., Yang, J., Brand, R., and Tanbour, E. (2004). Towards understanding the workspace of human limbs. *Ergonomics*, 47(13):1386–405.

[Aspert et al., 2002] Aspert, N., Santa-Cruz, D., and Ebrahimi, T. (2002). MESH: Measuring Errors between Surfaces using the Hausdorff Distance. In *Proceedings of the IEEE International Conference on Multimedia and Expo*, volume I, pages 705–708.

[Barraquand and Latombe, 1991] Barraquand, J. and Latombe, J.-C. (1991). Robot Motion Planning: A Distributed Representation Approach. *The International Journal of Robotics Research*, 10(6):628–649.

[Beall et al., 2005] Beall, D. P., Sweet, C. F., Martin, H. D., Lastine, C. L., Grayson, D. E., Ly, J. Q., and Fish, J. R. (2005). Imaging findings of femoroacetabular impingement syndrome. *Skeletal radiology*, 34(11):691–701.

[Beaulé et al., 2005] Beaulé, P. E., Zaragoza, E., Motamedi, K., Copelan, N., and Dorey, F. J. (2005). Three-dimensional computed tomography of the hip in the assessment of femoroacetabular impingement. *Journal of orthopaedic research : official publication of the Orthopaedic Research Society*, 23(6):1286–92.

[Beck et al., 2005] Beck, M., Kalhor, M., Leunig, M., and Ganz, R. (2005). Hip morphology influences the pattern of damage to the acetabular cartilage: femoroacetabular impingement as a cause of early osteoarthritis of the hip. *The Journal of bone and joint surgery. British volume*, 87(7):1012–8.

[Beck et al., 2004] Beck, M., Leunig, M., Parvizi, J., Boutier, V., Wyss, D., and Ganz, R. (2004). Anterior femoroacetabular impingement: part II. Midterm results of surgical treatment. *Clinical orthopaedics and related research*, (418):67–73.

[Bernstein et al., 1996] Bernstein, J., Adler, L. M., Blank, J. E., Dalsey, R. M., Williams, G. R., and Iannotti, J. P. (1996). Evaluation of the Neer system of classification of proximal humeral fractures with computerized tomographic scans and plain radiographs. *The Journal of bone and joint surgery. American volume*, 78(9):1371–5.

[Blaas et al., 2005] Blaas, J., Botha, C. P., Peters, B., Vos, F. M., and Post, F. H. (2005). Fast and reproducible fiber bundle selection in {DTI} visualization. In Silva, C., Gröller, E., and Rushmeier, H., editors, *Proceedings of IEEE Visualization 2005*, pages 59–64.

[Boileau and Walch, 1997] Boileau, P. and Walch, G. (1997). The three-dimensional geometry of the proximal humerus. Implications for surgical technique and prosthetic design. *J Bone Joint Surg Br*, 79:857–865.

[Botha and Post, 2008] Botha, C. and Post, F. (2008). Hybrid Scheduling in the DeVIDE Dataflow Visualisation Environment. In Hauser, H., Strassburger, S., and Theisel, H., editors, *Proceedings of Simulation and Visualization*, pages 309–322. SCS Publishing House Erlangen.

[Botha, 2005] Botha, C. P. (2005). *Techniques and Software Architectures for Medical Visualisation and Image Processing*. PhD thesis.

[Branzan-Albu et al., 2004] Branzan-Albu, A., Laurendeau, D., Hébert, L., Moffet, H., Dufour, M., and Moisan, C. (2004). Image-Guided Analysis of Shoulder Pathologies: Modeling the 3D Deformation of the Subacromial Space during Arm Flexion and Abduction. In Stephane Cotin, D. M., editor, *International Symposium on Medical Simulation (ISMS 2004)*, volume 1 of *Lecture Notes in Computer Science*, pages 193–202, Cambridge, MA, USA. Springer Verlag.

[Bresenham, 1965] Bresenham, J. E. (1965). Algorithm for computer control of a digital plotter. *IBM Systems Journal*, 4:25–30.

[Chambers et al., 2008] Chambers, E. W., de Verdière, E. C., Erickson, J., Lazarus, F., and Whittlesey, K. (2008). Splitting (complicated) surfaces is hard. *Computational Geometry*, 41:94–110.

[Chen et al., 2007] Chen, J., Forsberg, A. S., Swartz, S. M., and Laidlaw, D. H. (2007). Interactive Multiple Scale Small Multiples. In *Proceedings of IEEE Visualization*.

[Christ, 1975] Christ, R. E. (1975). Review and Analysis of Color Coding Research for Visual Displays. *Human Factors: The Journal of the Human Factors and Ergonomics Society*, 17(6):29.

[Cicchetti and Sparrow, 1981] Cicchetti, D. V. and Sparrow, S. A. (1981). Developing criteria for establishing interrater reliability of specific items: applications to assessment of adaptive behavior. *American journal of mental deficiency*, 86(2):127–37.

[Cobb et al., 2010] Cobb, J., Logishetty, K., Davda, K., and Iranpour, F. (2010). Cams and Pincer Impingement Are Distinct, Not Mixed: The Acetabular Pathomorphology of Femoroacetabular Impingement. *Clinical orthopaedics and related research*.

[Codman, 1934] Codman, E. (1934). *The Shoulder: Rupture of the Supraspinatus Tendon and Other Lesions in or about the Subacromial Bursa*. Thomas Todd Co., Boston.

[Côté et al., 2005] Côté, J. N., Raymond, D., Mathieu, P. A., Feldman, A. G., and Levin, M. F. (2005). Differences in multi-joint kinematic patterns of repetitive hammering in healthy, fatigued and shoulder-injured individuals. *Clinical biomechanics (Bristol, Avon)*, 20(6):581–90.

[De Bruin et al., 2007] De Bruin, P. W., Krekel, P. R., Valstar, E. R., and Rozing, P. M. (2007). Bony landmark registration for computer navigation of the shoulder: evaluation of accuracy. In *7th Annual Meeting of Computer Assisted Orthopaedic Surgery - International*.

[De Filippis et al., 2004] De Filippis, L., Gulli, S., Caliri, A., Romano, C., Munaò, F., Trimarchi, G., La Torre, D., Fichera, C., Pappalardo, A., Triolo, G., Gallo, M., Valentini, G., and Bagnato, G. (2004). Epidemiology and risk factors in osteoarthritis: literature review data from "OASIS" study. *Reumatismo*, 56(3):169–84.

[De Groot, 1997] De Groot, J. (1997). The variability of shoulder motions recorded by means of palpation. *Clinical Biomechanics*, 12(7-8):461–472.

[Dempster, 1955] Dempster, W. T. (1955). Space Requirements of the Seated Operator.

[Di Gioia III et al., 2007] Di Gioia III, M. D. A. M., Blendea, S., and Jaramaz, B. (2007). Surgical Navigation for Total Hip Arthroplasty. In J.J. Callaghan A.G. Rosenberg, H. E. R., editor, *The Adult Hip, 2nd Edition*, volume 2, pages 1053–1059. Lippincott Williams & Wilkins.

[Dick et al., 2008] Dick, C., Georgii, J., Burgkart, R., and Westermann, R. (2008). Computational Steering for Patient-Specific Implant Planning in Orthopedics. In *Proceedings of Visual Computing for Biomedicine*, pages 83–92.

[Dijkstra, 1959] Dijkstra, E. W. (1959). A note on two problems in connexion with graphs. *Numerische Mathematik*, 1:269–271.

[Dines et al., 2001] Dines, D. M., Warren, R. F., and Rodriguez, D. F. (2001). Revision Shoulder Arthroplasty. *Techniques in Shoulder & Elbow Surgery*, 2:26–37.

[Duda and Hart, 1972] Duda, R. O. and Hart, P. E. (1972). Use of the Hough transform to detect lines and curves in pictures. *Comm. ACM*, 15:11–15.

[Ebaugh et al., 2005] Ebaugh, D. D., McClure, P. W., and Karduna, A. R. (2005). Three-dimensional scapulothoracic motion during active and passive arm elevation. *Clinical Biomechanics*, 20(7):700–709.

[Edelson et al., 2004] Edelson, G., Kelly, I., Vigder, F., and Reis, N. D. (2004). A three-dimensional classification for fractures of the proximal humerus. *The Journal of bone and joint surgery. British volume*, 86(3):413–25.

[Fleute and Lavallee, 1998] Fleute, M. and Lavallee, S. (1998). Building a complete surface model from sparse data using statistical shape models: application to computer assisted knee surgery system. In *MICCAI*, pages 879–887.

[Frankle et al., 2005] Frankle, M., Siegal, S., Pupello, D., Saleem, A., Mighell, M., and Vasey, M. (2005). The Reverse Shoulder Prosthesis for glenohumeral arthritis associated with severe rotator cuff deficiency. A minimum two-year follow-up study of sixty patients. *J Bone Joint Surg Am*, 87:1697–1705.

[Ganz et al., 2003] Ganz, R., Parvizi, J., Beck, M., Leunig, M., Nötzli, H., and Siebenrock, K. A. (2003). Femoroacetabular impingement: a cause for osteoarthritis of the hip. *Clinical orthopaedics and related research*, (417):112–20.

[Goldman et al., 1995] Goldman, R., Koval, K., Cuomo, F., Gallagher, M., and Zuckerman, J. (1995). Functional outcome after humeral head replacement for acute three- and four-part proximal humeral fractures. *Journal of Shoulder and Elbow Surgery*, 4(2):81–86.

[Gosvig et al., 2008] Gosvig, K. K., Jacobsen, S., Sonne-Holm, S., and Gebuhr, P. (2008). The prevalence of cam-type deformity of the hip joint: a survey of 4151 subjects of the Copenhagen Osteoarthritis Study. *Acta radiologica (Stockholm, Sweden : 1987)*, 49(4):436–41.

[Graham and Kennedy, 2003] Graham, M. and Kennedy, J. (2003). Using curves to enhance parallel coordinate visualisations. *Information Visualization, 2003. IV 2003. Proceedings. Seventh International Conference on*.

[Grammont et al., 1987] Grammont, P., Trouilloud, P., Laffay, J. P., and Deries, X. (1987). Etude et réalisation d'une nouvelle prothèse d'épaule. *Rhumatologie*, 39:407–418.

[Guery et al., 2006] Guery, J., Favard, L., Sirveaux, F., Oudet, D., Mole, D., and Walch, G. (2006). Reverse total shoulder arthroplasty. Survivorship analysis of eighty replacements followed for five to ten years. *J Bone Joint Surg Am.*, 88(8):1742–1747.

[Hagen et al., 2010] Hagen, T. P., Vaughan-Sarrazin, M. S., and Cram, P. (2010). Relation between hospital orthopaedic specialisation and outcomes in patients aged 65 and older: retrospective analysis of US Medicare data. *BMJ (Clinical research ed.)*, 340:c165.

[Hagino et al., 1999] Hagino, H., Yamamoto, K., Ohshiro, H., Nakamura, T., Kishimoto, H., and Nose, T. (1999). Changing incidence of hip, distal radius, and proximal humerus fractures in Tottori Prefecture, Japan. *Bone*, 24(3):265–70.

[Hasan et al., 2001] Hasan, S. S., Leith, J. M., Smith, K. L., and Matsen, F. A. (2001). The distribution of shoulder replacements among surgeons is significantly different than that of hip or knee replacements. In *Annual Meeting of the American Academy of Orthopaedic Surgeons, San Francisco, CA*.

[Hasan et al., 2003] Hasan, S. S., Leith, J. M., Smith, K. L., and Matsen, F. A. (2003). The distribution of shoulder replacement among surgeons and hospitals is significantly different than that of hip or knee replacement. *Journal of shoulder and elbow surgery / American Shoulder and Elbow Surgery*, 12(2):164–9.

[Hertel et al., 2004] Hertel, R., Hempfing, A., Stiehler, M., and Leunig, M. (2004). Predictors of humeral head ischemia after intracapsular fracture of the proximal humerus. *Journal of Shoulder and Elbow Surgery*, 13(4):427–433.

[Hoeymans et al., 2010] Hoeymans, N., Melse, J., and Schoemaker, C. (2010). Gezondheid en determinanten. Deelrapport van de Volksgezondheid Toekomst Verkenning 2010 Van gezond naar beter.

[Huiskes and Chao, 1986] Huiskes, R. and Chao, E. Y. (1986). Guidelines for external fixation frame rigidity and stresses. *Journal of orthopaedic research : official publication of the Orthopaedic Research Society*, 4(1):68–75.

[Iannotti et al., 2005] Iannotti, J. P., Spencer, E. E., Winter, U., Deffenbaugh, D., and Williams, G. (2005). Prosthetic positioning in total shoulder arthroplasty. *J Shoulder Elbow Surg*, 14:111S—-121S.

[Illingworth and Kittler, 1988] Illingworth, J. and Kittler, J. (1988). A survey of the hough transform. *Computer Vision, Graphics, and Image Processing*, 44(1):87–116.

[Jaramaz et al., 1997] Jaramaz, B., Nikou, C., Simon, D., and Di Gioia, A. M. (1997). Range of Motion After Total Hip Arthroplasty: Experimental Verification of the Analytical Simulator. Technical report, Robotics Institute, Carnegie Mellon University, Pittsburgh, PA.

[Juvenspan et al., 2005] Juvenspan, M., Nourissat, G., and L., D. (2005). La prothèse inversée dépaule dans les ruptures massives et irréparables de la coiffe des rotateurs. *Maîtrise Orthopédique*, 148.

[Kang et al., 2003] Kang, Y., Engelke, K., and Kalender, W. A. (2003). A New Accurate and Precise 3-D Segmentation Method for Skeletal Structures in Volumetric CT Data. *IEEE Trans. on Med. Imaging*, 22:586–598.

[Karduna et al., 2001] Karduna, A. R., McClure, P. W., Michener, L. A., and Sennett, B. (2001). Dynamic measurements of three-dimensional scapular kinematics: a validation study. *Journal of biomechanical engineering*, 123(2):184–90.

[Keefe et al., 2009] Keefe, D., Ewert, M., Ribarsky, W., and Chang, R. (2009). Interactive Coordinated Multiple-View Visualization of Biomechanical Motion Data. *viscenter.uncc.edu*, 15(6):1383–1390.

[Koenig et al., 2006] Koenig, M., Spindler, W., Rexilius, J., Jomier, J., Link, F., and Peitgen, H.-O. (2006). Embedding VTK and ITK into a visual programming and rapid prototyping platform. In Cleary, K. R., Galloway, R. L., and Jr., editors, *Medical Imaging 2006: Visualization, Image-Guided Procedures, and Display*, volume 6141, pages 61412O–11, San Diego, CA, USA. SPIE.

[Kontaxis et al., 2009] Kontaxis, A., Cutti, A. G., Johnson, G. R., and Veeger, H. E. J. (2009). A framework for the definition of standardized protocols for measuring upper-extremity kinematics. *Clinical biomechanics (Bristol, Avon)*, 24(3):246–53.

[Krekel, 2005] Krekel, P. R. (2005). Collision detection for the pre-operative planning of shoulder arthroplasty. Technical report, Delft University of Technology.

[Krekel et al., 2006] Krekel, P. R., Botha, C. P., Valstar, E. R., de Bruin, P. W., Rozing, P. M., and Post, F. H. (2006). Interactive simulation and comparative visualisation of the bone-determined range of motion of the human shoulder. In Schulze, T., Horton, G., Preim, B., and Schlechtweg, S., editors, *Proceedings of Simulation and Visualization*, pages 275–288. SCS Publishing House Erlangen.

[Krekel et al., 2009] Krekel, P. R., de Bruin, P. W., Valstar, E. R., Post, F. H., Rozing, P. M., and Botha, C. P. (2009). Evaluation of bone impingement prediction in preoperative planning for shoulder arthroplasty. *J. Engineering in Medicine Part H: Proc. IMechE*, Vol. 223.

[Kristiansen et al., 1988] Kristiansen, B., Andersen, U. L. S., Olsen, C. A., and Varmarken, J.-E. (1988). The Neer classification of fractures of the proximal humerus. *Skeletal Radiology*, 17(6):420–422.

[Krueger et al., 2007] Krueger, A., Leunig, M., Siebenrock, K. A., and Beck, M. (2007). Hip arthroscopy after previous surgical hip dislocation for femoroacetabular impingement. *Arthroscopy : the journal of arthroscopic & related surgery : official publication of the Arthroscopy Association of North America and the International Arthroscopy Association*, 23(12):1285–1289.e1.

[Lang et al., 2005] Lang, H., Radtke, A., Hindennach, M., Schroeder, T., Frühauf, N. R., Malagó, M., Bourquain, H., Peitgen, H.-O., Oldhafer, K. J., and Broelsch, C. E. (2005). Impact of virtual tumor resection and computer-assisted risk analysis on operation planning and intraoperative strategy in major hepatic resection. *Archives of surgery (Chicago, Ill. : 1960)*, 140(7):629–38; discussion 638.

[Larsen, 1995] Larsen, A. (1995). How to apply Larsen score in evaluating radiographs of rheumatoid arthritis in long-term studies. *J Rheumatol 22,* page 19745.

[Larson and Giveans, 2008] Larson, C. M. and Giveans, M. R. (2008). Arthroscopic management of femoroacetabular impingement: early outcomes measures. *Arthroscopy : the journal of arthroscopic & related surgery : official publication of the Arthroscopy Association of North America and the International Arthroscopy Association*, 24(5):540–6.

[Lattanzi et al., 2002] Lattanzi, R., Petrone, M., Quadrani, P., Zannoni, C., and Viceconti, M. (2002). Applications of 3D Medical Imaging in Orthopaedic Surgery: Introducing the Hip-Op System. *Proc. First International Symposium on 3D Data Processing Visualization and Transmission*, pages 808–811.

[Lenarčič and Klopčar, 2006] Lenarčič, J. and Klopčar, N. (2006). Positional kinematics of humanoid arms. *Robotica*, 24(1).

[Leunig et al., 2005] Leunig, M., Beck, M., Dora, C., and Ganz, R. (2005). Femoroacetabular Impingement: Etiology and Surgical Concept. *Operative Techniques in Orthopaedics*, 15(3):247–255.

[Lind et al., 1989] Lind, T., Krø ner, K., and Jensen, J. (1989). The epidemiology of fractures of the proximal humerus. *Archives of Orthopaedic and Trauma Surgery*, 108(5):285–287.

[Lindberg et al., 1982] Lindberg, H. O., Carlsson, A. S., Gentz, C. F., and Pettersson, H. (1982). Recurrent and non-recurrent dislocation following total hip arthroplasty. *Acta orthopaedica Scandinavica*, 53(6):947–52.

[Lo et al., 2003] Lo, I., Bishop, J., and Flatow, E. (2003). Revision shoulder arthroplasty after failed total shoulder arthroplasty. *Operative Techniques in Orthopaedics*, 13(4):277–289.

[Lorensen and Cline, 1987] Lorensen, W. E. and Cline, H. E. (1987). Marching Cubes: A high resolution 3D surface construction algorithm. *Computer Graphics*, 21.

[Lozano-Pérez, 1990] Lozano-Pérez, T. (1990). Spatial planning: a configuration space approach. *Autonomous robot vehicles*.

[Mackinlay, 1986] Mackinlay, J. D. (1986). Automating the Design of Graphical Presentations of Relational Information. *ACM Transactions on Graphics*, 5:110–141.

[Magermans et al., 2005] Magermans, D. J., Chadwick, E. K. J., Veeger, H. E. J., and van Der Helm, F. C. T. (2005). Requirements for upper extremity motions during activities of daily living. *Clinical biomechanics (Bristol, Avon)*, 20(6):591–9.

[Majed et al., 2011a] Majed, A., Macleod, I., Bull, A. M., Zyto, K., Resch, H., Hertel, R., Reilly, P., and Emery, R. J. (2011a). Proximal Humeral Fracture Classification Systems Revisited. *Journal of Shoulder and Elbow Surgery*.

[Majed et al., 2011b] Majed, A., Tardugno, A., Reilly, P., Bull, A. M., and Emery, R. J. (2011b). Digital 3D Geometric Assessment of Proximal Humeral Fractures. *Submitted, reviews pending*.

[Manal et al., 2005] Manal, K., Chang, C.-C., Hamill, J., and Stanhope, S. J. (2005). A three-dimensional data visualization technique for reporting movement pattern deviations. *Journal of biomechanics*, 38(11):2151–6.

[Manal and Stanhope, 2004] Manal, K. and Stanhope, S. J. (2004). A novel method for displaying gait and clinical movement analysis data. *Gait & posture*, 20(2):222–6.

[Mangan and Whitaker, 1999] Mangan, A. P. and Whitaker, R. T. (1999). Partitioning 3D Surface Meshes Using Watershed Segmentation. *IEEE Transactions on Visualization and Computer Graphics*, 5:308–321.

[Mardones et al., 2005] Mardones, R. M., Gonzalez, C., Chen, Q., Zobitz, M., Kaufman, K. R., and Trousdale, R. T. (2005). Surgical treatment of femoroacetabular impingement: evaluation of the effect of the size of the resection. *The Journal of bone and joint surgery. American volume*, 87(2):273–9.

[Maurel, 1999] Maurel, W. (1999). *3D Modeling of the Human Upper Limb including the Biomechanics of Joints, Muscles and Soft Tissues*. PhD thesis.

[Maurel et al., 2002] Maurel, W., Thalmann, D., Hoffmeyer, P., Beylot, P., Gingins, P., Kalra, P., and Magnenat Thalmann, N. (2002). *A biomechanical musculoskeletal model of human upper limb for dynamic simulation*. IEEE.

[Meskers et al., 1998] Meskers, C. G. M., Van der Helm, F. C. T., Rozendaal, L. A., and Rozing, P. M. (1998). In vivo estimation of the glenohumeral joint rotation center from scapular bony landmarks by linear regression. *Journal of Biomechanics*, 31:93–96.

[Metz et al., 2008] Metz, C., Schaap, M., Walsum, T. V., Giessen, A. V. D., Weustink, A., Mollet, N., Krestin, G., and Niessen, W. (2008). 3D Segmentation in the Clinic: A Grand Challenge II Coronary Artery Tracking. *Medical Image Computing and Computer-Assisted Intervention MICCAI*.

[Müller et al., 1994] Müller, M. E., Nazarian, S., Koch, P., and Schatzker, J. (1994). *The Comprehensive Classification of Fractures of Long Bones*. Springer.

[Munzner, 2009] Munzner, T. (2009). A Nested Process Model for Visualization Design and Validation. *IEEE Transactions on Visualization and Computer Graphics*, 15:921–928.

[Nanidis et al., 2010] Nanidis, T. G., Majed, A., Liddle, A. D., Constantinides, V. A., Sivagnanam, P., Tekkis, P. P., Reilly, P., and Emery, R. J. (2010). Conservative Versus Operative Management of Complex Proximal Humeral Fractures A Meta-Analysis. *Journal of Shoulder and Elbow Surgery*.

[Neer, 1970] Neer, C. S. (1970). Displaced proximal humeral fractures. I. Classification and evaluation. *The Journal of bone and joint surgery. American volume*, 52(6):1077–89.

[Nötzli et al., 2002] Nötzli, H. P., Wyss, T. F., Stoecklin, C. H., Schmid, M. R., Treiber, K., and Hodler, J. (2002). The contour of the femoral head-neck junction as a predictor for the risk of anterior impingement. *The Journal of Bone and Joint Surgery*, 84(4):556–560.

[Nyffeler et al., 2005] Nyffeler, R. W., Werner, C. M. L., and Gerber, C. (2005). Biomechanical relevance of glenoid component positioning in the reverse Delta III total shoulder prosthesis. *J Shoulder Elbow Surg*, 14:524–528.

[Outerbridge, 1961] Outerbridge, R. E. (1961). The etiology of chondromalacia patellae. *The Journal of bone and joint surgery. British volume*, 43-B:752–7.

[Page et al., 2003] Page, D. L., Koschan, A. F., and Abidi, M. A. (2003). Perception-based 3D Triangle Mesh Segmentation Using Fast Marching Watersheds. *cvpr*, 02:27.

[Page et al., 2002] Page, D. L., Sun, Y., Koschan, A. F., Paik, J., and Abidi, M. A. (2002). Normal vector voting:crease detection and curvature estimation on large, noisy meshes. *Graphical Models*, 64(3).

[Palvanen et al., 2006] Palvanen, M., Kannus, P., Niemi, S., and Parkkari, J. (2006). Update in the epidemiology of proximal humeral fractures. *Clinical orthopaedics and related research*, 442:87–92.

[Pang et al., 1997] Pang, A. T., Wittenbrink, C. M., and Lodha, S. K. (1997). Approaches to uncertainty visualization. *The Visual Computer*, 13(8):370–390.

[Philippon et al., 2009] Philippon, M. J., Briggs, K. K., Yen, Y.-M., and Kuppersmith, D. A. (2009). Outcomes following hip arthroscopy for femoroacetabular impingement with associated chondrolabral dysfunction: minimum two-year follow-up. *The Journal of bone and joint surgery. British volume*, 91(1):16–23.

[Philippon et al., 2007] Philippon, M. J., Schenker, M. L., Briggs, K. K., Kuppersmith, D. A., Maxwell, R. B., and Stubbs, A. J. (2007). Revision hip arthroscopy. *The American journal of sports medicine*, 35(11):1918–21.

[Phillips et al., 2003] Phillips, C. B., Barrett, J. A., Losina, E., Mahomed, N. N., Lingard, E. A., Guadagnoli, E., Baron, J. A., Harris, W. H., Poss, R., and Katz, J. N. (2003). Incidence rates of dislocation, pulmonary embolism, and deep infection during the first six months after elective total hip replacement. *The Journal of bone and joint surgery. American volume*, 85-A(1):20–6.

[Pitiot et al., 2004] Pitiot, A., Delingette, H., Thompson, P. M., and Ayache, N. (2004). Expert knowledge-guided segmentation system for brain MRI. *Neuroimage*, 23 Suppl 1:S85—-S96.

[Plumlee and Ware, 2006] Plumlee, M. D. and Ware, C. (2006). Zooming versus multiple window interfaces:Cognitive costs of visual comparisons. *ACM Transactions on Computer-Human Interaction (TOCHI)*, 13(2):179.

[Preim and Bartz, 2007] Preim, B. and Bartz, D. (2007). *Visualization in Medicine: Theory, Algorithms, and Applications (The Morgan Kaufmann Series in Computer Graphics)*. Morgan Kaufmann.

[Prescher, 2000] Prescher, A. (2000). Anatomical basics, variations, and degenerative changes of the shoulder joint and shoulder girdle. *Eur J Radiol*, 35:88–102.

[Rajamani et al., 2007] Rajamani, K. T., Styner, M. A., Talib, H., Zheng, G., Nolte, L. P., and lez Ballester, M. A. G. (2007). Statistical deformable bone models for robust 3D surface extrapolation from sparse data. *Med Image Anal*, 11:99–109.

[Richolt et al., 1998] Richolt, J. A., Teschner, M., Everett, P., Girod, B., Millis, M. B., and Kikinis, R. (1998). Planning and Evaluation of Reorienting Osteotomies of the Proximal Femur in Cases of SCFE Using Virtual Three-Dimensional Models. In *MICCAI '98*, pages 1–8, London, UK. Springer-Verlag.

[Rockwood, 2007] Rockwood, C. A. (2007). The reverse total shoulder prosthesis. The new kid on the block. *J Bone Joint Surg Am*, 89:233–235.

[Rowe and Wright, 1999] Rowe, G. and Wright, G. (1999). The Delphi technique as a forecasting tool: issues and analysis. *International Journal of Forecasting*, 15(4):353–375.

[Saase et al., 1989] Saase, J. L. V., Romunde, L. K. V., Cats, A., Vandenbroucke, J. P., and Valkenburg, H. A. (1989). Epidemiology of osteoarthritis: Zoetermeer survey. Comparison of radiological osteoarthritis in a Dutch population with that in 10 other populations. *Ann Rheum Dis*, 48(4):271–280.

[Sato et al., 2000] Sato, Y., Sasama, T., Sugano, N., Nakahodo, K., Nishii, T., Ozono, K., Yonenobu, K., Ochi, T., and Tamura, S. (2000). Intraoperative Simulation and Planning Using a Combined Acetabular and Femoral (CAF) Navigation System for Total Hip Replacement. In *Medical Image Computing and Computer-Assisted Intervention MICCAI 2000*, pages 1114–1125.

[Shneiderman, 1996] Shneiderman, B. (1996). The Eyes Have It:A Task by Data Type Taxonomy for Information Visualizations. *VL*.

[Sidor et al., 1993] Sidor, M. L., Zuckerman, J. D., Lyon, T., Koval, K., Cuomo, F., and Schoenberg, N. (1993). The Neer classification system for proximal humeral fractures. An assessment of interobserver reliability and intraobserver reproducibility. *The Journal of bone and joint surgery. American volume*, 75(12):1745–50.

[Siebenrock and Gerber, 1993] Siebenrock, K. A. and Gerber, C. (1993). The reproducibility of classification of fractures of the proximal end of the humerus. *The Journal of bone and joint surgery. American volume*, 75(12):1751–5.

[Simon et al., 1997] Simon, D. A., Jaramaz, B., Blackwell, M., Morgan, F., DiGioia, A. M., Kischell, E., Colgan, B., and Kanade, T. (1997). Development And Validation Of A Navigational Guidance System For Acetabular Implant Placement. *Proc. of the First Joint CVRMed / MRCAS Conference*, pages 583–592.

[Simovitch et al., 2007] Simovitch, R. W., Zumstein, M. A., Lohri, E., Helmy, N., and Gerber, C. (2007). Predictors of scapular notching in patients managed with the Delta III reverse total shoulder replacement. *J Bone Joint Surg Am*, 89:588–600.

[Sirveaux et al., 2004] Sirveaux, F., Favard, L., Oudet, D., Huquet, D., Walch, G., and Mol, D. (2004). Grammont inverted total shoulder arthroplasty in the treatment of glenohumeral osteoarthritis with massive rupture of the cuff. Results of a multicentre study of 80 shoulders. *J Bone Joint Surg Br*, 86:388–395.

[Symmons et al., 1994] Symmons, D. P., Barrett, E. M., Bankhead, C. R., Scott, D. G., and Silman, A. J. (1994). The incidence of rheumatoid arthritis in the United Kingdom: results from the Norfolk Arthritis Register. *British journal of rheumatology*, 33(8):735–9.

[Tannast et al., 2007a] Tannast, M., Kubiak-Langer, M., Langlotz, F., Puls, M., Murphy, S. B., and Siebenrock, K. A. (2007a). Noninvasive three-dimensional assessment of femoroacetabular impingement. *Journal of orthopaedic research : official publication of the Orthopaedic Research Society*, 25(1):122–31.

[Tannast et al., 2007b] Tannast, M., Siebenrock, K. A., and Anderson, S. E. (2007b). Femoroacetabular impingement: radiographic diagnosis–what the radiologist should know. *AJR. American journal of roentgenology*, 188(6):1540–52.

[Tao et al., 2002] Tao, X., Prince, J. L., and Davatzikos, C. (2002). Using a statistical shape model to extract sulcal curves on the outer cortex of the human brain. *IEEE Trans Med Imaging*, 21:513–524.

[Taubin, 1995] Taubin, G. (1995). A signal processing approach to fair surface design. In *SIGGRAPH '95: Proceedings of the 22nd annual conference on Computer graphics and interactive techniques*, pages 351–358, New York, NY, USA. ACM.

[Terdiman, 2001] Terdiman, P. (2001). Memory-optimized bounding-volume hierarchies.

[Tory and Möller, 2004] Tory, M. and Möller, T. (2004). Human Factors in Visualization Research. *IEEE Transactions on Visualization and Computer Graphics*, 10(1).

[Tremblay et al., 2004] Tremblay, M.-E., Branzan-Albu, A., Laurendeau, D., and Hébert, L. (2004). Integrating Region and Edge Information for the Automatic Segmentation for Interventional Magnetic Resonance Images of the Shoulder Complex. In *1st Canadian Conference on Computer and Robot Vision (CRV2004)*, volume 1, pages 279–286, London, Ontario, Canada. IEEE Computer Society.

[Van der Glas et al., 2002] Van der Glas, M., Vos, F. M., Botha, C. P., and Vossepoel, A. M. (2002). Determination of Position and Radius of Ball Joints. In Sonka, M., editor, *Proceedings of the SPIE International Symposium on Medical Imaging*, volume 4684 - Ima.

[Van der Helm, 1994] Van der Helm, F. C. T. (1994). A finite element musculo-skeletal model of the shoulder mechanism. *Journal of Biomechanics*, 27:551–569.

[Van Ginneken et al., 2007] Van Ginneken, B., Heimann, T., and Styner, M. (2007). 3D Segmentation in the Clinic: A Grand Challenge. *3D Segmentation in the Clinic: A Grand Challenge*, pages 7–15.

[Van Sint Jan et al., 1998] Van Sint Jan, S. L., Clapworthy, G. J., and Rooze, M. (1998). Visualization of Combined Motions in Human Joints. *IEEE Computer Graphics and Applications*, 18(6).

[Van Staa et al., 2001] Van Staa, T. P., Dennison, E. M., Leufkens, H. G., and Cooper, C. (2001). Epidemiology of fractures in England and Wales. *Bone*, 29(6):517–22.

[Van Wijk, 2005] Van Wijk, J. (2005). The value of visualization. In *Proc. IEEE Visualization*, pages 79–86.

[Vollmer et al., 1999] Vollmer, J., Mencel, R., and Mueller, H. (1999). Improved laplacian smoothing of noisy surface meshes. In *Computer Graphics Forum*, volume 18, pages 131–138.

[Von Schroeder et al., 2001] Von Schroeder, H. P., Kuiper, S. D., and Botte, M. J. (2001). Osseous anatomy of the scapula. *Clin Orthop Relat Res*, pages 131–139.

[Whittle, 2006] Whittle, M. (2006). *Gait analysis: an introduction*. Butterworth-Heinemann Publishing, Oxford, 4th edition.

[Williams et al., 2001] Williams, G. R., Wong, K. L., Pepe, M. D., Tan, V., Silverberg, D., Ramsey, M. L., Karduna, A., and Iannotti, J. P. (2001). The effect of articular

malposition after total shoulder arthroplasty on glenohumeral translations, range of motion, and subacromial impingement. *J Shoulder Elbow Surg*, 10:399–409.

[Wirth and Rockwood, 1994] Wirth, M. A. and Rockwood, C. A. (1994). Complications of shoulder arthroplasty. *Clinical orthopaedics and related research*, (307):47–69.

[Wu and Sun, 2006] Wu, C.-H. and Sun, Y.-N. (2006). Segmentation of kidney from ultrasound B-mode images with texture-based classification. *Comput Methods Programs Biomed*, 84:114–123.

[Wu et al., 2005] Wu, G., van der Helm, F. C. T., Veeger, H. E. J., Makhsous, M., Van Roy, P., Anglin, C., Nagels, J., Karduna, A. R., McQuade, K., Wang, X., and al., E. (2005). ISB recommendation on definitions of joint coordinate systems of various joints for the reporting of human joint motion–Part II: shoulder, elbow, wrist and hand. *Journal of Biomech*, 38:987–992.

[Yoshimine and Ginbayashi, 2002] Yoshimine, F. and Ginbayashi, K. (2002). A mathematical formula to calculate the theoretical range of motion for total hip replacement. *J Biomech*, 35:989–993.

[Zhao et al., 2006] Zhao, L., Botha, C., Bescos, J., Truyen, R., Vos, F., and Post, F. (2006). Lines of Curvature for Polyp Detection in Virtual Colonoscopy. *IEEE Transactions on Visualization and Computer Graphics*, 12:885–892.

[Zoroofi et al., 2003] Zoroofi, R. A., Sato, Y., Sasama, T., Nishii, T., Sugano, N., Yonenobu, K., Yoshikawa, H., Ochi, T., and Tamura, S. (2003). Automated segmentation of acetabulum and femoral head from 3-d CT images. *IEEE Transactions on Information Technology in Biomedicine*, 7:329–343.

[Zyto, 1998] Zyto, K. (1998). Non-operative treatment of comminuted fractures of the proximal humerus in elderly patients. *Injury*, 29(5):349–352.

[Zyto et al., 1997] Zyto, K., Ahrengart, L., Sperber, A., and Törnkvist, H. (1997). Treatment of displaced proximal humeral fractures in elderly patients. *The Journal of bone and joint surgery. British volume*, 79(3):412–7.

[Zyto et al., 1995] Zyto, K., Kronberg, M., and Broström, L. A. (1995). Shoulder function after displaced fractures of the proximal humerus. *Journal of shoulder and elbow surgery / American Shoulder and Elbow Surgeons*, 4(5):331–6.

Summary

In this thesis we investigate how medical visualisation provides insight into the articulation and range of motion (ROM) of joints, with the purpose of supporting surgical decision-making that addresses pathology at the articulating joint. To this aim, we study medical visualisation applications in image processing, diagnostic decision-making, pre-operative planning and evaluation of kinematics.

We present a technique for the segmentation of bony structures in computed tomography (CT) scans of rheumatoid shoulders (*chapter 2*). The segmentation process is complicated by holes (i.e. bone cysts), irregularities and a non-uniform density of the bone tissue, which are caused by the pathological state of the joint. For the specific case of the shoulder joint, existing segmentation techniques often fail and lead to poor results. Our approach enables users to quickly and accurately segment CT scans of gleno-humeral joints that have a varying bone density and a small joint space.

The technique consists of three steps and starts with a rough surface model of the bones. First, a loop that encircles the joint is extracted by calculating the minimum curvature of the surface model. Subsequently, the intersection points of this loop with the separate CT-slices are connected by means of a path search algorithm. Finally, errors in the segmentation are corrected by iteratively applying a Hough transform to the segmentation result.

The segmentation routine was developed to facilitate the extraction of surface models from CT scans for a pre-operative planning system. The limited time available in clinical practice introduces the requirement that the segmentation routine must lead to a sufficiently accurate segmentation result in under two minutes. This criterion was satisfied by our approach. We conclude that the combination of surface curvature, limited user interaction and iterative refinement via a Hough transform forms a satisfactory approach for the segmentation of severely damaged arthritic shoulder joints.

The segmented volumes can be converted to surface models of the shoulder bo-

nes. The models play an important role in a system we developed for pre-operative planning of shoulder replacement surgery. The system includes a fast and efficient method for highly interactive visualisation of patient-specific bone-determined ROM for the gleno-humeral joint (*chapter 3*). The gleno-humeral ROM is visualised with motion envelopes that indicate the maximum ROM of the humerus in every direction. In our pre-operative planning system, the prosthesis alignment can be adjusted interactively, during which a novel comparative visualisation technique depicts the differences between the current and previous ROM. By using geometry clipping-based optimisation, as well as precalculation and interpolation techniques, it was possible to show in real-time the consequences of adjustments made to a planned shoulder prosthesis alignment.

Subsequently, the results of an evaluation experiment for the ROM simulator are presented (*chapter 4*). Both shoulders of a cadaver were replaced with a modular shoulder prosthesis. A data connection between the software environment and an existing intra-operative guidance system was created to track the relative positions of the bones. With the data connection, the position and alignment of patient-specific surface models within our visualisation software were matched with the position and alignment of the real bones. Using this set-up, all of the occurrences of impingement of a series of systematic movements were registered. These registrations were compared to the results of the ROM simulator. We conclude that the ROM simulator is sufficiently accurate to fulfil its role as a supportive instrument for orthopaedic surgeons during shoulder replacement surgery.

The use of the ROM simulator as a method to categorically analyse impingement and joint articulation of proximal humerus fractures (PHFs) is described in *chapter 5*. The morphology of the fractured shoulders varies greatly. Classification systems attempt to formalise these differences and relate them to clinical results. However, the repeatability of these classification systems has been shown to be poor, giving rise to the question whether a more objective measure entails improved predictability of outcome.

We demonstrate that it is possible to reproducibly evaluate the bone-determined ROM of a fractured shoulder joint and relate the results to morphological properties. It follows from this work that intra-articular fractures generally have a worse prognosis with regards to bone-determined ROM when compared to fractures with an intact articular surface. The bone-determined ROM of fractures with a displaced tuberculum major and minor is generally larger than that of intra-articular fractures, but often still limited in abduction by the coracoacromial arch. Finally, our results indicate that a low head inclination angle leads to a high probability of sub-acromial and gleno-humeral impingement.

We present a new analysis system that allows users to investigate multi-joint ki-

nematics (*chapter 6*). Kinematic analysis is the analysis of motions without regarding forces or inertial effects, with the purpose of understanding joint behaviour. Kinematic data of the upper extremity contains many interrelated degrees of freedom of several joints, complicating numerical analysis. The analysis process can be supported by visualisation techniques, thereby improving the effectiveness of kinematic experiments.

In our case, the kinematic data is acquired using motion registration systems. The data is used to evaluate clinical results. The challenge inherent in the data is that the upper extremity is comprised of five cooperating joints (excluding the hand) with a total of fifteen degrees of freedom. The ROM may be affected by subtle deficiencies of individual joints that are difficult to pinpoint. To highlight the subtle interplay between the joints our approach combines interactive filtering and multiple visualisation techniques.

Our system integrates simultaneous acquisition and visual analysis of kinematic data and forms an effective approach specifically tailored for the investigation and comparison of large collections of kinematic data. To facilitate complex queries, we have designed a visual query interface with visualisation and interaction elements that are based on the domain-specific anatomical representation of the data. An evaluation experiment is described where the technique was successfully used to view the kinematics of the left and right arm of a patient with a healed proximal humerus fracture, i.e. a healed shoulder fracture.

Finally, clinical case studies where the ROM simulation system was used to support treatment and diagnostic decision-making are presented in *chapter 7*:

1. The first case report concerns a patient with a PHF. Through analysis of the fracture by means of the ROM simulation system it was possible to calculate the correction required to prevent impingement.

2. The second case report concerns the evaluation of the risk of dislocation of a total hip prosthesis. Using the ROM simulation system it is possible to detect malalignment of prostheses and impingement, a possible cause for luxation.

3. The third case report concerns a patient who was diagnosed with femoroacetabular impingement. Primary arthroscopic treatment did not have satisfactory results. The ROM simulation system showed that there was still bony impingement that limited ROM. This was successfully removed in a second arthroscopic procedure, as was proved with a post-operative CT scan and ROM simulation.

The ROM simulator contributes in the decision-making process involved in patients with potential impingement.

Samenvatting (Dutch summary)

In dit proefschrift onderzoeken we hoe medische visualisatie inzicht kan geven in de articulatie en bewegingsvrijheid van gewrichten, met als doel om chirurgische beslissingen die betrekking hebben op de behandeling van pathologie van gewrichten te ondersteunen. Hiervoor bestuderen we medische visualisatieapplicaties op het gebied van beeldverwerking, diagnose, pre-operatieve planning en kinematische evaluatie.

Een techniek voor het segmenteren van botstructuren in computer tomografie (CT) scans van reumatoïde schouders wordt beschreven in *hoofdstuk 2*). Het segmentatieproces wordt gecompliceerd door gaten (botcystes), onregelmatigheden en een niet uniforme dichtheid van het botweefsel, een gevolg van de pathologische staat van het gewricht. Voor het specifieke geval van het schoudergewricht zijn bestaande segmentatietechnieken onvoldoende nauwkeurig. Onze benadering stelt gebruikers in staat om snel en accuraat CT scans van gleno-humerale gewrichten met variërende botdichtheid en een smalle gewrichtsspleet (door slijtage) te segmenteren.

De techniek bestaat uit drie stappen en begint met een grof oppervlaktemodel van de botten. Het gewricht wordt omcirkeld door de minimale curvatuur van het oppervlaktemodel te berekenen. Vervolgens worden de intersectiepunten van deze cirkel met de verschillende CT-plakken verbonden door middel van een kortste pad routine. Tenslotte worden de fouten van deze segmentatie verbeterd door iteratief een Hough transform toe te passen op het segmentatieresultaat. De Hough transform filtert oneffenheden uit de segmentatie en maakt hiervoor gebruik van de curvatuur van het segmentatieoppervlak.

De segmentatieroutine is ontwikkeld om het extraheren van botmodellen uit CT scans voor een pre-operatief planningssysteem te faciliteren. De beperkte beschikbare tijd in de klinische praktijk introduceert de vereiste dat onze segmentatieroutine een voldoende accuraat segmentatieresultaat moet produceren in minder dan twee minuten. De beschreven techniek voldoet aan dit criterium. We concluderen hieruit dat een combinatie van curvatuurberekeningen, beperkte gebruikersinteractie en een

iteratieve verfijning door middel van een Hough transform tot bevredigende segmentatieresultaten leidt bij zeer ernstig aangetaste reumatoïde schoudergewrichten.

De gesegmenteerde volumes worden omgezet naar botmodellen die een belangrijke rol spelen in pre-operatieve planning voor schoudervervangingschirurgie. Een snelle en efficiënte methode voor interactieve visualisatie van patiënt-specifieke door bot bepaalde bewegingsvrijheid van het gleno-humerale gewricht wordt beschreven in *hoofdstuk 3*. De gleno-humerale bewegingsvrijheid wordt gevisualiseerd door middel van bewegingsenvelopen die de maximale bewegingsvrijheid van de humerus t.o.v. het glenoid weergeven in elke richting van het gewricht. In het gepresenteerde pre-operatieve planningssysteem kan de protheseplaatsing interactief aangepast worden. Tegelijkertijd geeft het systeem met een speciale visualisatietechniek het verschil aan tussen de huidige en de vorige bewegingsvrijheid van het gewricht. Door optimalisatietechnieken kunnen we de gevolgen van een aanpassing aan de planning van een schoudervervanging in real-time laten zien.

De resultaten van een evaluatie-experiment voor de bewegingsvrijheidsimulator worden gepresenteerd in *hoofdstuk 4*. In het experiment werden beide schouders van een kadaver vervangen door een modulaire schouderprothese. Een dataverbinding werd gecreëerd tussen ons systeem en een bestaand computernavigatiesysteem. Dit stelde ons in staat om real-time de positie en oriëntatie van de patiëntspecifieke botten te volgen in de door ons ontwikkelde software. Met deze opstelling hebben we alle gevallen van impingement van een serie opgelegde bewegingen geregistreerd. Deze registraties hebben we vervolgens vergeleken met de resultaten van onze bewegingsvrijheidsimulatiesysteem. Uit de resultaten blijkt dat het bewegingsvrijheidsimulatiesysteem voldoende accuraat is om als ondersteunend instrument te gebruiken bij schoudervervangingschirurgie.

In *hoofdstuk 5* wordt beschreven hoe het bewegingsvrijheidsimulatiesysteem gebruikt kan worden om benige impingement en gewrichtsarticulatie van proximale humerus fracturen (PHF) te bestuderen. De morfologie van deze breuken varieert aanzienlijk. Classificatiesystemen proberen deze verschillen te formaliseren om zo de relatie te leggen met klinische resultaten. Echter, in de literatuur is aangetoond dat de validiteit van deze classificatiesystemen matig is. Daarom is een objectievere methode nodig als voorspeller voor uitkomst.

Het blijkt mogelijk te zijn om de door bot bepaalde bewegingsvrijheid van een gewricht reproduceerbaar te evalueren en te relateren aan morfologische eigenschappen. Een conclusie van deze studie is dat intra-articulaire breuken over het algemeen tot een slechtere prognose leiden met betrekking tot bewegingsvrijheid, in vergelijking met breuken waarbij het gewrichtsvlak nog intact is. De door bot bepaalde bewegingsvrijheid van breuken met een verplaatst tuberculum major en minor is over het algemeen groter dan die van intra-articulaire breuken, maar deze leiden vaak nog

steeds tot een beperking van abductie door de coraco-acromiale boog. Tenslotte blijkt dat een lage inclinatiehoek een indicator is voor een grote kans op impingementcomplicaties, zowel glenohumeraal als subacromiaal.

Een nieuw analysesysteem voor kinematische data wordt beschreven in *hoofdstuk 6*. Kinematische analyse is de analyse van bewegingen zonder dat daarbij krachten of inertiële krachten worden beschouwd. Kinematische data van meerdere gewrichten, zoals bijvoorbeeld bij de bovenste extremiteit, omvat veel aan elkaar gerelateerde vrijheidsgraden die numerieke analyse bemoeilijken. Het analyseproces kan ondersteund worden door visualisatietechnieken die de effectiviteit van kinematische experimenten vergroten.

In ons specifieke geval zijn de kinematische data afkomstig uit bewegingsregistratiesystemen. De data worden gebruikt om klinische resultaten te evalueren. De bovenste extremiteit bestaat uit vijf samenwerkende gewrichten die samen 15 vrijheidsgraden hebben. De bewegingsvrijheid kan beperkt worden door subtiele beperkingen van individuele gewrichten. Om dit zichtbaar te maken combineren wij in onze benadering interactieve filters met meerdere visualisatietechnieken.

Ons systeem integreert simultane acquisitie en visuele analyse van kinematische data en vormt een effectieve benadering die specifiek ontworpen is voor het onderzoeken en vergelijken van grote hoeveelheden kinematische data. Om complexe zoekopdrachten mogelijk te maken hebben we een visuele query-interface ontworpen met visualisatie en interactie-elementen die gebaseerd zijn op domein-specifieke anatomische representaties van de data. We beschrijven een evaluatie-experiment waarbij we het systeem hebben gebruikt om de kinematica van de linker- en rechterschouder van een patiënt met een geheelde schouderfractuur te bestuderen. Het systeem stelde ons in staat om afwijkende bewegingspatronen te constateren en te beschrijven.

Tenslotte geven we voorbeelden van orthopaedische problemen waarbij de bewegingsvrijheidsimulator gebruikt kan worden om een behandelingsbeslissing te ondersteunen (*hoofdstuk 7*). Dit doen we door middel van drie casus:

1. De eerste casus betreft een patiënt met een schouderfractuur. Door analyse van de fractuur met de bewegingsvrijheidsimulator was het mogelijk om te berekenen wat de benodigde correctie was teneinde impingement te voorkomen.

2. De tweede casus betreft de evaluatie van het risico van een luxatie van een totale heupprothese. Met de bewegingsvrijheidsimulator is het mogelijk om de verkeerde oriëntatie van een prothese te detecteren, die een mogelijke oorzaak van een luxatie kan zijn.

3. De derde casus betreft een patiënt die gediagnostiseerd was met femoroacetabular impingement. Dit is een afwijking waarbij beweging van het heupgewricht

beperkt wordt door ossificaties. Arthroscopische behandeling, waarbij bot werd weggehaald, leidde niet tot een bevredigend resultaat. Met de bewegingsvrij-heidsimulator werd de kinematica van het gewricht geanalyseerd. Aan de hand van deze simulaties werd vastgesteld waar er bot verwijderd moest worden tij-dens een tweede arthroscopische behandeling. Het succes van deze tweede operatie kon aangetoond worden met behulp van een post-operatieve CT scan en bewegingsvrijheidsimulaties.

Het in dit proefschrift gepresenteerde bewegingsvrijheidsimulatiesysteem draagt bij aan het beslissingsproces dat vooraf gaat aan de behandeling van patiënten met potentiële impingementproblemen.

List of publications

Krekel PR, Botha CP, Valstar ER, DeBruin PW, Post FH, Rozing PM (2006). Interactive simulation and comparative visualisation of the bone-determined range of motion of the human shoulder. *Proceedings of Simulation and Visualization* (T. Schulze, G. Horton, B. Preim, and S. Schlechtweg, eds.), 275-288, Best Paper Award.

Krekel PR, de Bruin PW, Valstar ER, Post FH, Rozing PM, Botha CP (2009). Evaluation of bone impingement prediction in preoperative planning for shoulder arthroplasty. *J. Engineering in Medicine Part H: Proc. IMechE.* 223(7), 813-822.

Krekel PR, Valstar ER, Post FH, Rozing PM, Botha CP (2010). Combined surface and volume processing for fused joint segmentation. *The International Journal for Computer Assisted Radiology and Surgery* 5(3), 263-273.

Krekel PR, Valstar ER, DeGroot J, Post FH, Nelissen RGHH, Botha CP (2010). Visual Analysis of Multi-Joint Kinematic Data. *Computer Graphics Forum*, 29(3), 1123-1132.

Botha CP, Krekel PR, Valstar ER, DeBruin PM, Rozing PM, Post FH (2010). Pre-operative planning and intra-operative guidance for shoulder replacement surgery. *Scientific Visualization: Advanced Concepts* (H. Hagen, Schloss Dagstuhl-Leibniz-Zentrum für Informatik), 1, 179-195.

Krekel PR, Vochteloo AJH, Bloem RM, Nelissen RGHH (2011). Femoroacetabular impingement and its implications on range of motion: a case report. *Journal of Medical Case Reports*, Accepted to appear.

Curriculum Vitae

Peter Krekel was born on the 20th of June 1982 in the Bronovo Hospital in Den Haag, The Netherlands. After graduating from the 'Oranje Nassau College' in Zoetermeer (VWO) in the year 2000 he commenced his studies in Computer Science at Delft University of Technology. During a practical in 2004 he came into contact with dr. C.P. Botha, who efficaciously conveyed his enthusiasm for the field of medical visualisation. A Master's project followed, which was completed in 2006. The research was showcased in a national television series and was awarded a Best Paper award at Simulation and Visualization 2006 in Magdeburg, Germany and the 1st prize of the Young Investigator Award of the Dutch Biomedical Engineering conference 2007 in Egmond aan Zee, the Netherlands.

He continued the work on medical visualisation for orthopaedics as a Ph.D. student in May 2006. The project was carried out as a joint effort between the Orthopaedics Department of Leiden University Medical Center (Head: prof. dr. P.M. Rozing; followed up in 2006 by prof. dr. R.G.H.H. Nelissen) and the Computer Graphics & CAD/CAM group of the Department of Mediamatics of Delft University of Technology (Head: prof. dr. ir. F.W. Jansen).

In May 2010 he founded a company called Clinical Graphics. Clinical Graphics specialises in decision-supporting visualisation software for clinical challenges.

Acknowledgements

This thesis was realised at the Department of Orthopaedics of Leiden University Medical Center (Head: prof. dr. P.M. Rozing; and prof. dr. R.G.H.H. Nelissen) and the Computer Graphics & CAD/CAM group of the Faculty of Electrical Engineering, Mathematics and Computer Science of Delft University of Technology (Head: Prof. dr. ir. F.W. Jansen). The described research was supervised by Charl Botha, Edward Valstar and Frits Post. Its completion I owe to many.

I am greatly indebted to Professor Emery and Addie Majed, who have believed in this work from our first encounter at a pleasant small-sized conference in London. They have been vital for a large part of this thesis, as well as for the continuation of the research.

I would like to thank Rolf, Tom, Heinse and Stefan for being early adopters in (r)evolutionary hip research. Furthermore, the people at J9, especially Nienke, Daniel, André and Bouke, who were colleagues from the beginning and perfectly played their part in a never dull work environment. Jurriaan, thank you for your advice on orientation and direction. A special thanks goes to Ruud and Bart for their knowledgeable technical support.

I would like to thank, in order of appearance, but not necessarily in order of importance: Jorik, Gerwin, Eric, Peter Schaafsma, Stef, Lingxiao, Paul de Bruin, Thisbe, Vesna, Paolo, Tim, Stef, Andriy, Emiel and last and quite the contrary of least, François. Your social roles and in depth discussions have been of utmost importance.

Dear Frans, it would be impossible for me to imagine the past four years without your friendship. You already finished your thesis, a masterpiece you can be extremely proud of. A reminder of an important period in both our lives, I will keep the books side-by-side and frequently look back with a smile. I was told that nothing really ends; we should do this again some time.

With the final dot drawing nearer I am thankful to my parents, who have always encouraged me to pursue and to persist. Sacha, thank you for being there for me

when I need you. Fleur, I am extremely proud of having you as a sister.

Dear Charl, the final spot is rightfully yours. I can honestly say that the decision to do my Master's graduation work under your supervision has been the best decision of my life. For everything that followed from it I am thoroughly grateful.